A-760 DEC 23 1946

ACR No. L5G31a

3 1176 00125 3328

NATIONAL ADVISORY COMMITTEE FOR AERONAUTICS

WARTIME REPORT

ORIGINALLY ISSUED
January 1946 as
Advance Confidential Report L5G31a

1.1.2.1
1.2.1.3
1.2.1.8
1.9.1
1.8.2.5

EFFECT OF COMPRESSIBILITY ON THE PRESSURES AND FORCES ACTING ON A MODIFIED NACA 65,3-019 AIRFOIL HAVING A 0.20-CHORD FLAP

By W. F. Lindsey

Langley Memorial Aeronautical Laboratory
Langley Field, Va.

NACA

WASHINGTON

N A C A LIBRARY
LANGLEY MEMORIAL AERONAUTICAL LABORATORY
Langley Field, Va.

NACA WARTIME REPORTS are reprints of papers originally issued to provide rapid distribution of advance research results to an authorized group requiring them for the war effort. They were previously held under a security status but are now unclassified. Some of these reports were not technically edited. All have been reproduced without change in order to expedite general distribution.

NACA ACR No. L5G31a

NATIONAL ADVISORY COMMITTEE FOR AERONAUTICS

ADVANCE CONFIDENTIAL REPORT

EFFECT OF COMPRESSIBILITY ON THE PRESSURES AND FORCES ACTING ON A MODIFIED NACA 65,3-019 AIRFOIL HAVING A 0.20-CHORD FLAP

By W. F. Lindsey

SUMMARY

An investigation has been conducted in the Langley rectangular high-speed tunnel to determine the effect of compressibility on the pressure distribution for a modified NACA 65,3-019 airfoil having a 0.20-chord flap. The investigation was made for an angle-of-attack range extending from -2° to 12° at flap deflections from 0° to -12°. Test data were obtained for Mach numbers from 0.28 to approximately 0.74.

The results show that the effectiveness of the trailing-edge-type control surface rapidly decreased and approached zero as the Mach number increased above the critical value.

INTRODUCTION

The available information on the aerodynamic characteristics of airfoils, with and without flaps, at low speeds is quite extensive and previous investigations have shown the general effects of compressibility on airfoils without flaps. For airfoils with flaps, however, the available information at high speeds is limited.

The earlier investigations at high speeds demonstrated the limitations of the theoretical methods in extrapolating low-speed data to high speeds (reference 1). In addition, the investigations illustrated the inapplicability of the theoretical methods in the supercritical-speed range, in which pressures and forces change radically. These radical changes in pressures and forces are the adverse effects of compressibility, a knowledge of

which is necessary in the design of high-speed airplanes. Because of the inadequacy of the theoretical method in applications to the supercritical region, recourse to experiment is necessary to determine the adverse effects of compressibility.

Data at high speeds were required in connection with the design of a specific airplane; accordingly, an investigation was conducted in the Langley rectangular high-speed tunnel to determine the effect of compressibility on the pressures and forces acting on a modified NACA 65,3-019 airfoil having a 0.20-chord flap. Pressure-distribution measurements were made at Mach numbers between 0.28 and 0.74 for angles of attack from -2° to 12° and flap deflections from 0° to -12°.

APPARATUS AND TESTS

The tests were conducted in the Langley rectangular high-speed tunnel, which is an induction-type tunnel without return passages and has an 18-inch by 4-inch test section. The variation in the Mach number in the test section along the tunnel axis without a model installed in the tunnel is ±0.4 percent of the stream Mach number. In a plane normal to the tunnel axis the variation is ±0.8 percent of the test-section Mach number at a stream Mach number of 0.60. The direction of the air flow appears to be misalined by -0.1° with a possible variation of ±0.1°. No correction for misalinement has been made for the data presented herein.

The model completely spanned the test section along the 4-inch dimension and was supported by large circular end plates which were fitted into the tunnel walls in such a way as to rotate with the model and to retain continuity of the surface of the tunnel walls. The juncture between the model and the end plate was sealed.

The profile of the 5-inch-chord model having a 0.20-chord flap differed from the modified NACA 65,3-019 airfoil section in that the profile from approximately the 81-percent station to the trailing edge was formed by straight lines having an included angle between 20° and 21°. Forty pressure orifices were installed in the model surface in two chordwise rows $\frac{1}{4}$ inch from and on

either side of the model center line. The model profile and pressure-orifice locations are shown in figure 1. The airfoil ordinates are given in table I.

Pressure-distribution measurements were made for a range of Mach numbers from 0.28 to approximately 0.74 at angles of attack from -2° to 12° and flap deflections from 0° to -12° (up). Additional pressure-distribution measurements were made for positive (down) deflections of the flap at angles of attack of 2° and 4°. These tests were supplemented by schlieren photographs of the flow in the supercritical speed region for a few of the lower angle-of-attack configurations. These photographs show density gradients in the flow by changes in light intensity. (For details, see reference 1.)

SYMBOLS

M	Mach number
M_{cr}	Mach number at which sonic velocity was obtained locally within the flow field (as at the model surface)
q	dynamic pressure
p_o	free-stream static pressure
p	local static pressure (as at model surface)
α	angle of attack
P	pressure coefficient $\left(\frac{p - p_o}{q}\right)$
P_{cr}	critical pressure coefficient, corresponding to local Mach number of 1.0 $\left(\frac{0.528H - p_o}{q}\right)$
H	total pressure
P_U	upper-balance-chamber pressure coefficient
P_L	lower-balance-chamber pressure coefficient
c_n	section normal-force coefficient

[redacted]

$c_{m_{c/4}}$ section pitching-moment coefficient of normal force about quarter-chord location

c_{n_f} flap normal-force coefficient

c_h flap hinge-moment coefficient (determined by the pressure distribution from flap hinge axis to trailing edge)

δ flap deflection measured with reference to the model chord; negative deflection is up

RESULTS AND DISCUSSION

Tunnel-Wall Effects

The results of these tests have not been corrected for constriction or tunnel-wall effects. The most important constriction effect on these data in the supercritical region is the change in the Mach numbers given herein to higher effective stream Mach numbers. (See reference 2.) The difference between the two Mach numbers increases rapidly as the maximum tunnel speed is approached. It is further shown in reference 2 that very near or at the maximum speed attainable for a given model-tunnel configuration large gradients in velocity occurred at the walls. The maximum-speed test points given herein for each angular configuration are therefore considered to be of questionable value.

Pressure Distribution

The pressure distributions along the chord of the model are presented in figures 2 to 31, inclusive. Each figure shows the effect of compressibility on the pressure distribution for a given angular configuration. The effect of angle of attack and flap deflection can be obtained from a comparison of the various figures.

Subcritical region.- The figures for the lower angles of attack and small normal-force coefficients show that increases in Mach number in the subcritical ranges are accompanied by increases in the maximum negative pressure coefficient, which is in agreement with theory. In the high angle-of-attack and large normal-force-coefficient

range the change in the maximum negative pressure coefficient with Mach number is approximately zero and not in agreement with theory, probably as a result of the existence of separated flow.

A comparison of part (a) of figures 2 to 31 for a constant angle of attack and various flap deflections shows that the increment in load produced by a deflection of the flap is distributed approximately uniformly along the chord as could be expected from low-speed tests. It can be seen, however, at this Mach number (approx. 0.43) that the maximum relative change in loading on the main part of the wing occurs near the leading edge. This change has an appreciable effect in increasing or relieving the pressure peaks that occur near the leading edge for some angle-of-attack conditions. (See part (a) of figs. 2 to 5 and 18 to 21.)

Supercritical region.- Although it has been shown that in the subcritical Mach number range the action of the flap in changing the loading along the chord was similar to that shown by the low-speed tests, in the supercritical range, when the region of supersonic flow is relatively large, the loading in and ahead of the supersonic region is a function only of angle of attack. The extent of flow affected by the flap is limited to the region of subsonic flow behind the supersonic region and to the flow over the flap itself. (See parts (d) and (e) of figs. 6 to 9.) The chordwise influence of flap deflection on the flow over the main part of the wing could be expected to be limited to the subsonic flow region ahead of the flap, since pressures are propagated at the speed of sound. This effect of compressibility in producing a marked change in the flow over the forward portion of the airfoil at supercritical Mach numbers is comparable to that which occurs for cambered airfoils, as evidenced by the change in the angle of zero lift. The similarity can be more clearly seen when the cambered airfoil is considered to be a multiple flapped airfoil.

Comparison of the pressure distributions for the flap deflected and neutral shows that, for this model, the chordwise extent of the influence of the flap decreases gradually as the speed is increased above the critical speed.

If the fundamental aspects of the flow are considered, deflections of the flap could produce changes

[redacted]

in the pressures in the subsonic flow region, thereby changing the shock location. This effect, however, is not apparent in these results because of separated flow and the resulting absence of the usual discontinuities in the pressure-distribution diagrams which indicate the shock location.

Schlieren Photographs

Schlieren photographs of the flow in the higher Mach number range are shown in figures 32 to 37, inclusive, for the model at angles of attack of 0° and 4° with various flap deflections. (Note compressions are white on fig. 32, black on figs. 33 to 37.) These photographs show that for angles of attack from 0° to 4° the flow separates at approximately the 0.60-chord location for Mach numbers near the critical values, and with increasing Mach number the separation point moves forward. The forward movement of the separation point is accompanied by a rearward movement of the shock along the separation boundary.

A comparison of the schlieren photographs with the corresponding pressure-distribution diagrams shows that the existence of separated flow has a serious effect on the pressure distribution in the vicinity of compression shocks. (See, for example, figs. 9(d) and 35(d).) It will be noted that for the condition of a well-defined shock and separated flow the pressure-distribution diagram indicates smooth compression. In addition, the location of the pressure corresponding to the critical pressure coefficient generally occurs from 5 to 10 percent of the chord downstream from the shock location. This phenomenon is probably the result of the existence of large static pressure gradients in the separated-flow region between the boundary and the model surface where pressures were measured. The extent of the separated flow would be reduced for an airfoil having a smaller thickness-to-chord ratio.

Critical Mach Number

The variation of the critical Mach number of each surface with flap deflection for constant angles of attack is presented in figure 38. The large decrease in critical Mach number that occurs at angles of attack between 6°

and 8° for the upper surface is a result of a rapid increase in the magnitude of the negative pressure coefficients near the leading edge. The difference between the critical Mach numbers for the upper and lower surfaces for corresponding conditions can be attributed to airflow misalinement. The highest critical Mach number for this airfoil is approximately 0.65 and is obtained for angular configurations corresponding to a normal force of approximately zero.

Compressibility Effects on Force and Moment Coefficients

The normal-force, moment, flap normal-force, and hinge-moment coefficients obtained from integrations of pressure-distribution diagrams are presented in figures 39 and 40. Each figure shows the variation in the coefficient with Mach number at a constant angle of attack for each flap deflection. These figures are cross-plotted in figure 41 to show the variation in the coefficients at a constant Mach number.

Normal-force coefficients.-Figure 39 shows that, with the flap at 0°, the effect of compressibility on the normal-force coefficient at subcritical Mach numbers is in accord with previous experimental and theoretical results. The variation for the other flap deflections at a fixed angle of attack, however, appears to follow, to some extent, both in direction and magnitude the variation for the condition of the flap at 0°, as indicated by a lesser divergence of the curves than would have been expected from theoretical estimations. (See parts (c), (d), and (e), fig. 39.) A variation of this type shows that the effect of compressibility on $\frac{dc_n}{d\delta}$ is small in the subcritical Mach number range.

In the supercritical Mach number range above the value at which the peak normal-force coefficient occurs, the convergence of the curves for the various flap deflections at a given angle of attack indicates a rapidly decreasing $\frac{dc_n}{d\delta}$ with increasing Mach number. The effect of compressibility on $\frac{dc_n}{d\delta}$, presented in figure 42, is in accord with the variations indicated in figure 39.

[redacted]

In the supercritical Mach range for angles of attack not greater than 6° it can be seen in figure 39 that the peak normal-force coefficient for a given angular configuration occurred at a Mach number of approximately 0.65, which indicates that this airfoil section should be restricted to designs wherein the maximum Mach number does not exceed 0.65.

A comparison of the various parts of figure 41 in which is given the variation of the normal-force coefficient with angle of attack shows that as the Mach number increases $\frac{dc_n}{d\alpha}$ increases and reaches a maximum value at a Mach number of 0.65 as could have been expected from the preceding discussion.

A further examination of figure 41 shows that deflections of the flap produce a change in the angle of zero normal force, but have no appreciable effect on $\frac{dc_n}{d\alpha}$ for the more linear parts of the curves. The effect of compressibility on $\frac{dc_n}{d\alpha}$ for the more linear parts of these curves is presented in figure 42.

The flap effectiveness $\frac{d\alpha}{d\delta}$, obtained from the ratio of $\frac{dc_n}{d\delta}$ to $\frac{dc_n}{d\alpha}$ (fig. 42) and presented in figure 43, decreased with increased Mach number and rapidly approached zero as the Mach number was increased above the critical value.

Moment coefficients.- The variation of the moment coefficient with Mach number in the subcritical range as shown in figure 39 is small. In the supercritical region the moment coefficients generally increase with increasing Mach number. This increase is followed by a rapid decrease, which occurs at a Mach number above the value at which the decrease in normal-force coefficient occurs. The pressure-distribution diagrams show that the decrease in normal-force results from a general decrease in the magnitude of the loading, and at higher Mach numbers the continued decrease in loading is accompanied by a change in distribution which results in a decreased moment coefficient.

[redacted]

At the supercritical Mach numbers at which the normal forces for the various flap deflections tend to be approximately the same, the direction of the change in the moment coefficients is similar to the direction of the change in c_n. A variation of similar magnitude, however, could not be expected in these coefficients because of the large effect that a small change in load at the rear of the model has on the moment coefficient.

A comparison of the effects of angle of attack and flap deflections on the variation in moment coefficient with normal-force coefficient can be seen in figure 41.

For constant flap deflection there is a small positive increase in moment coefficient with an increase in normal-force coefficient. This slope remains approximately constant for Mach numbers to approximately 0.65. For Mach numbers above 0.65, the variation depends on the flap deflection.

At a constant angle of attack between -2° and 6°, large changes in moment coefficient occur in a negative direction with an increase in the normal-force coefficient. These slopes, which are approximately constant to a Mach number of 0.6, increase as the Mach number is further increased to 0.7.

Flap normal force.- The flap normal-force coefficients are presented in figure 40. In the supercritical region, the variations in the coefficients are large and irregular, probably being influenced by the effect of flow separation.

Hinge-moment coefficients.- The variation in the hinge-moment coefficients with Mach number, also shown in figure 40, are very similar to the variation in flap normal force.

At Mach numbers from 0.01 to 0.02 below the maximum test value, a flap deflection range is indicated in which the flap tends to become or is overbalanced. At the same Mach number and for the same angular configuration, in figure 39, no change occurs in the value of normal-force coefficient, and the control would therefore be unresisting and ineffective. Although the Mach number is near the maximum test value, for which the data are of questionable value, the possibility of this condition of the control should not be overlooked.

[redacted]

The hinge-moment coefficients are presented in figure 41 in the same manner as the moment coefficients. It can be seen that for a constant flap deflection the magnitude and direction of change of hinge-moment coefficient with increase in normal-force coefficient depends on the absolute value of the flap deflection. The slope for a given flap deflection increases positively with increases in Mach number to 0.675; further increases in Mach number are accompanied by increases in the slope in the negative direction.

At a Mach number of 0.40 the changes in hinge moment with flap deflection at a constant angle of attack are generally uniform over the flap deflection range. At a Mach number of 0.60 and above in the negative normal-force-coefficient range the changes in hinge-moment coefficient for flap deflections between 0° and -4° is very small compared with the changes at larger deflections. This effect is possibly a result of the reversals in the load over the flap produced by the very thick boundary layer or separated flow. (See pressure-distribution diagrams and schlieren photographs.)

Balance-chamber pressure-coefficient differential ($P_L - P_U$).- The difference between the pressure coefficients for the lower-surface and the upper-surface balance chambers is presented in figure 44. This figure shows the effect of Mach number, flap deflection, and angle of attack on the pressure-coefficient differential.

The effect of compressibility on the pressure-coefficient differential is generally small at Mach numbers below 0.65. This small effect could be expected when the magnitudes of the individual pressure coefficients are small and are measured at a station in rear of the position of the maximum negative pressure coefficient. The decrease in the magnitude of the pressure coefficient at the high Mach numbers is primarily a result of the effects of flow separation.

The balanced hinge-moment coefficient for this model can be obtained by adding the hinge-moment coefficient of figure 40 to the product of the balance-chamber pressure-coefficient differential ($P_L - P_U$) and a constant, the constant depending on the length of the balance tab. A brief comparison of figures 40 and 44 indicates that at

[redacted]

low speeds the effect of the balance would be to reduce $\frac{dc_h}{d\delta}$ as compared with the unbalanced condition. With increasing Mach number the effect of the balance decreases for the lower angle-of-attack range.

CONCLUDING REMARK

The results of the investigation on the modified NACA 65,3-019 airfoil having a 0.20-chord flap indicate that the effectiveness of a trailing-edge control surface of small chord rapidly decreases and approaches zero as the Mach number increases above the critical value.

Langley Memorial Aeronautical Laboratory
National Advisory Committee for Aeronautics
Langley Field, Va.

REFERENCES

1. Stack, John, Lindsey, W. F., and Littell, Robert E.: The Compressibility Burble and the Effect of Compressibility on Pressures and Forces Acting on an Airfoil. NACA Rep. No. 646, 1938.

2. Byrne, Robert W.: Experimental Constriction Effects in High-Speed Wind-Tunnels. NACA ACR No. L4L07a, 1944.

[redacted]

TABLE I.- BASIC SECTION ORDINATES FOR MODIFIED NACA 65,3-019 AIRFOIL SECTION

[Stations and ordinates are in percent chord]

Station	Ordinate	
	Upper surface	Lower surface
0	0	0
.3	1.108	-1.108
1	1.921	-1.921
2	2.598	-2.598
4	3.620	-3.620
6	4.437	-4.437
8	5.127	-5.127
10	5.723	-5.723
14	6.715	-6.715
18	7.525	-7.525
22	8.192	-8.192
26	8.721	-8.721
30	9.113	-9.113
34	9.371	-9.371
38	9.490	-9.490
39.5	9.500	-9.500
42	9.471	-9.471
46	9.315	-9.315
50	9.024	-9.024
54	8.597	-8.597
58	8.039	-8.039
62	7.370	-7.370
66	6.612	-6.612
70	5.791	-5.791
74	4.922	-4.922
78	4.029	-4.029
82	8.128	-8.128
86	2.247	-2.247
90	1.416	-1.416
94	.688	-.688
98	.138	-.138
100	0	0
L.E. radius: 2.139		

[redacted]

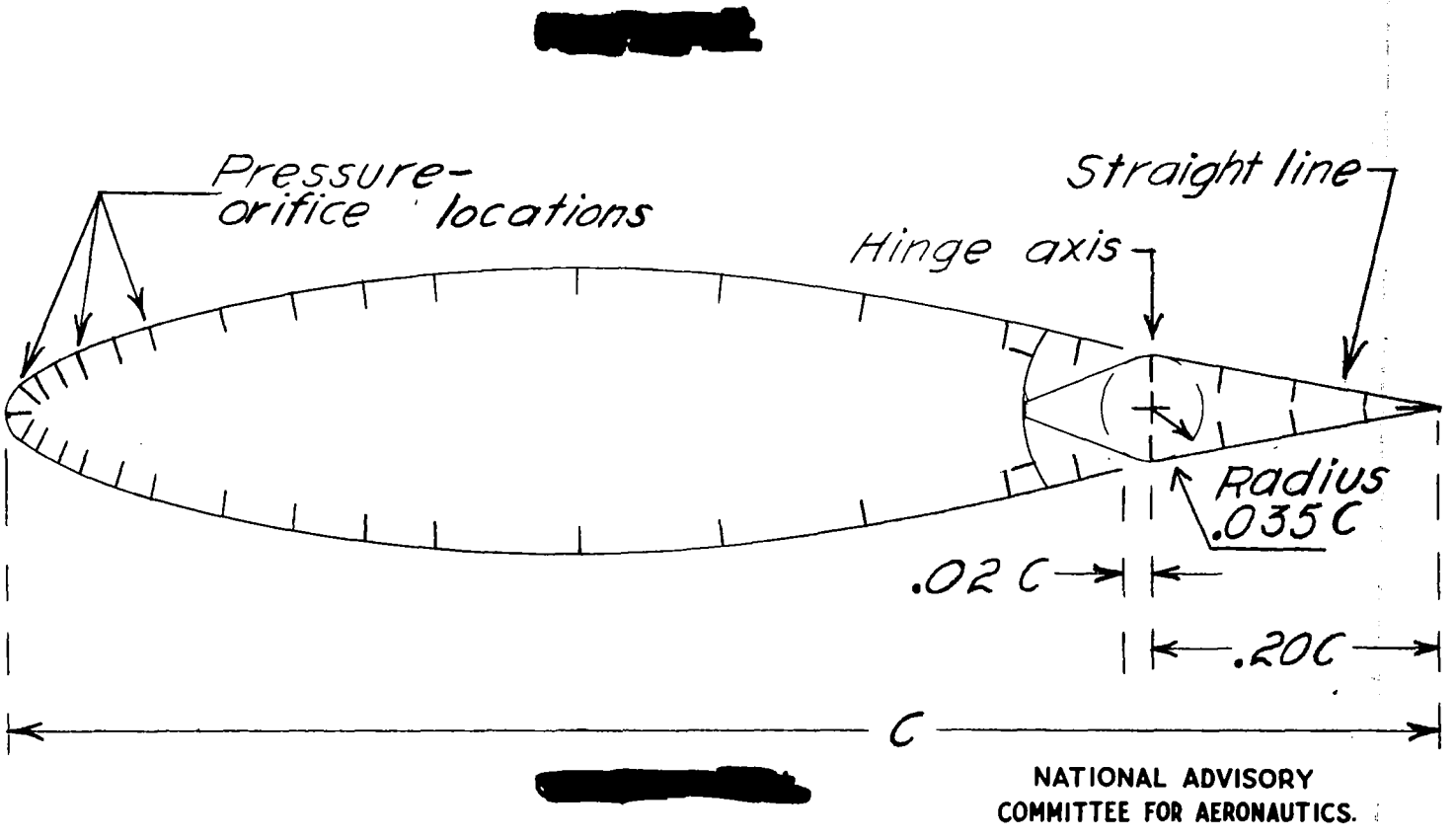

Figure 1.- Model profile.

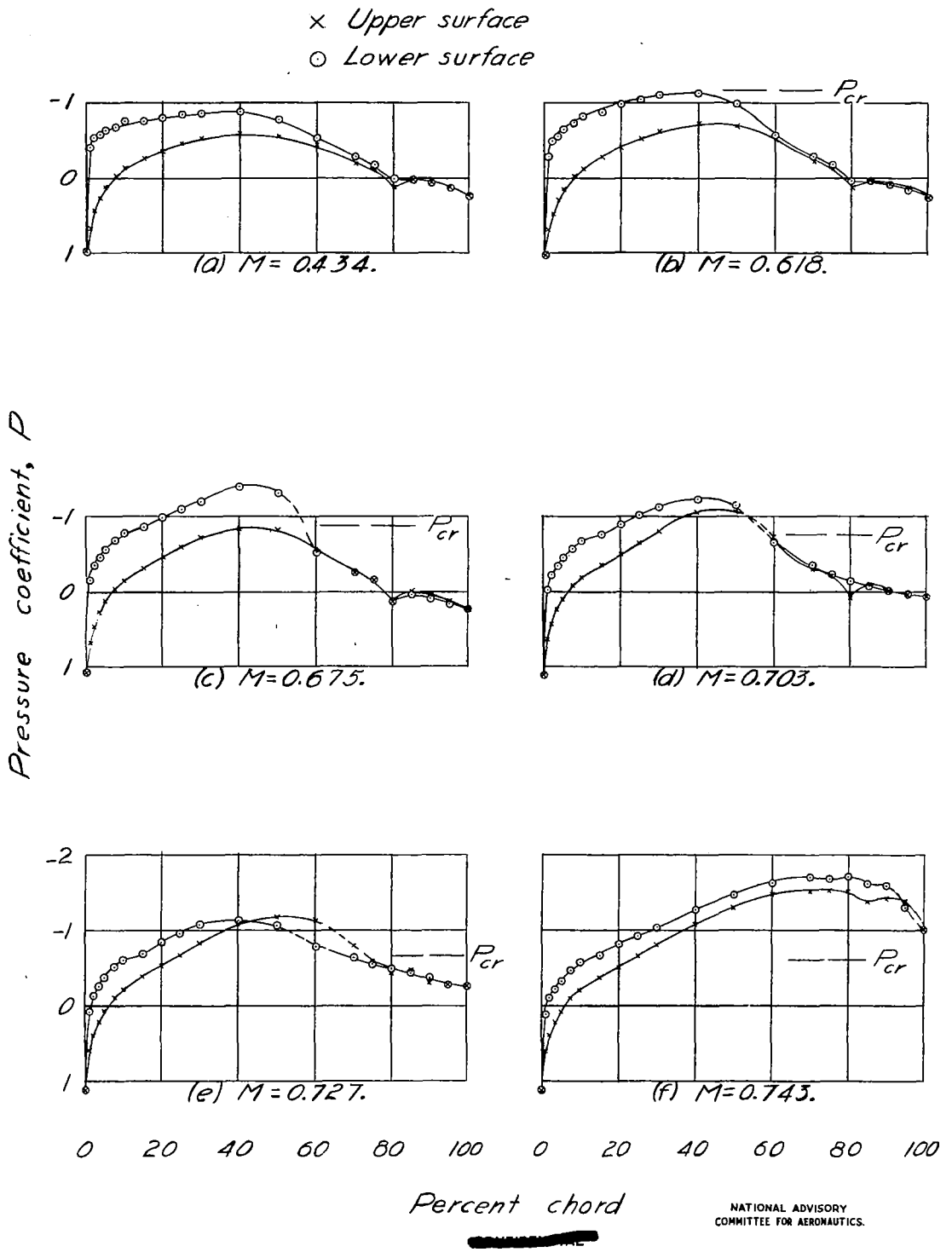

Figure 2.- Pressure distribution for a modified NACA 65,3-019 airfoil with 0.20-chord flap. $\alpha = -2^{\circ}$; $\delta = 0^{\circ}$.

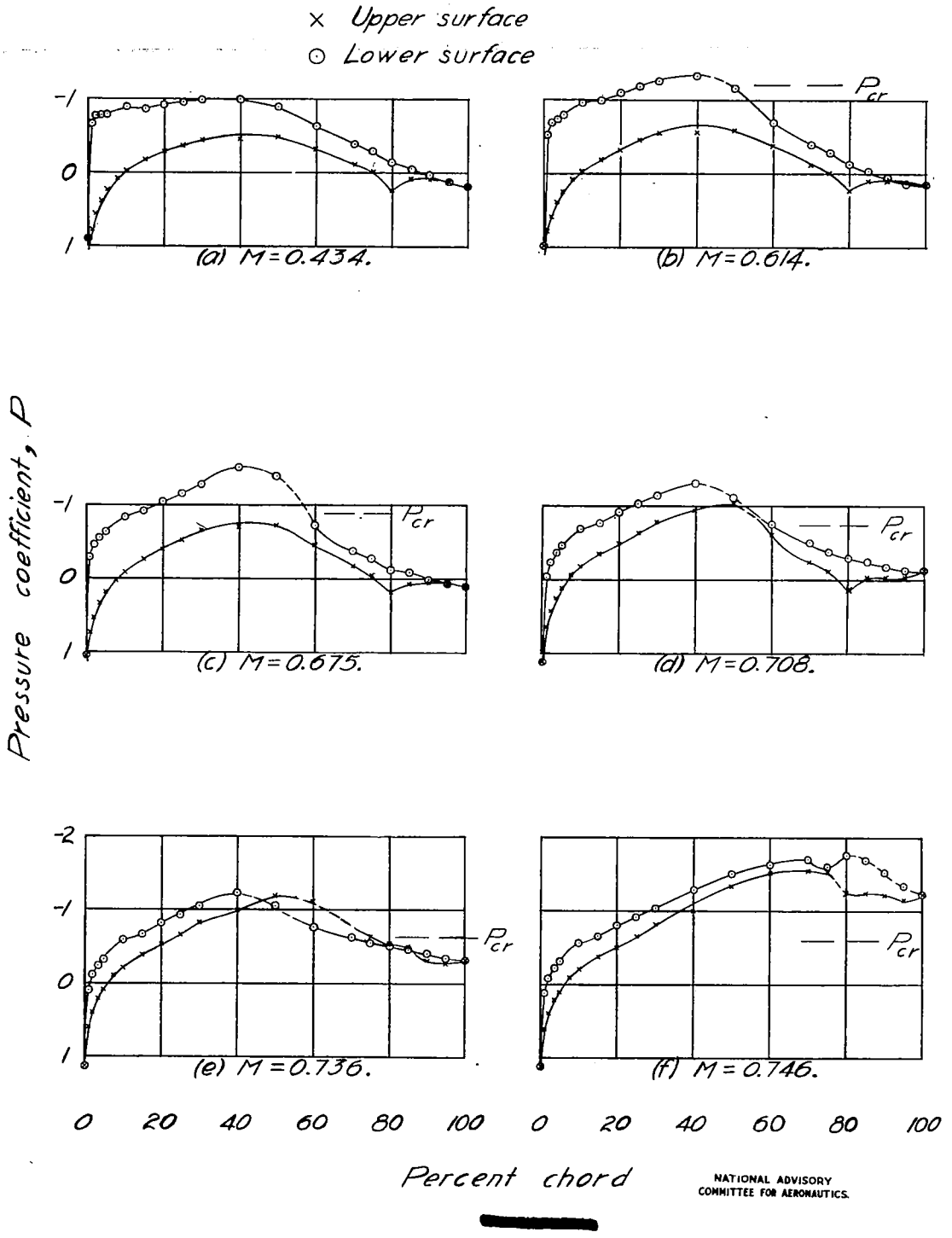

Figure 3.- Pressure distribution for a modified NACA 65,3-019 airfoil with 0.20-chord flap. $\alpha = -2^{\circ}$; $\delta = -4^{\circ}$.

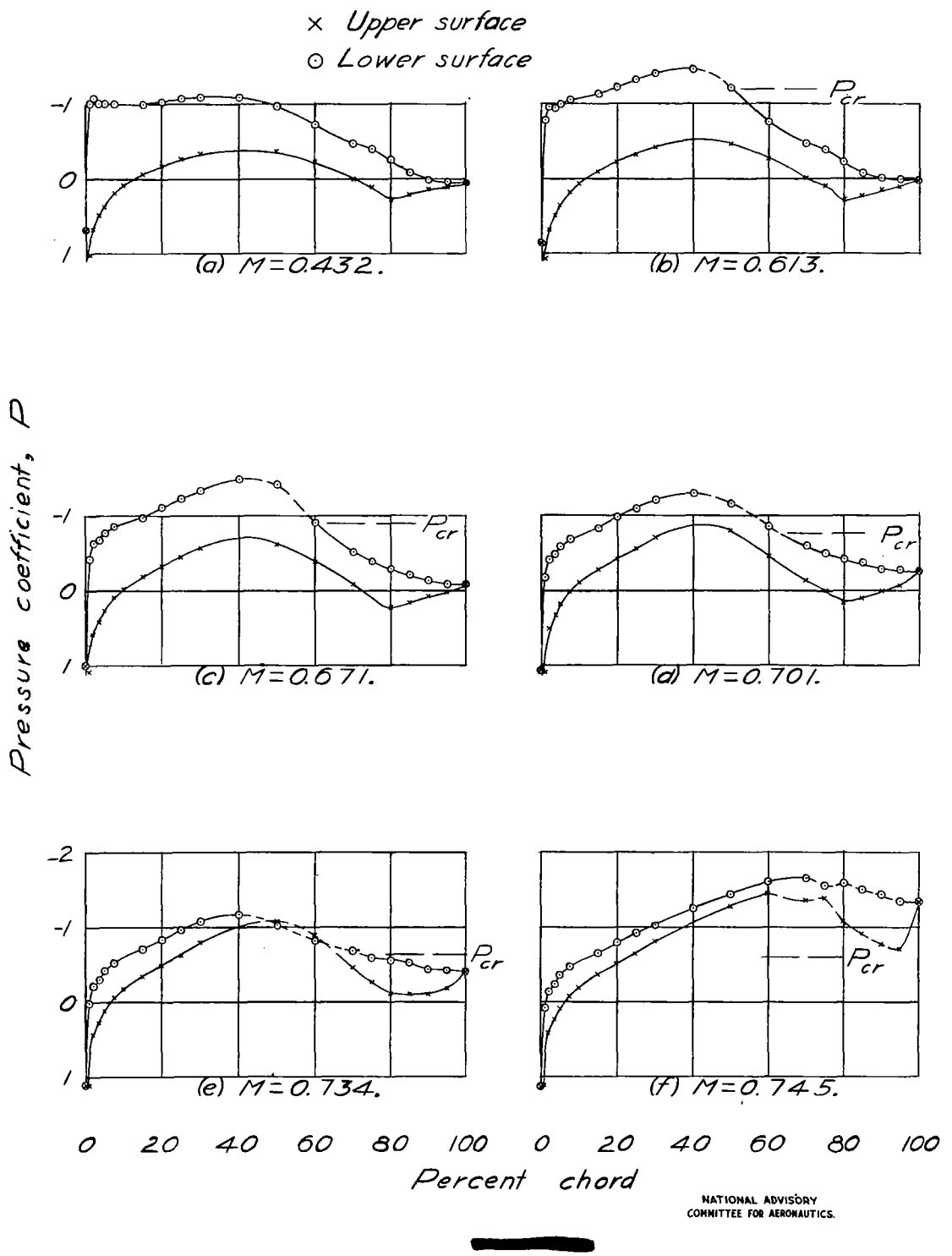

Figure 4.- Pressure distribution for a modified NACA 65,3-019 airfoil with 0.20-chord flap. $\alpha = -2^{\circ}$; $\delta = -8^{\circ}$.

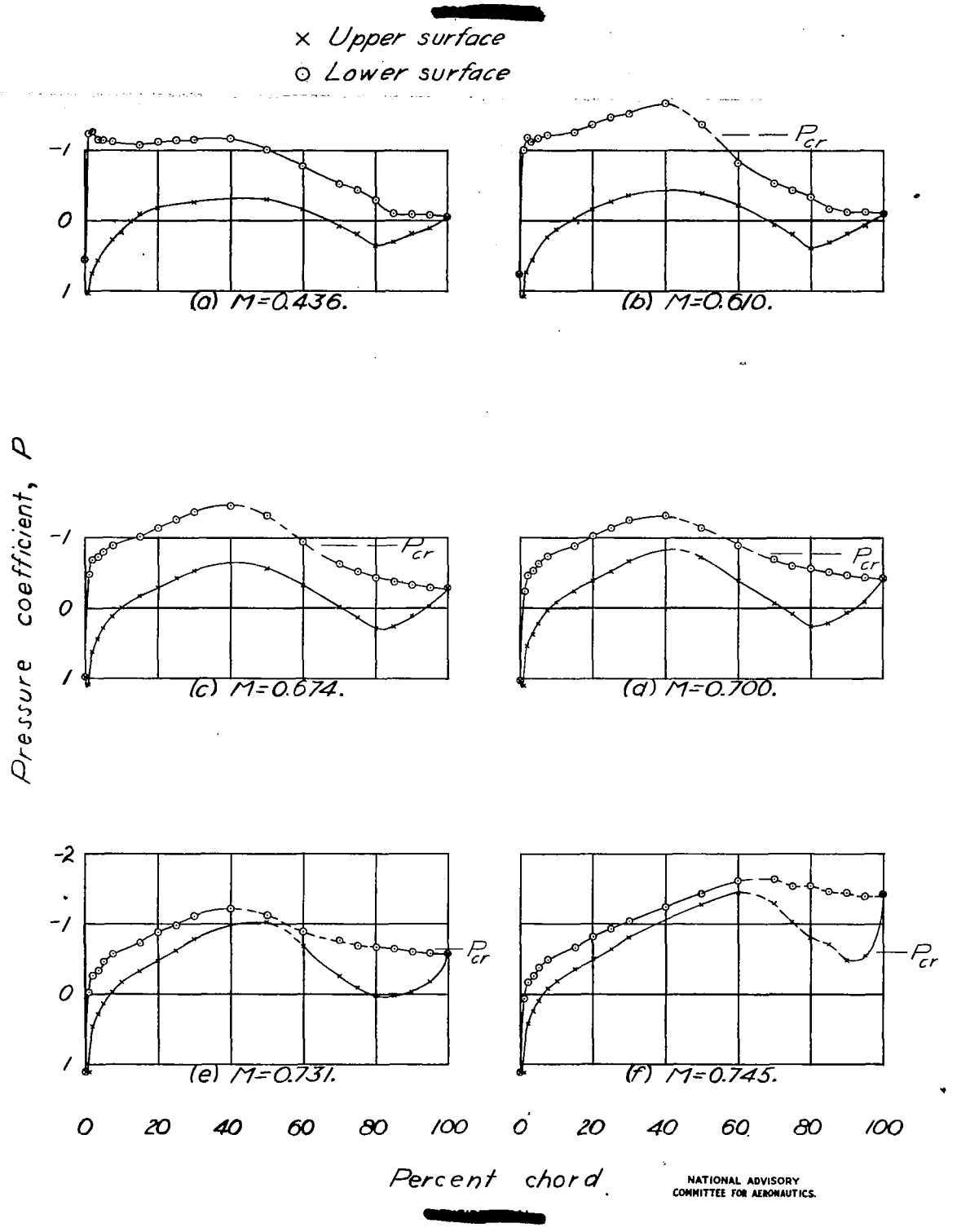

Figure 5.- Pressure distribution for a modified NACA 65,3-019 airfoil with 0.20-chord flap. $\alpha = -2^{\circ}$; $\delta = -12^{\circ}$.

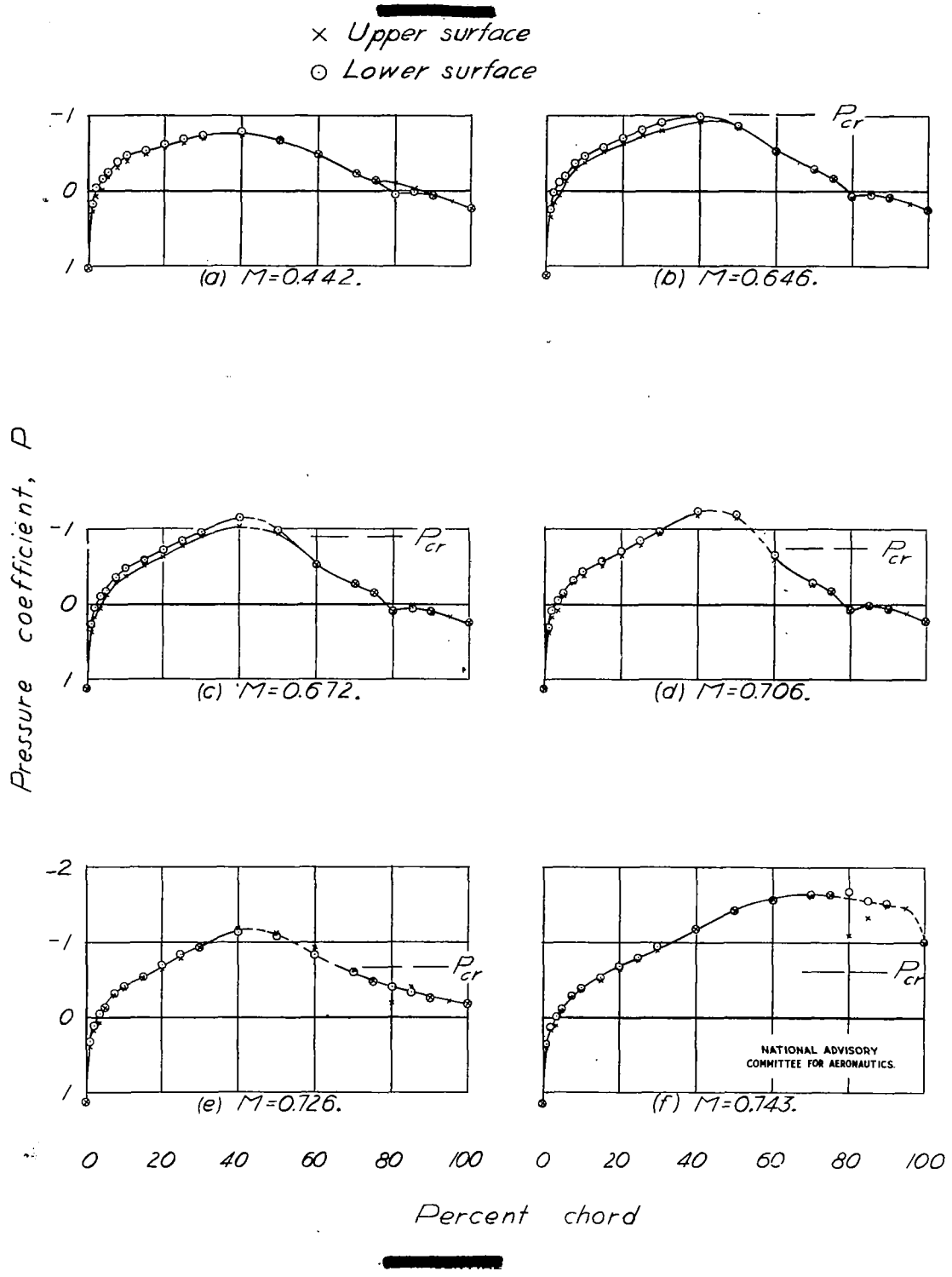

Figure 6.- Pressure distribution for a modified NACA 65,3-019 airfoil with 0.20-chord flap. $\alpha = 0^{\circ}$; $\delta = 0^{\circ}$.

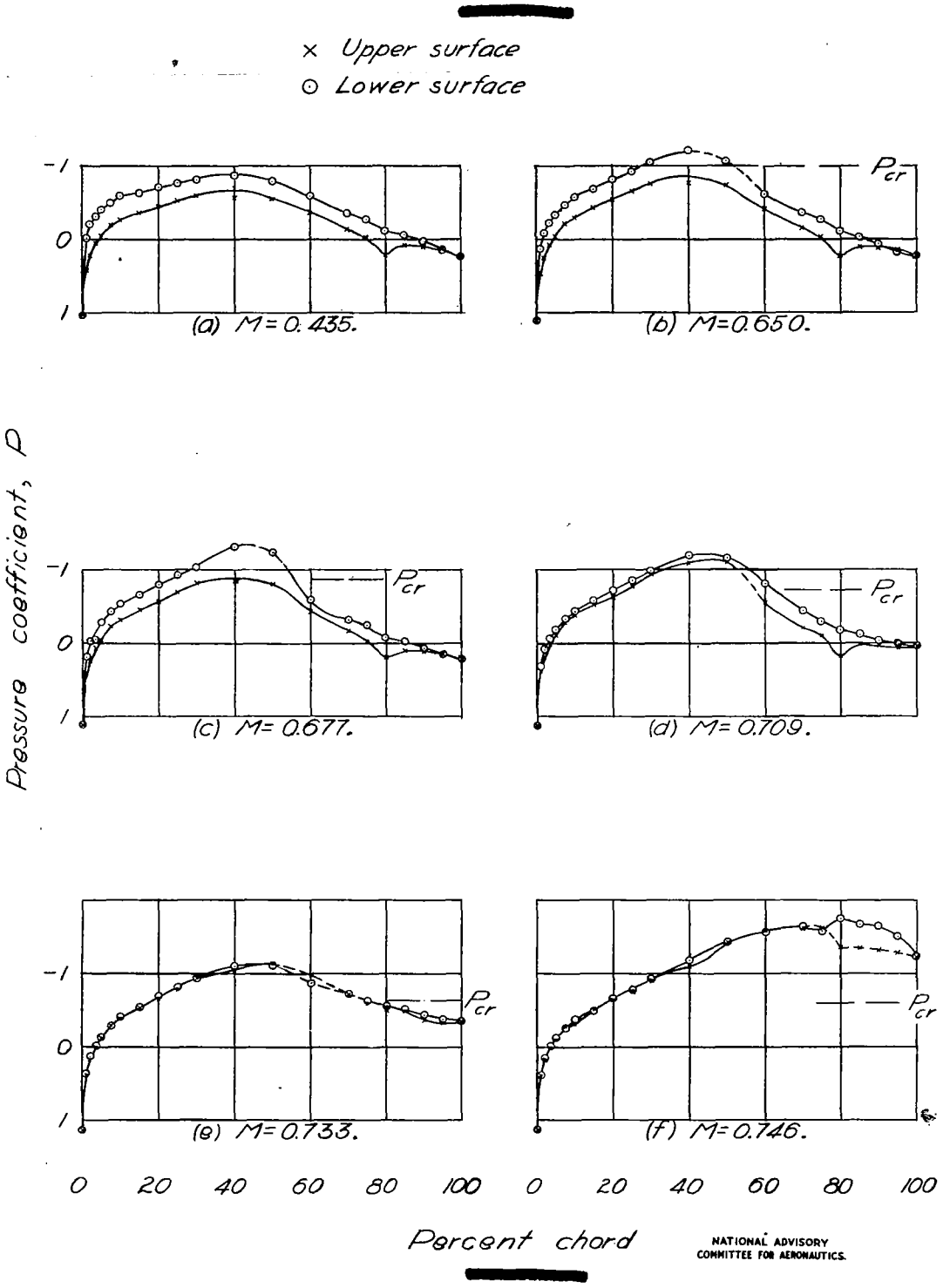

Figure 7.- Pressure distribution for a modified NACA 65,3-019 airfoil with 0.20-chord flap. $\alpha = 0^{\circ}$; $\delta = -4^{\circ}$.

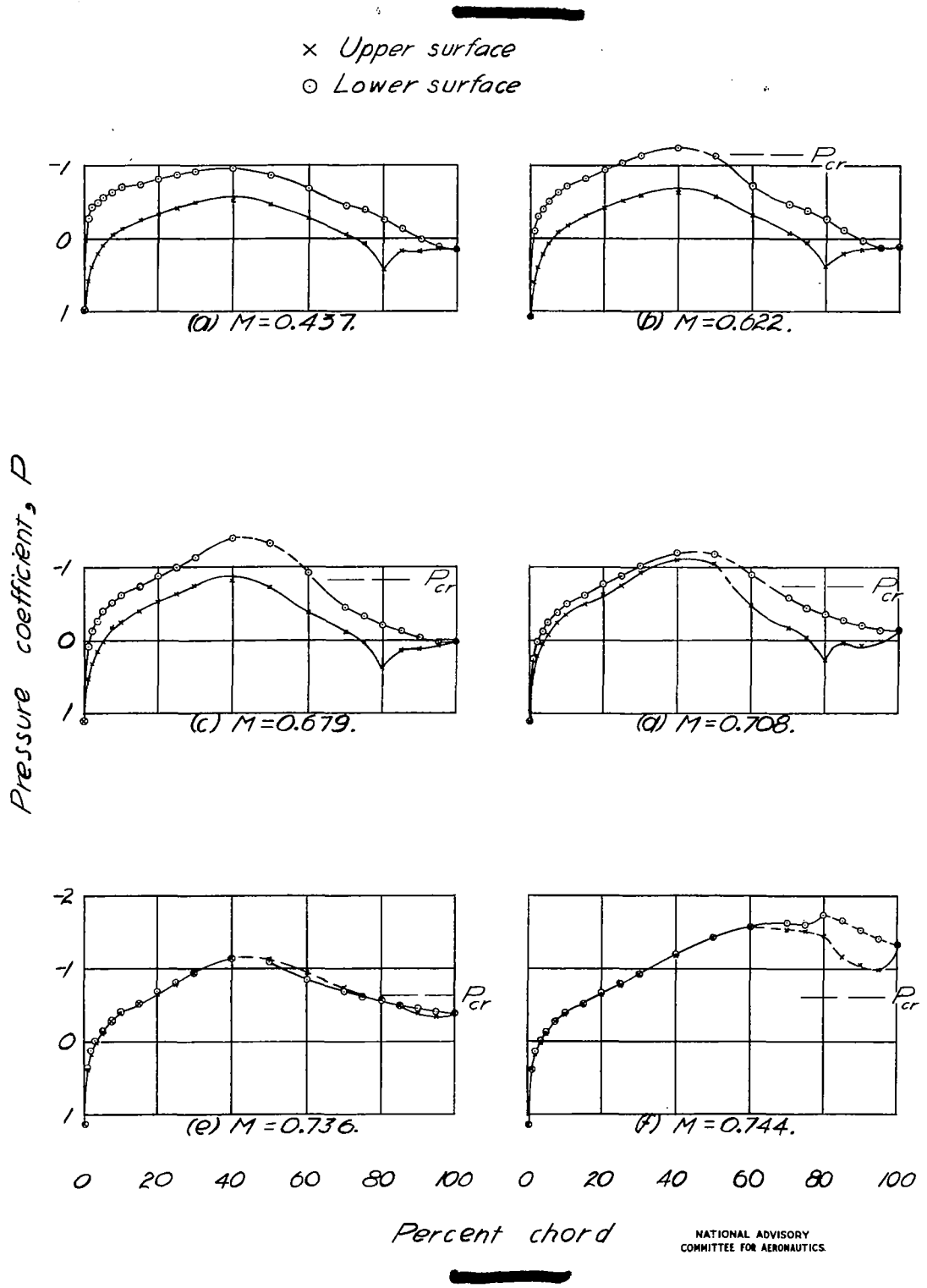

Figure 8.- Pressure distribution for a modified NACA 65,3-019 airfoil with 0.20-chord flap. $\alpha = 0^{\circ}$; $\delta = -8^{\circ}$.

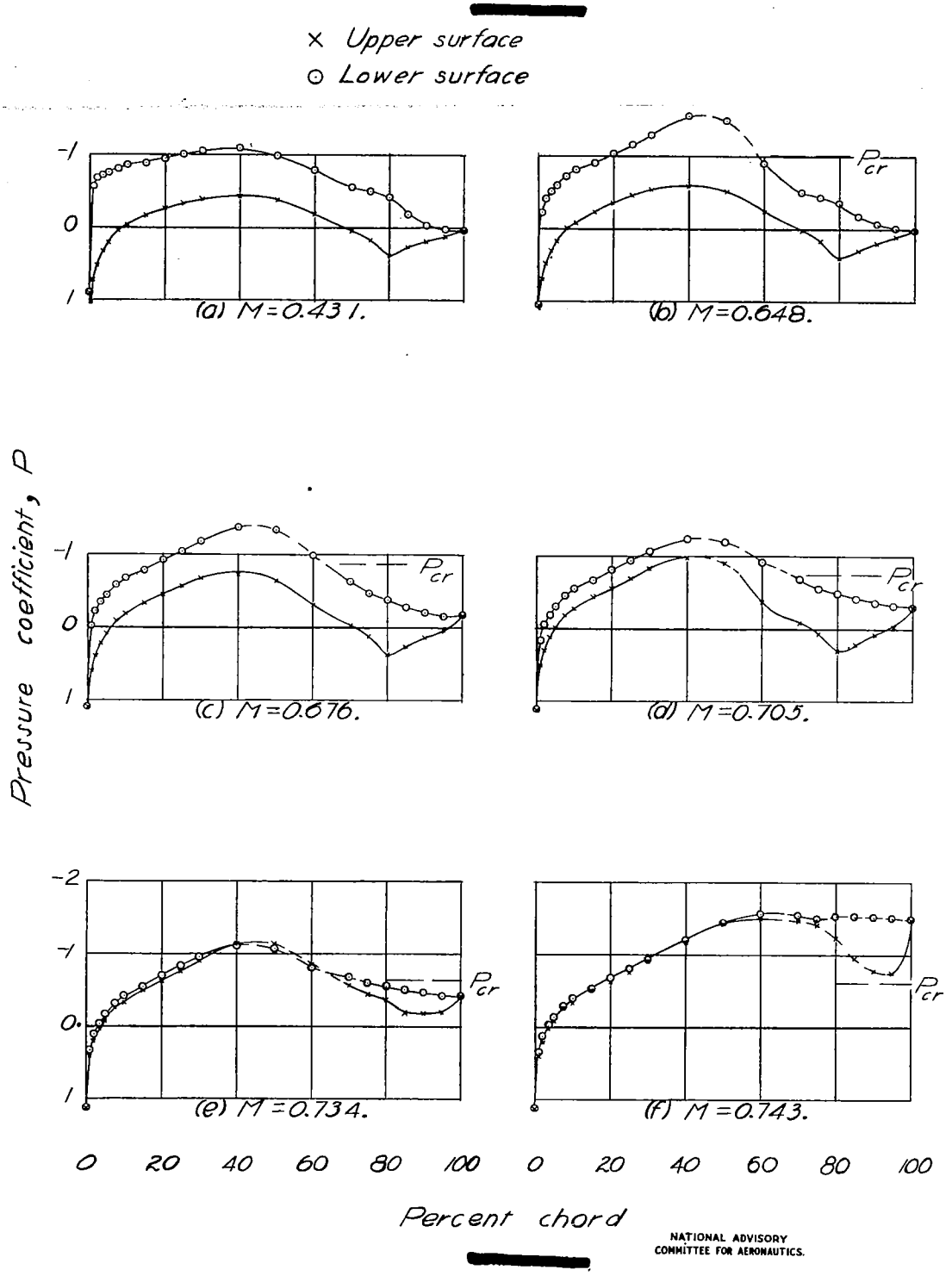

Figure 9.- Pressure distribution for a modified NACA 65,3-019 airfoil with 0.20-chord flap. $\alpha = 0^{\circ}$; $\delta = -12^{\circ}$.

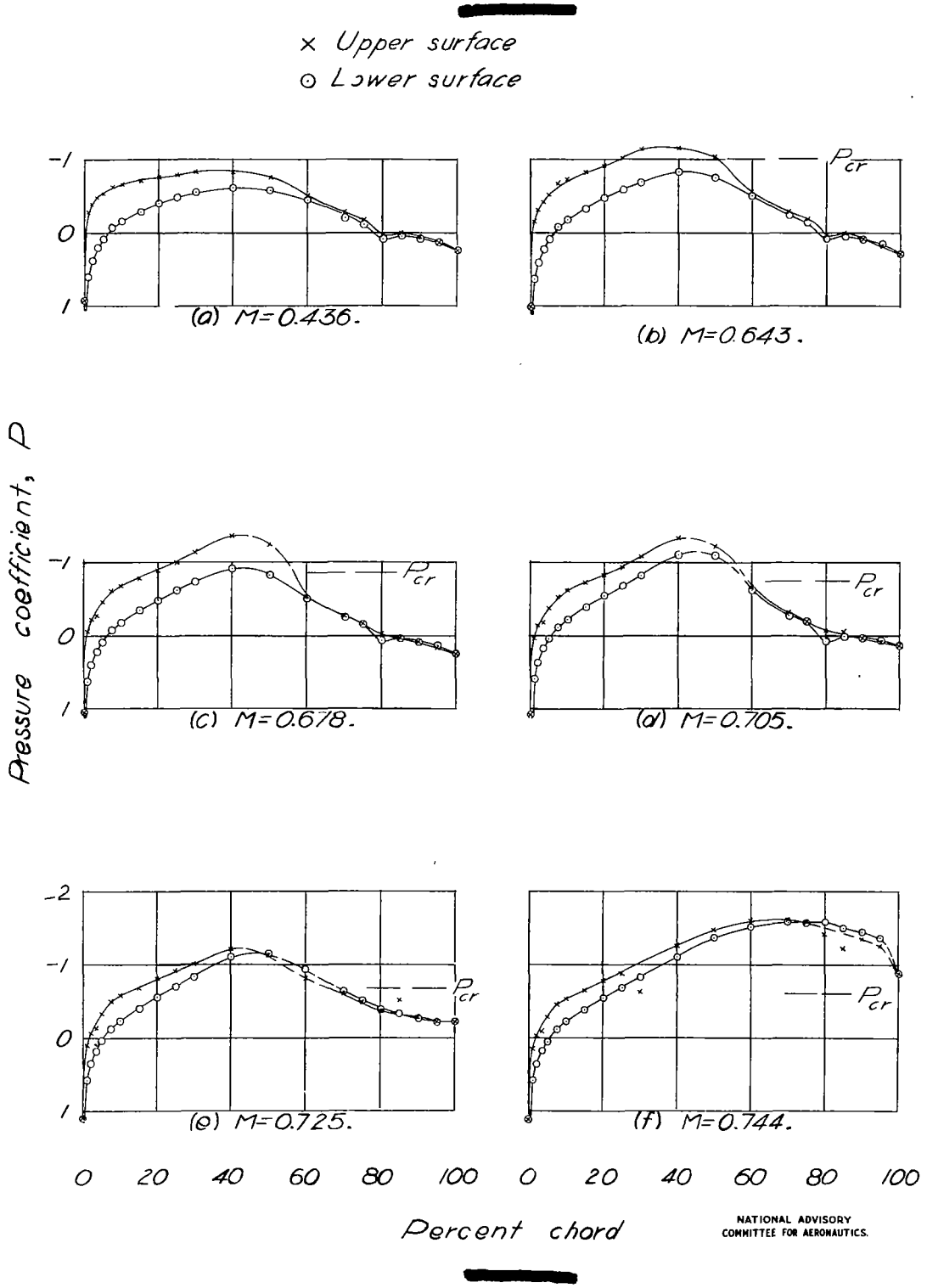

Figure 10.- Pressure distribution for a modified NACA 65,3-019 airfoil with 0.20-chord flap. $\alpha = 2^{\circ}$; $\delta = 0^{\circ}$.

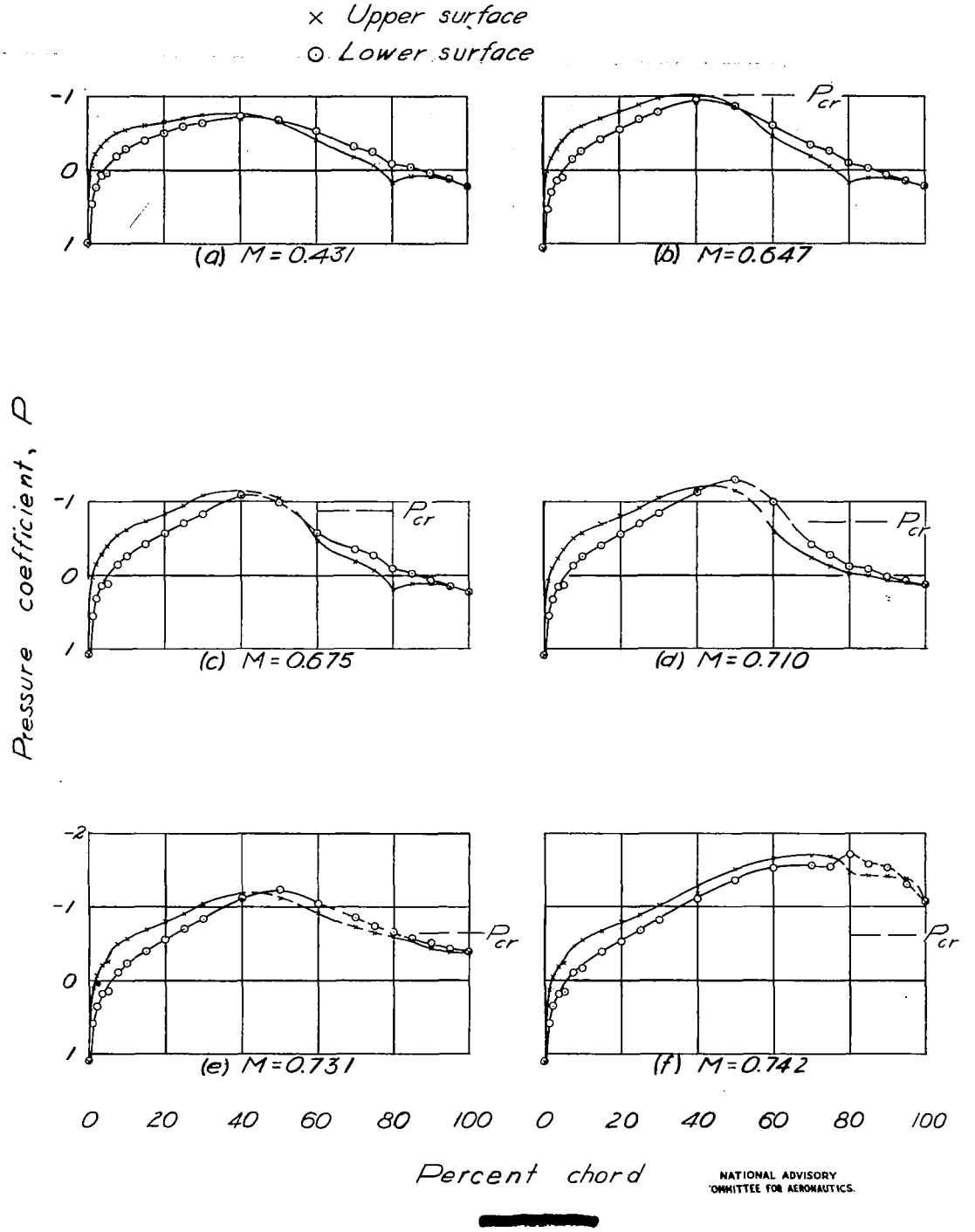

Figure 11.- Pressure distribution for a modified NACA 65,3-019 airfoil with 0.20-chord flap. $\alpha = 2^{\circ}$; $\delta = -4^{\circ}$.

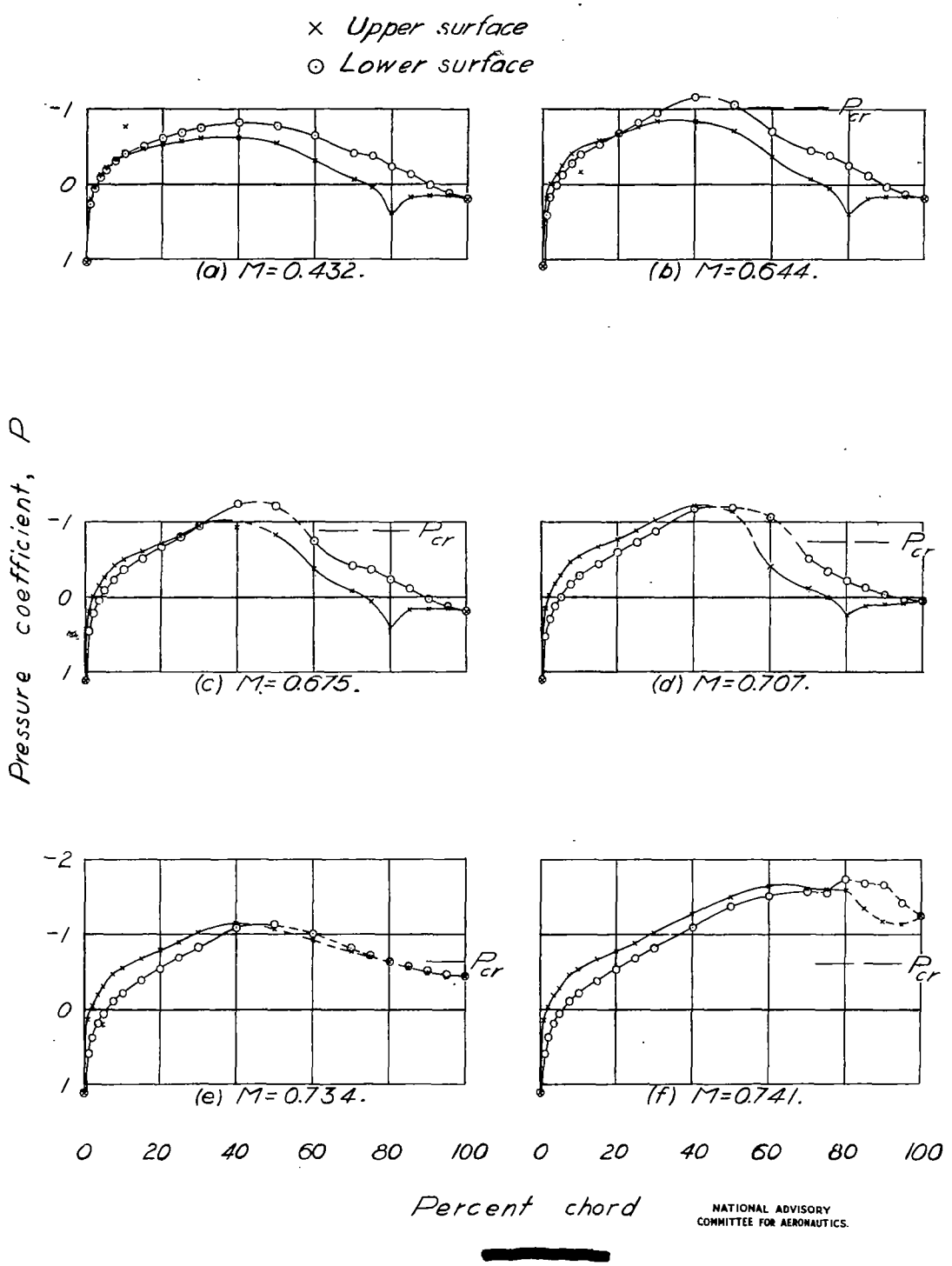

Figure 12.- Pressure distribution for a modified NACA 65,3-019 airfoil with 0.20-chord flap. $\alpha = 2^{\circ}$; $\delta = -8^{\circ}$.

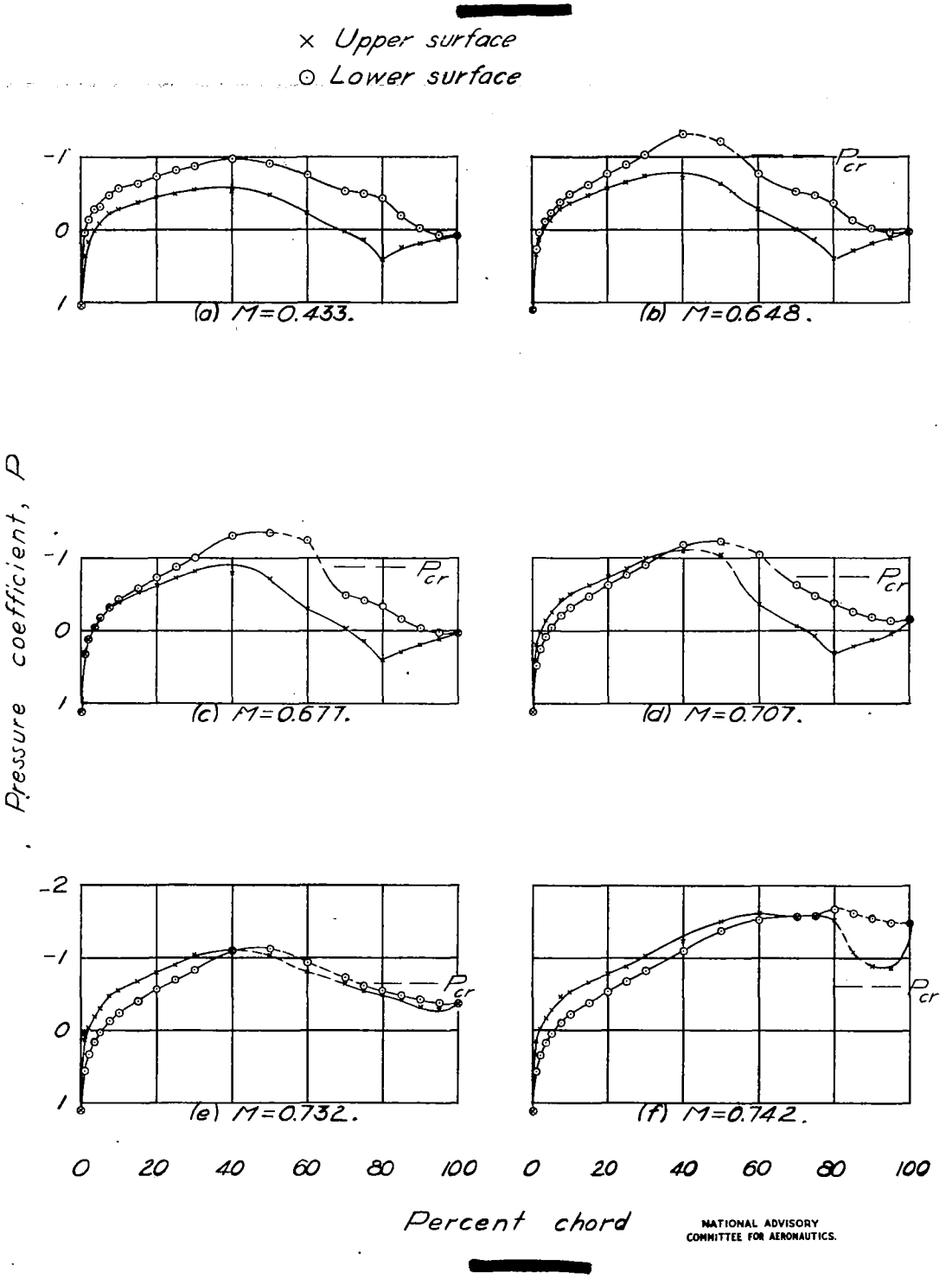

Figure 13.- Pressure distribution for a modified NACA 65,3-019 airfoil with 0.20-chord flap. $\alpha = 2^{\circ}$; $\delta = -12^{\circ}$.

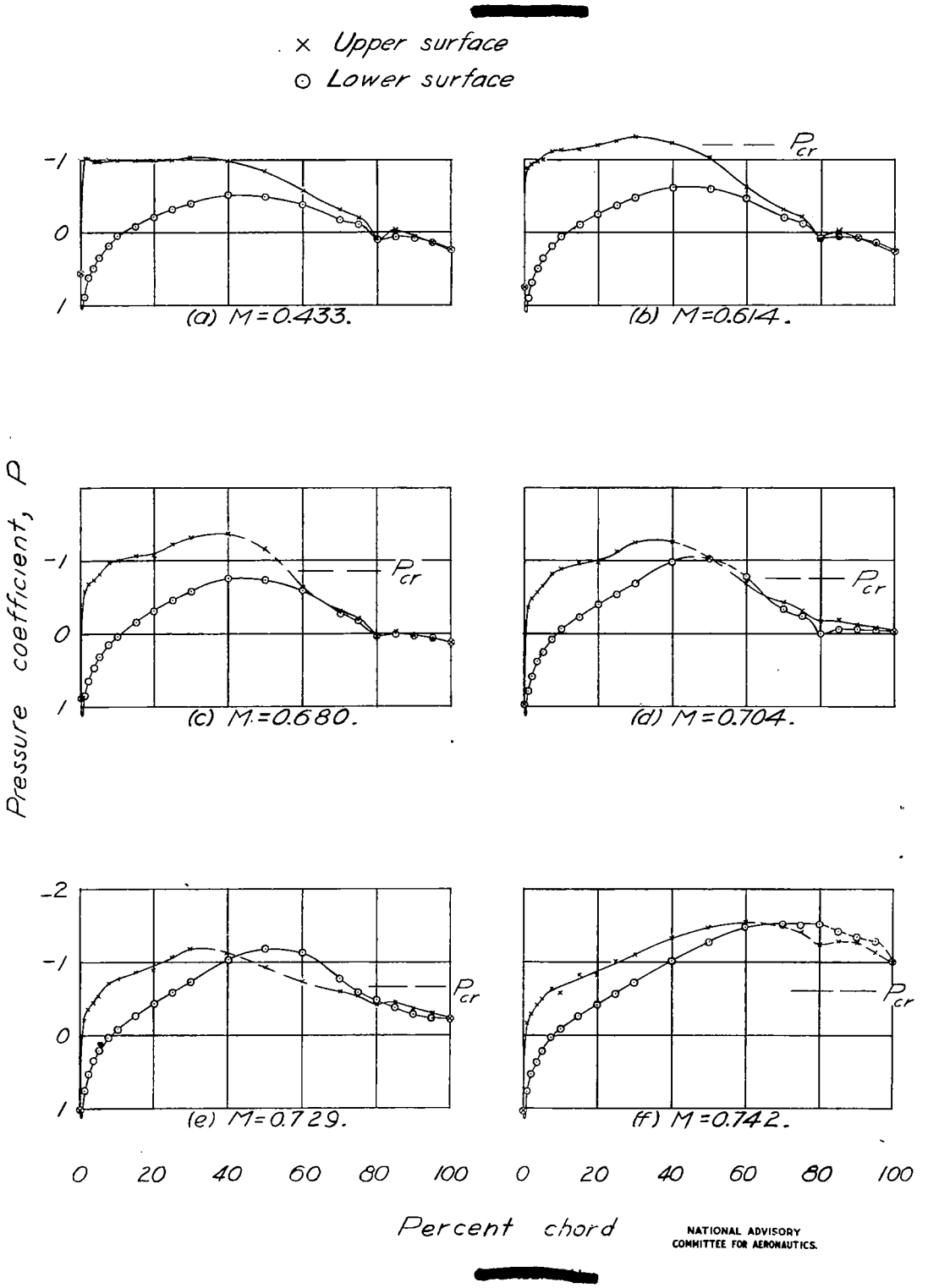

Figure 14.- Pressure distribution for a modified NACA 65,3-019 airfoil with 0.20-chord flap. $\alpha = 4^{\circ}$; $\delta = 0^{\circ}$.

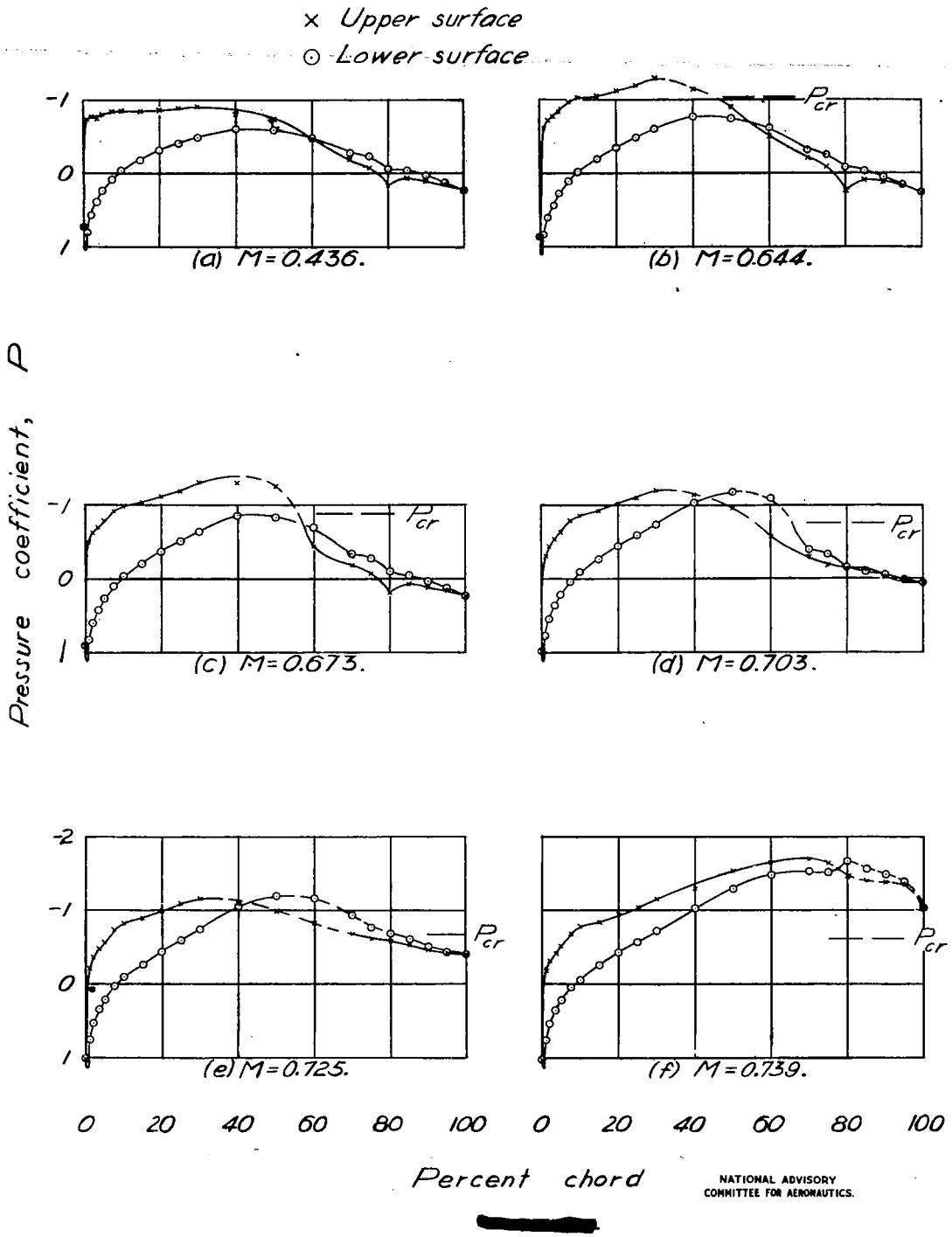

Figure 15.- Pressure distribution for a modified NACA 65,3-019 airfoil with 0.20-chord flap. $\alpha = 4^{\circ}$; $\delta = -4^{\circ}$.

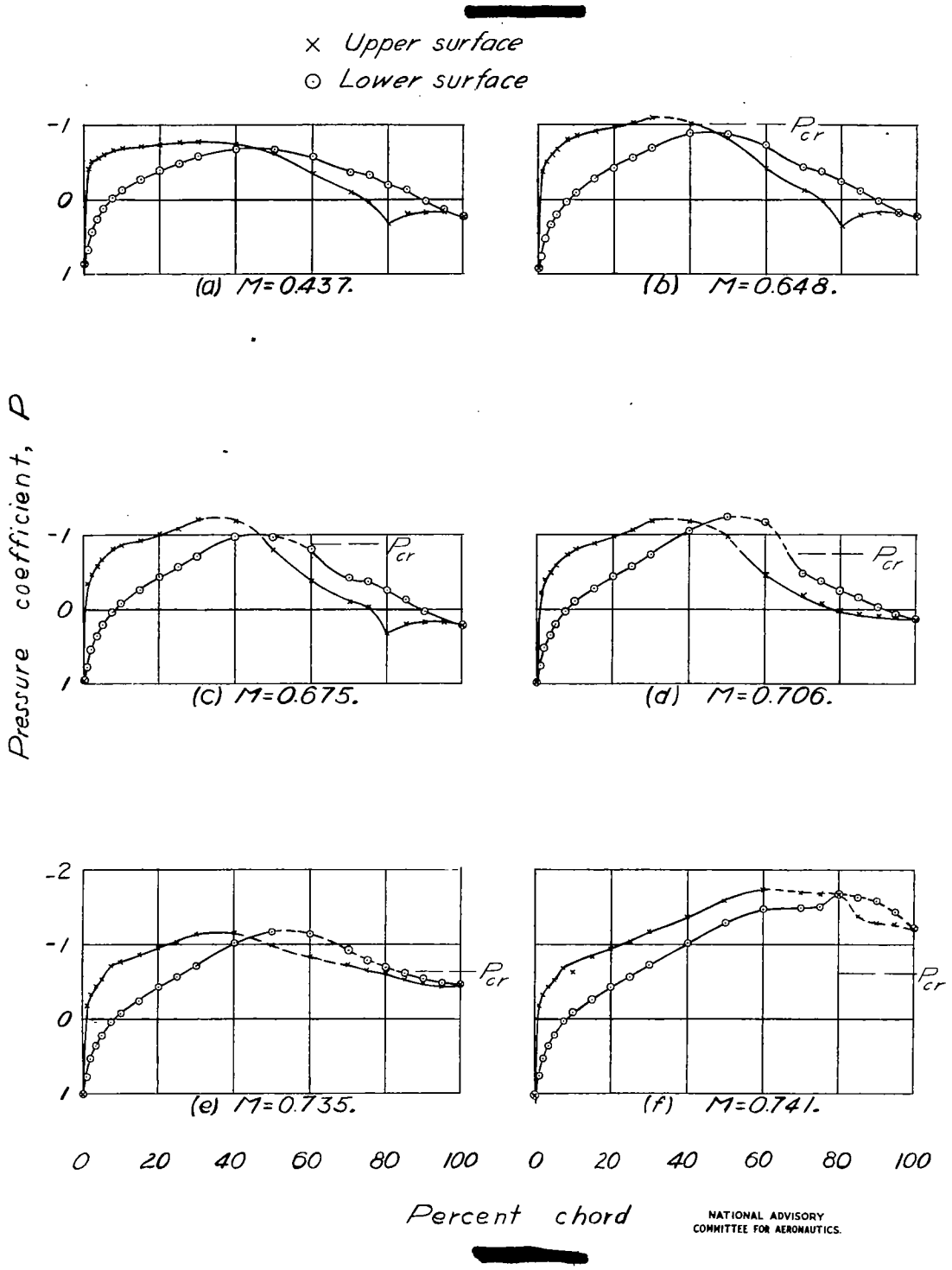

Figure 16. - Pressure distribution for a modified NACA 65,3-019 airfoil with 0.20-chord flap. $\alpha = 4^{\circ}$; $\delta = -8^{\circ}$.

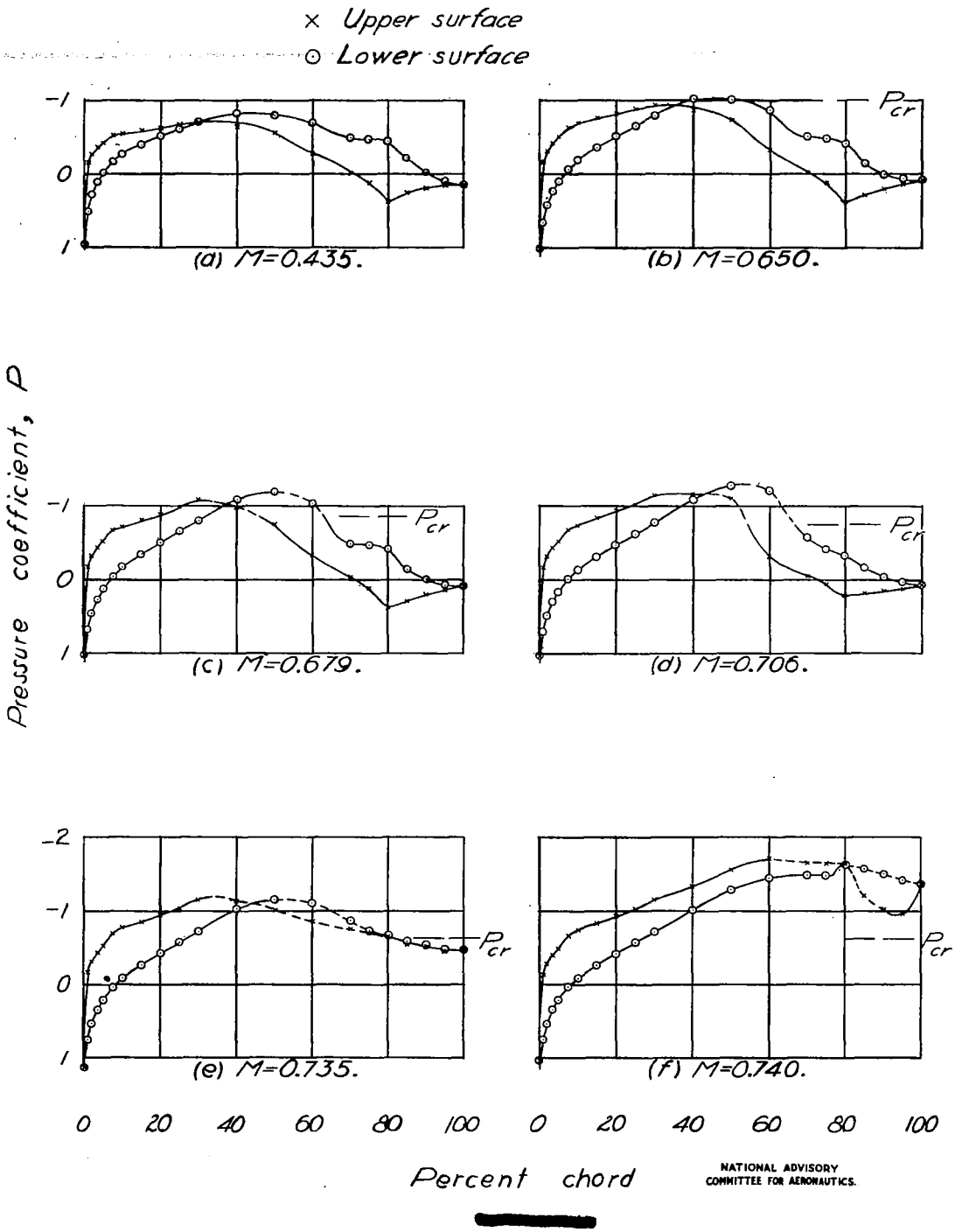

Figure 17.- Pressure distribution for a modified NACA 65,3-019 airfoil with 0.20-chord flap. $\alpha = 4^{\circ}$; $\delta = -12^{\circ}$.

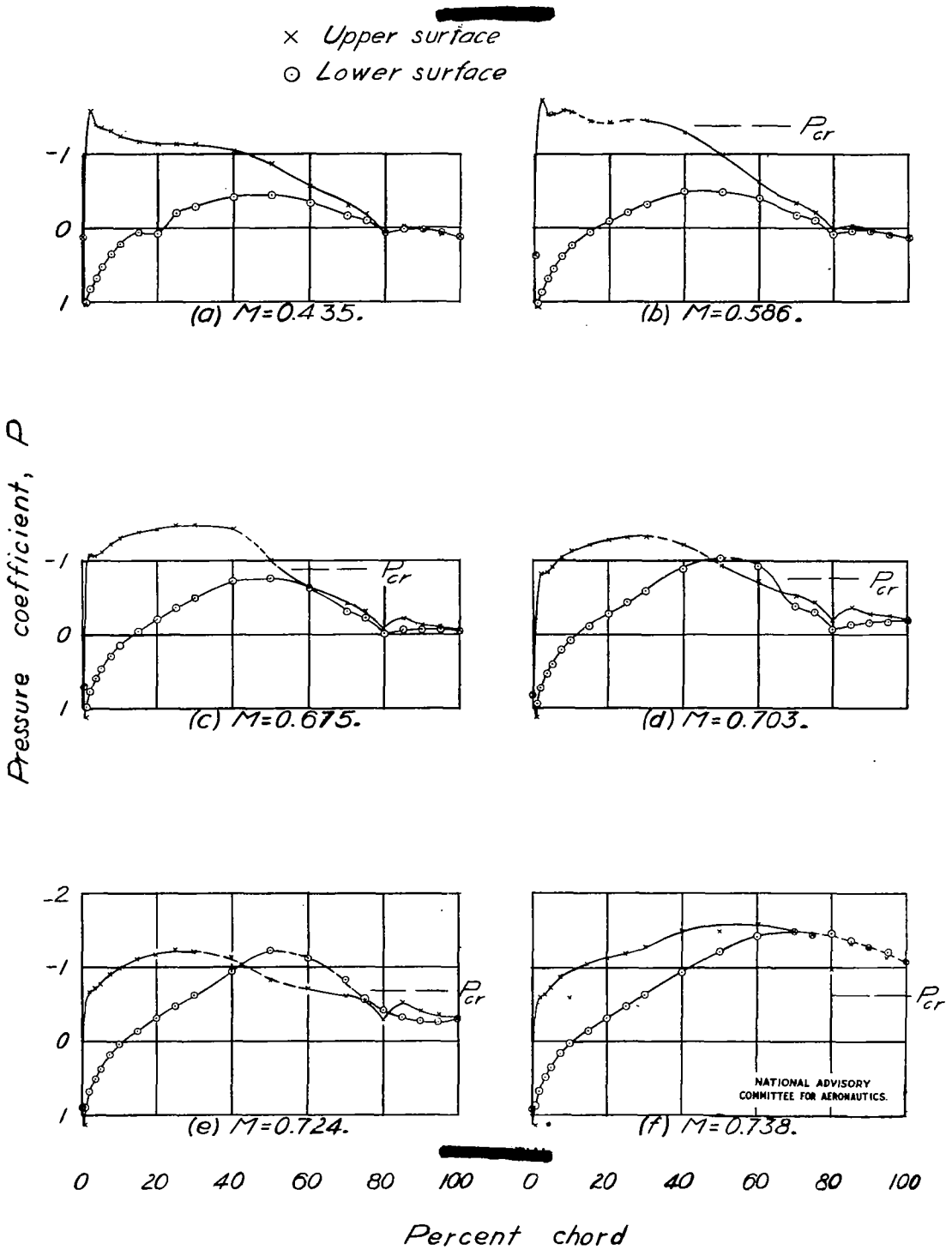

Figure 18.- Pressure distribution for a modified NACA 65,3-019 airfoil with 0.20-chord flap. $\alpha = 6^{\circ}$; $\delta = 0^{\circ}$.

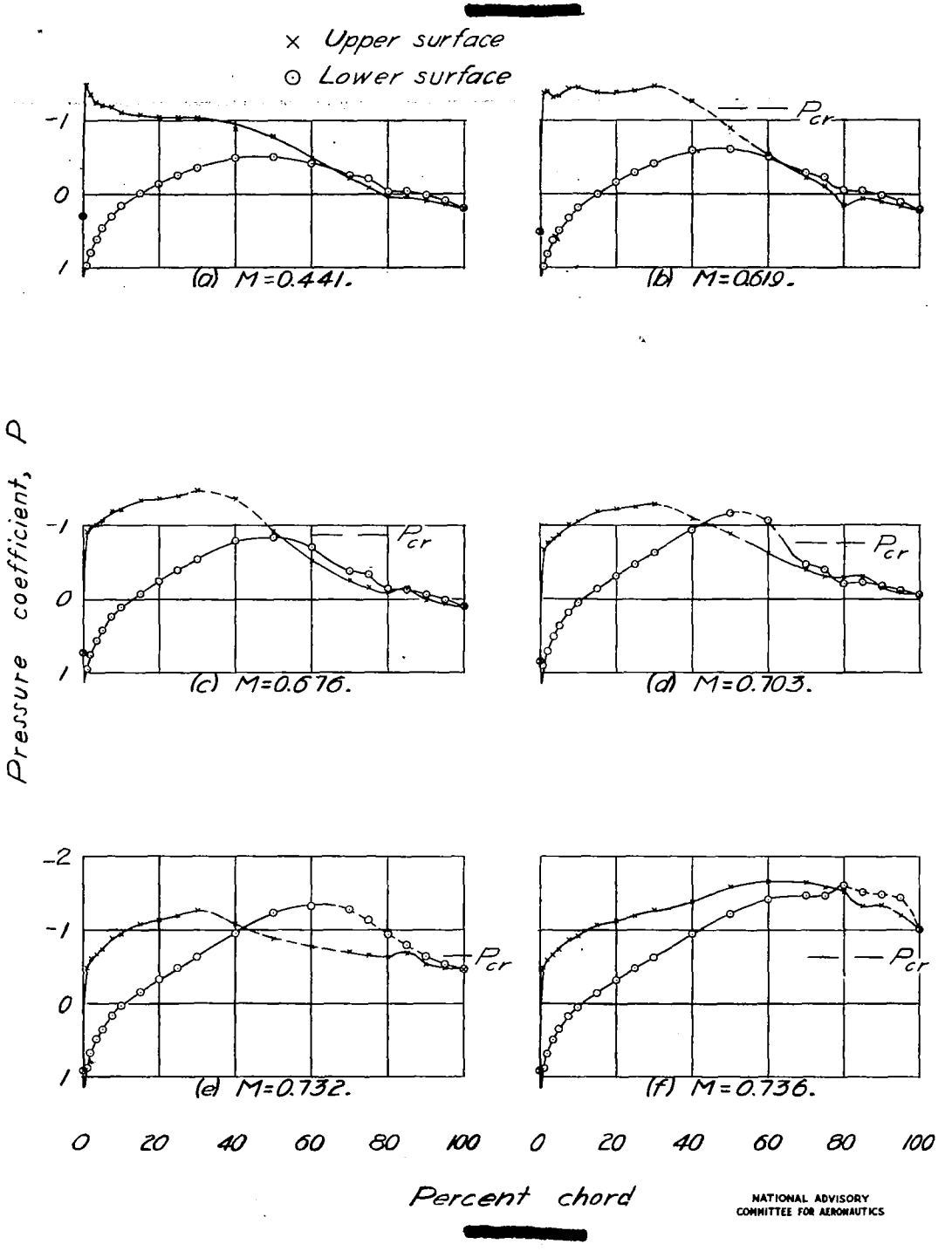

Figure 19.- Pressure distribution for a modified NACA 65,3-019 airfoil with 0.20-chord flap. $\alpha = 6^{\circ}$; $\delta = -4^{\circ}$.

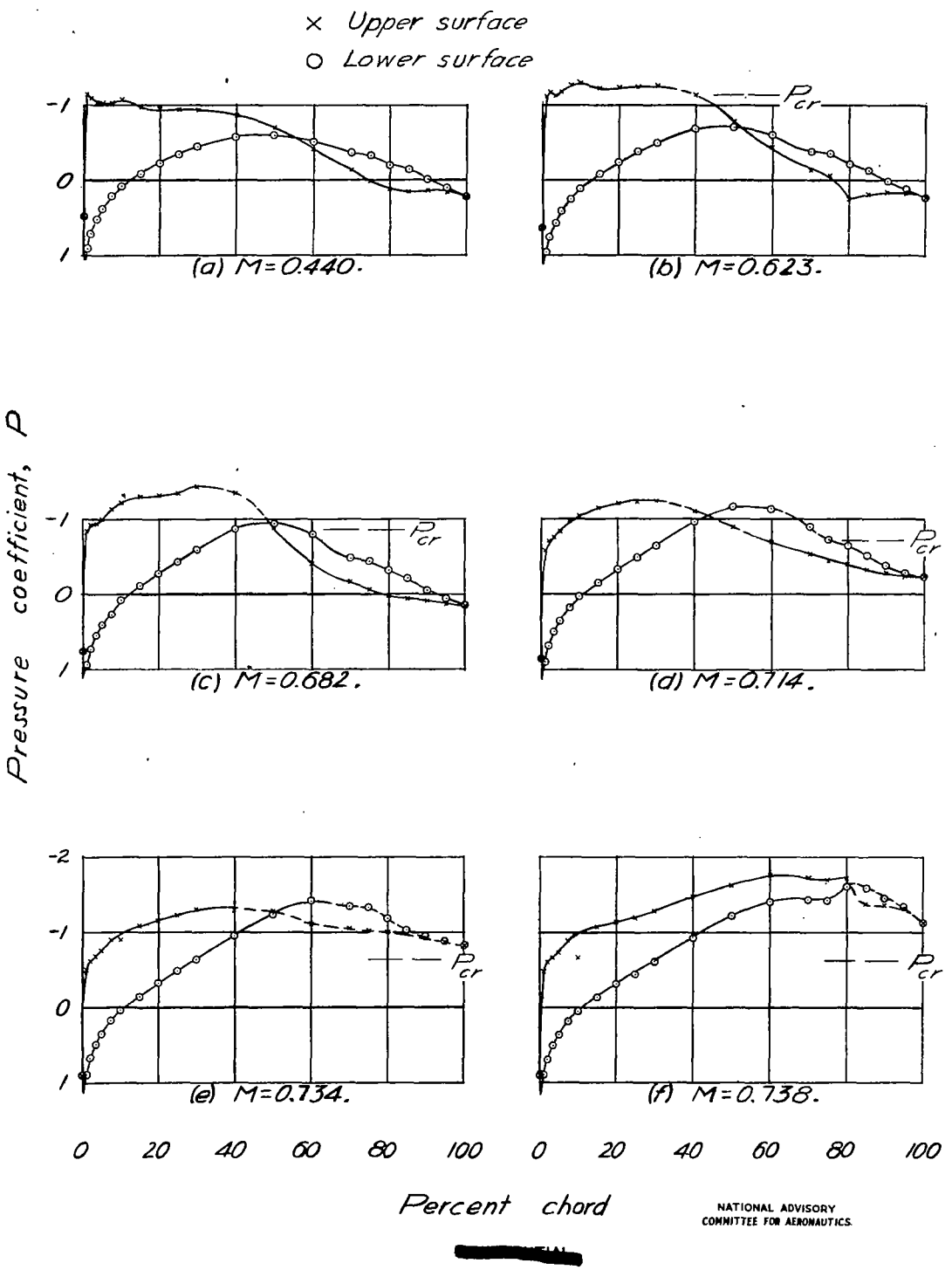

Figure 20.- Pressure distribution for a modified NACA 65,3-019 airfoil with 0.20-chord flap. $\alpha = 6^{\circ}$; $\delta = -8^{\circ}$.

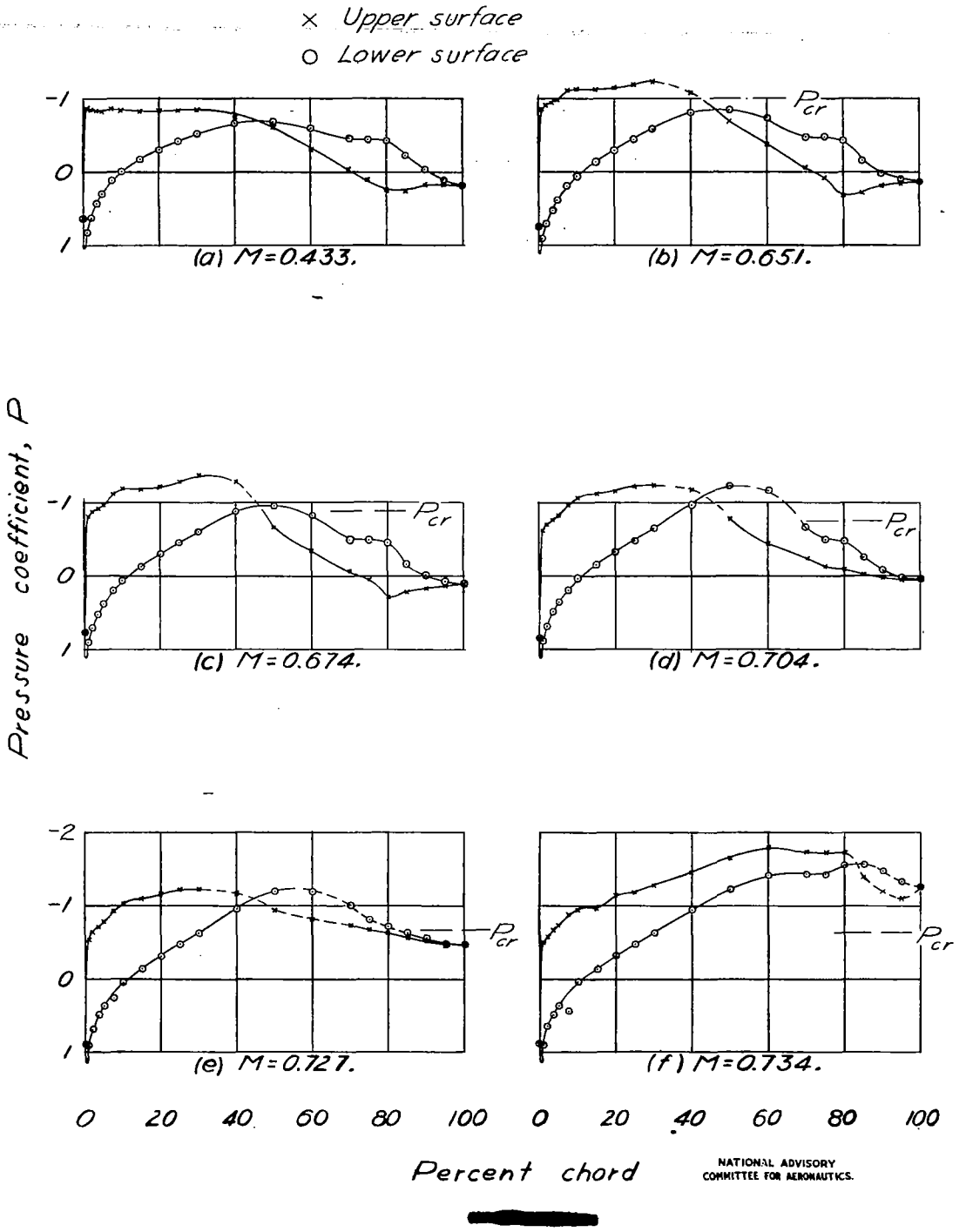

Figure 21.- Pressure distribution for a modified NACA 65,3-019 airfoil with 0.20-chord flap. $\alpha = 6^{\circ}$; $\delta = -12^{\circ}$.

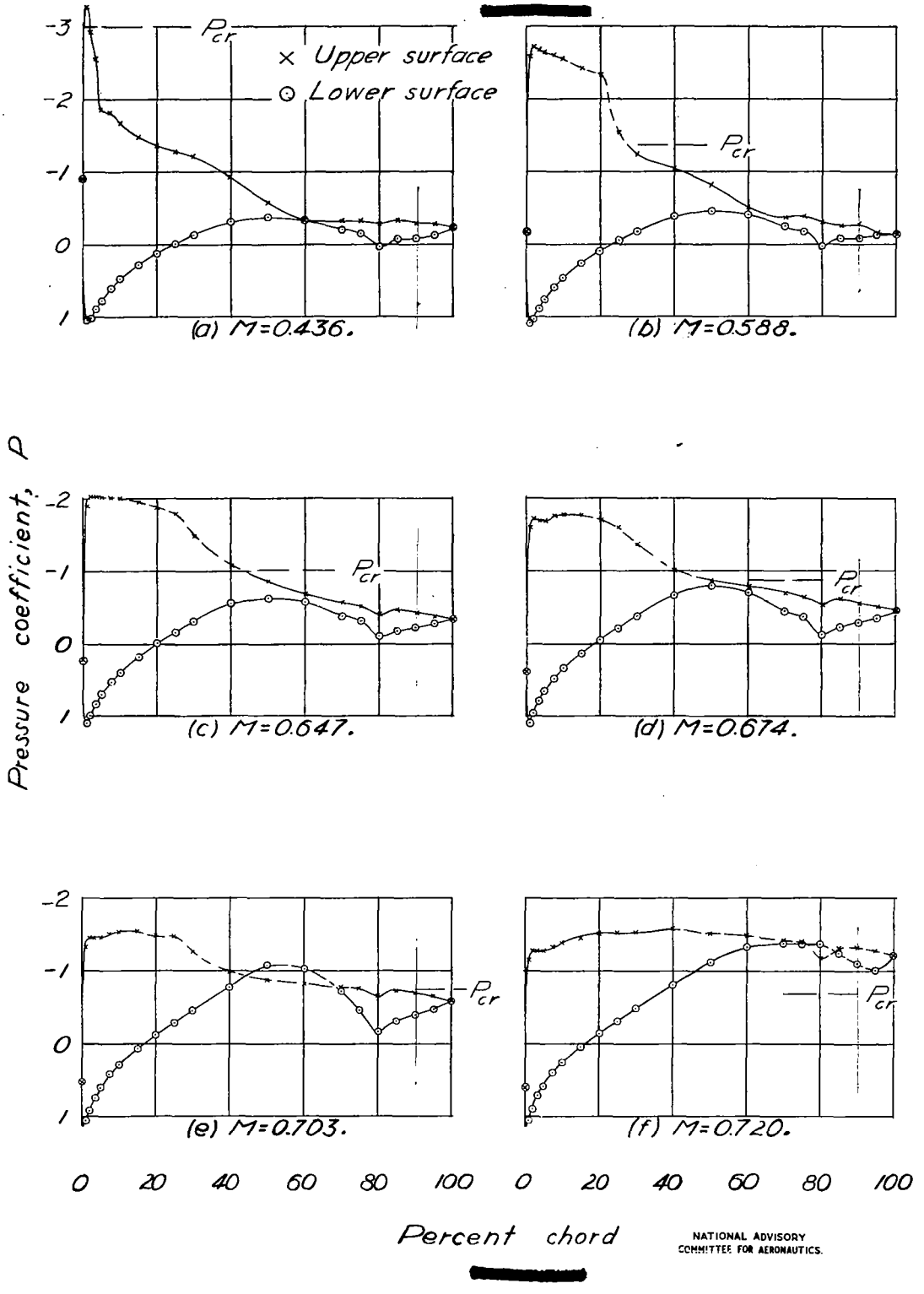

Figure 22.- Pressure distribution for a modified NACA 65,3-019 airfoil with 0.20-chord flap. $\alpha = 10^{\circ}$; $\delta = 0^{\circ}$.

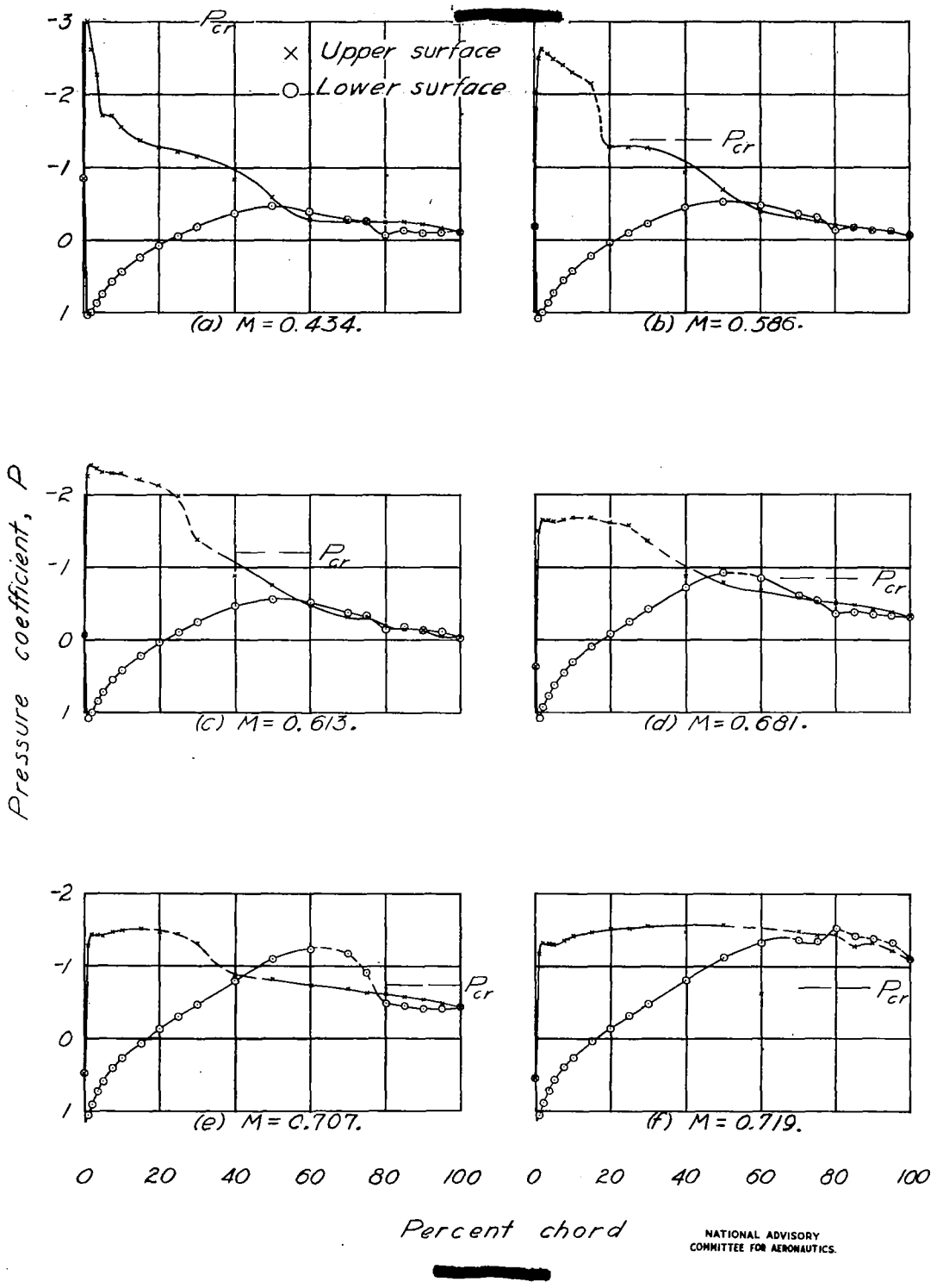

Figure 23.- Pressure distribution for a modified NACA 65,3-019 airfoil with 0.20-chord flap. $\alpha = 10^{\circ}$; $\delta = -4^{\circ}$.

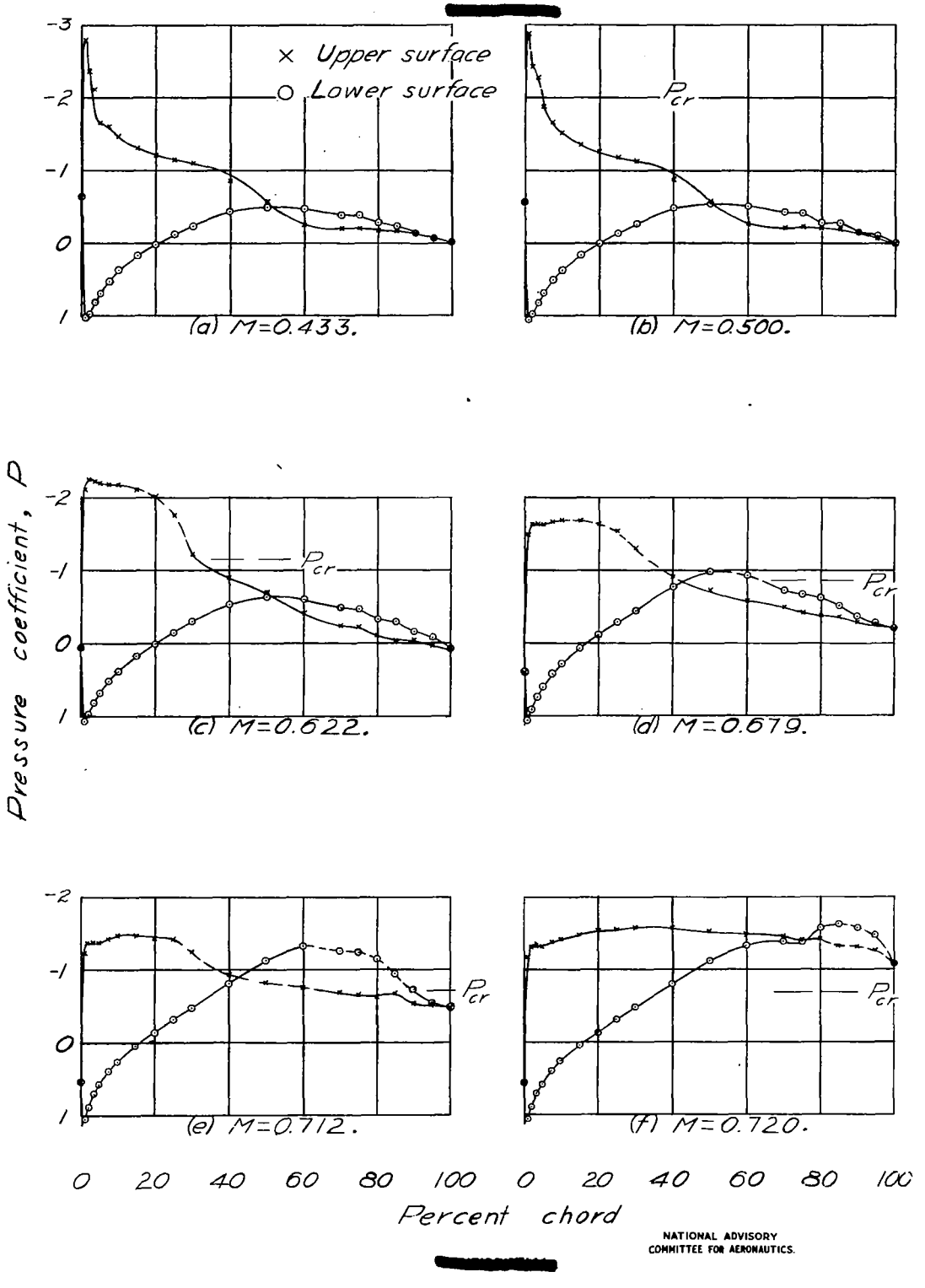

Figure 24.- Pressure distribution for a modified NACA 65,3-019 airfoil with 0.20-chord flap. $\alpha = 10^{\circ}$; $\delta = -8^{\circ}$.

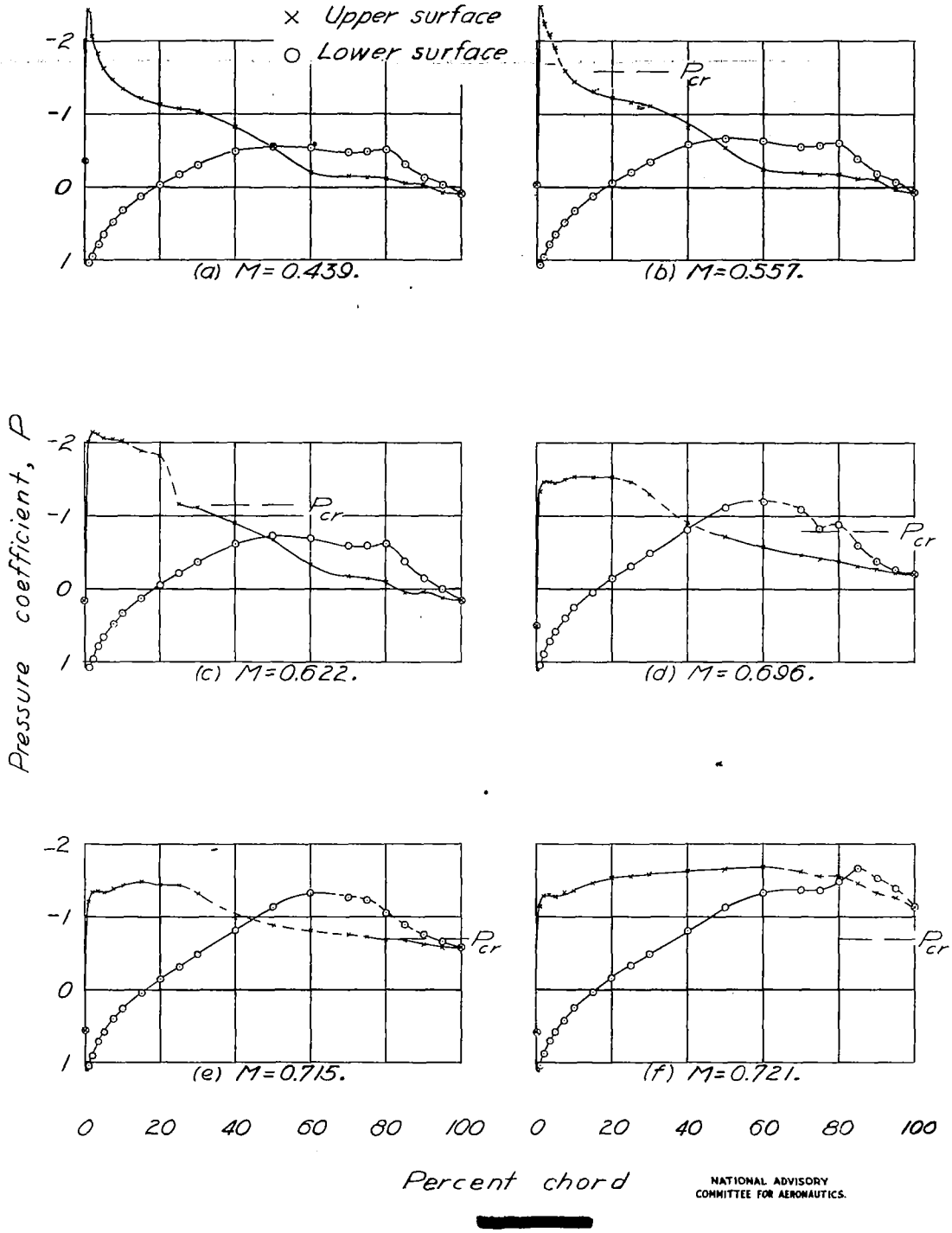

Figure 25. - Pressure distribution for a modified NACA 65,3-019 airfoil with 0.20-chord flap. $\alpha = 10^{\circ}$; $\delta = -12^{\circ}$.

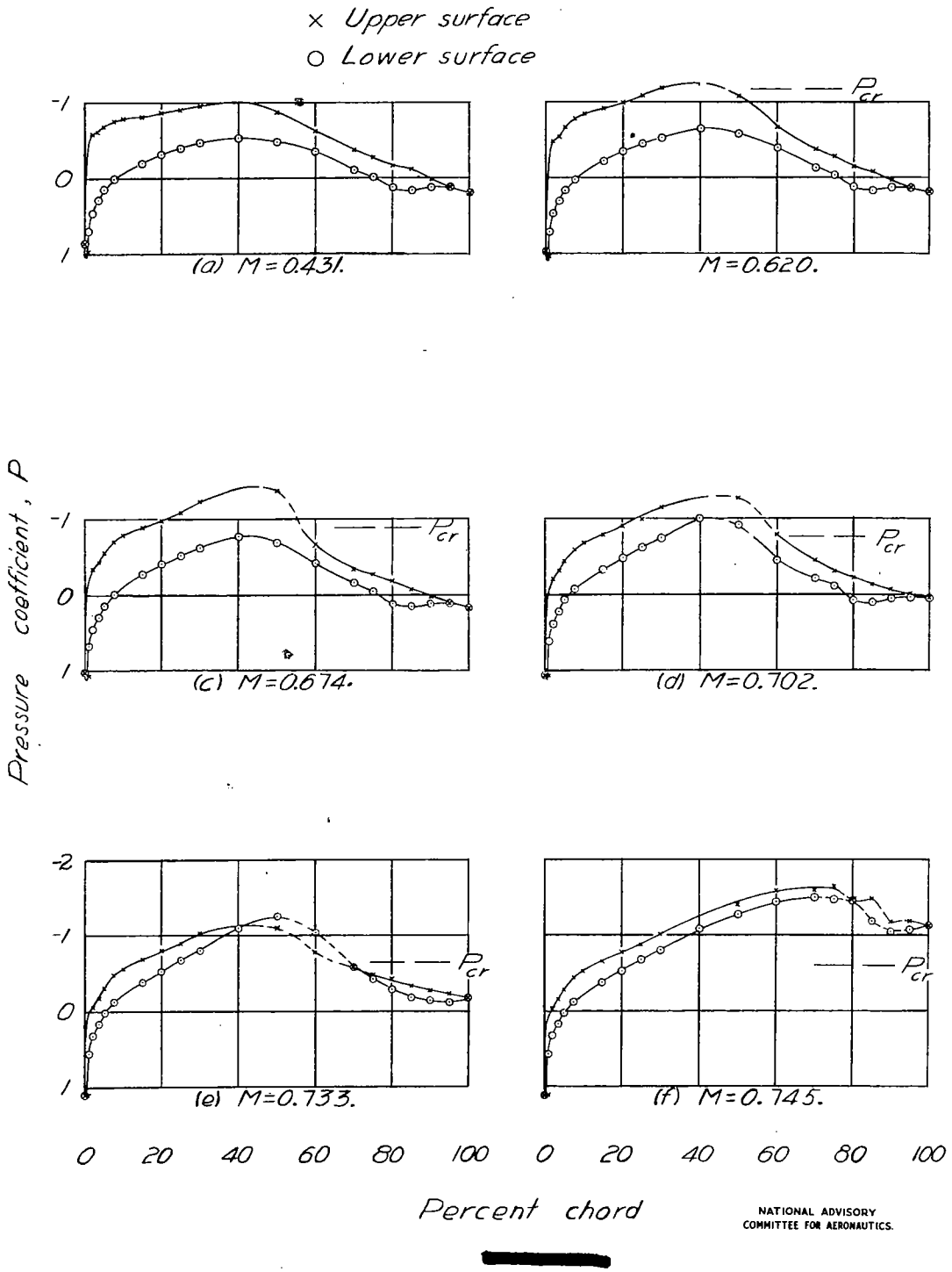

Figure 26.- Pressure distribution for a modified NACA 65,3-019 airfoil with 0.20-chord flap. $\alpha = 2^{\circ}$; $\delta = 4^{\circ}$.

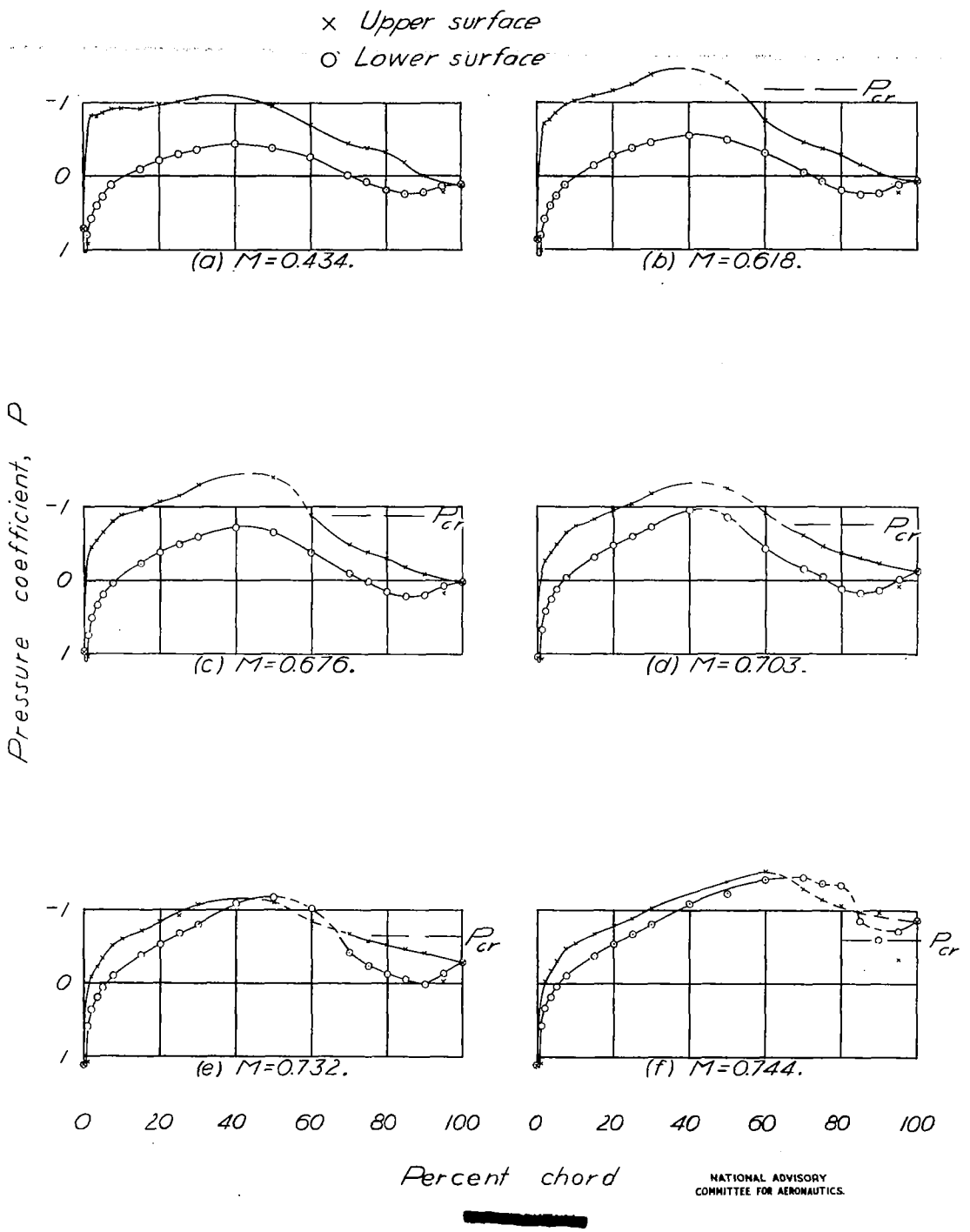

Figure 27.- Pressure distribution for a modified NACA 65,3-019 airfoil with 0.20-chord flap. $\alpha = 2^{\circ}$; $\delta = 8^{\circ}$.

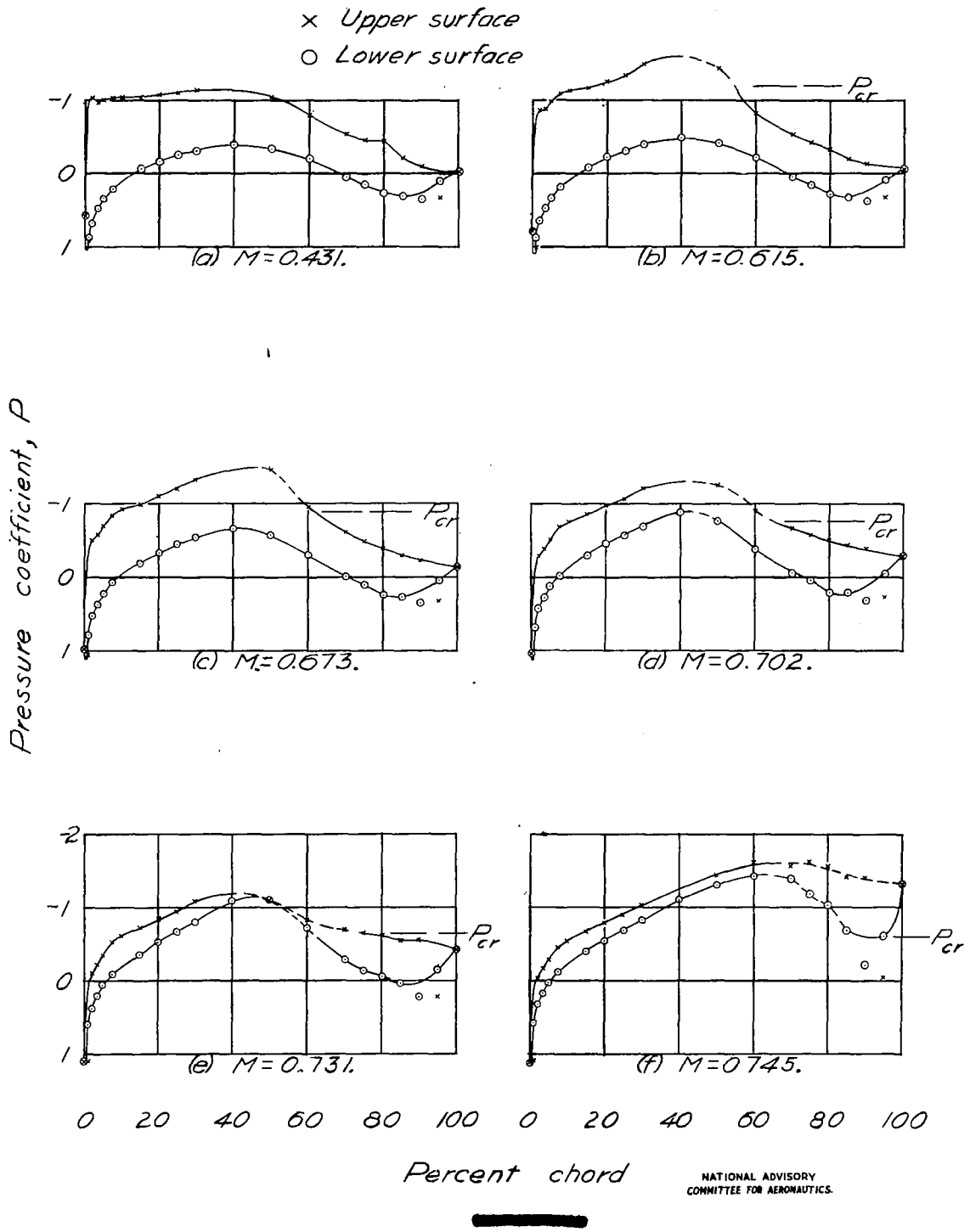

Figure 28.- Pressure distribution for a modified NACA 65,3-019 airfoil with 0.20-chord flap. $\alpha = 2^{\circ}$; $\delta = 12^{\circ}$.

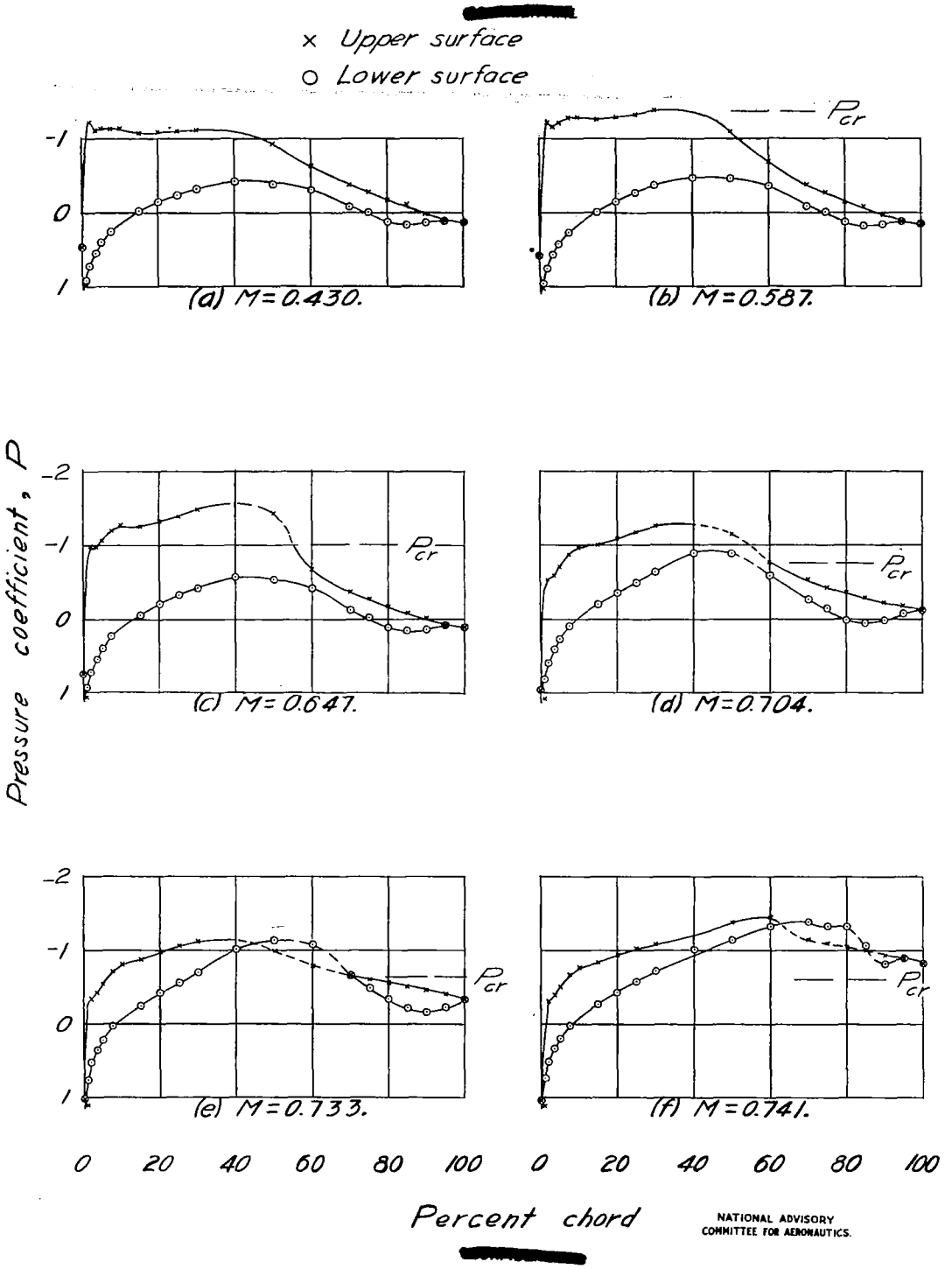

Figure 29.- Pressure distribution for a modified NACA 65,3-019 airfoil with 0.20-chord flap. $\alpha = 4^{\circ}$; $\delta = 4^{\circ}$.

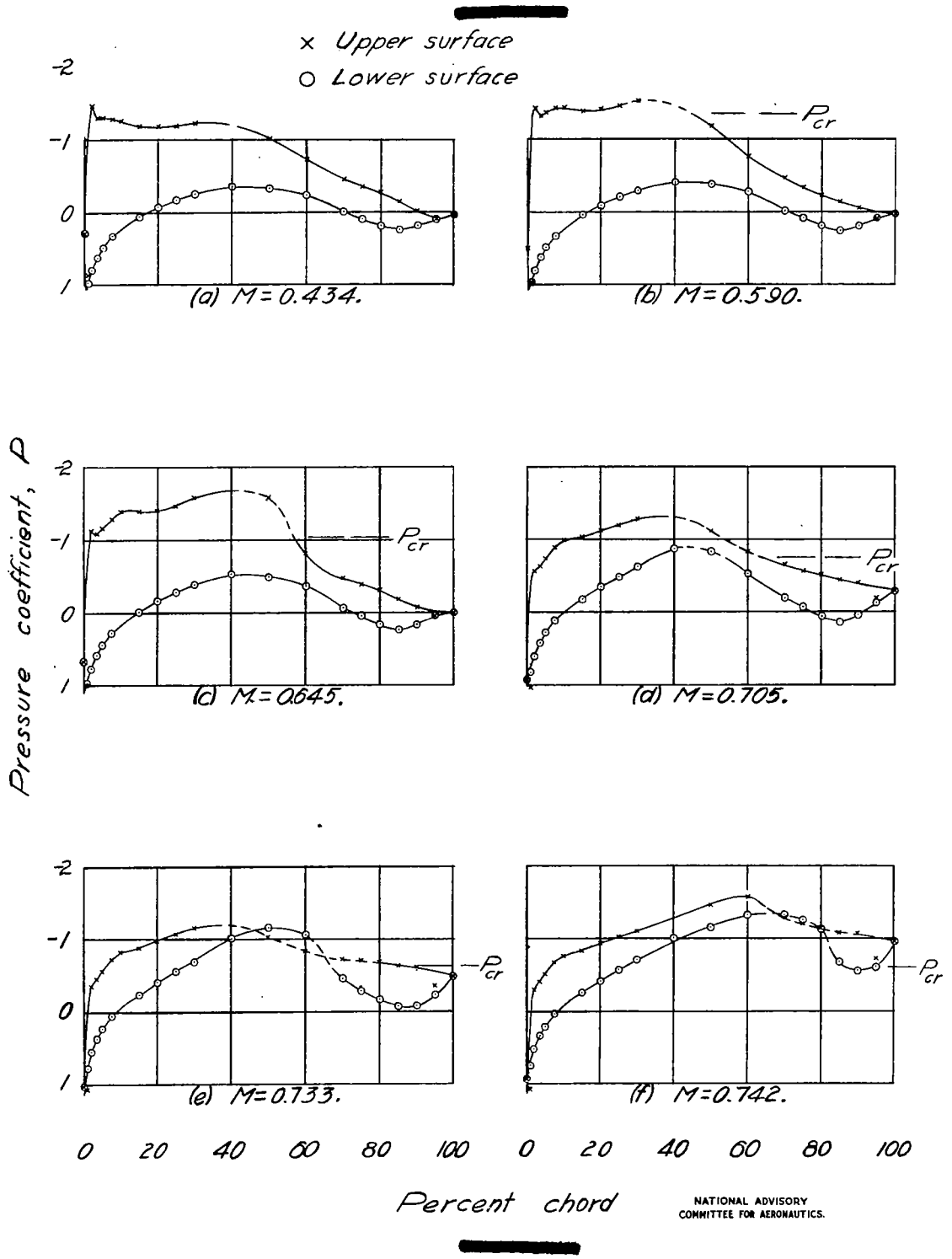

Figure 30.- Pressure distribution for a modified NACA 65,3-019 airfoil with 0.20-chord flap. $\alpha = 4^{\circ}$; $\delta = 8^{\circ}$.

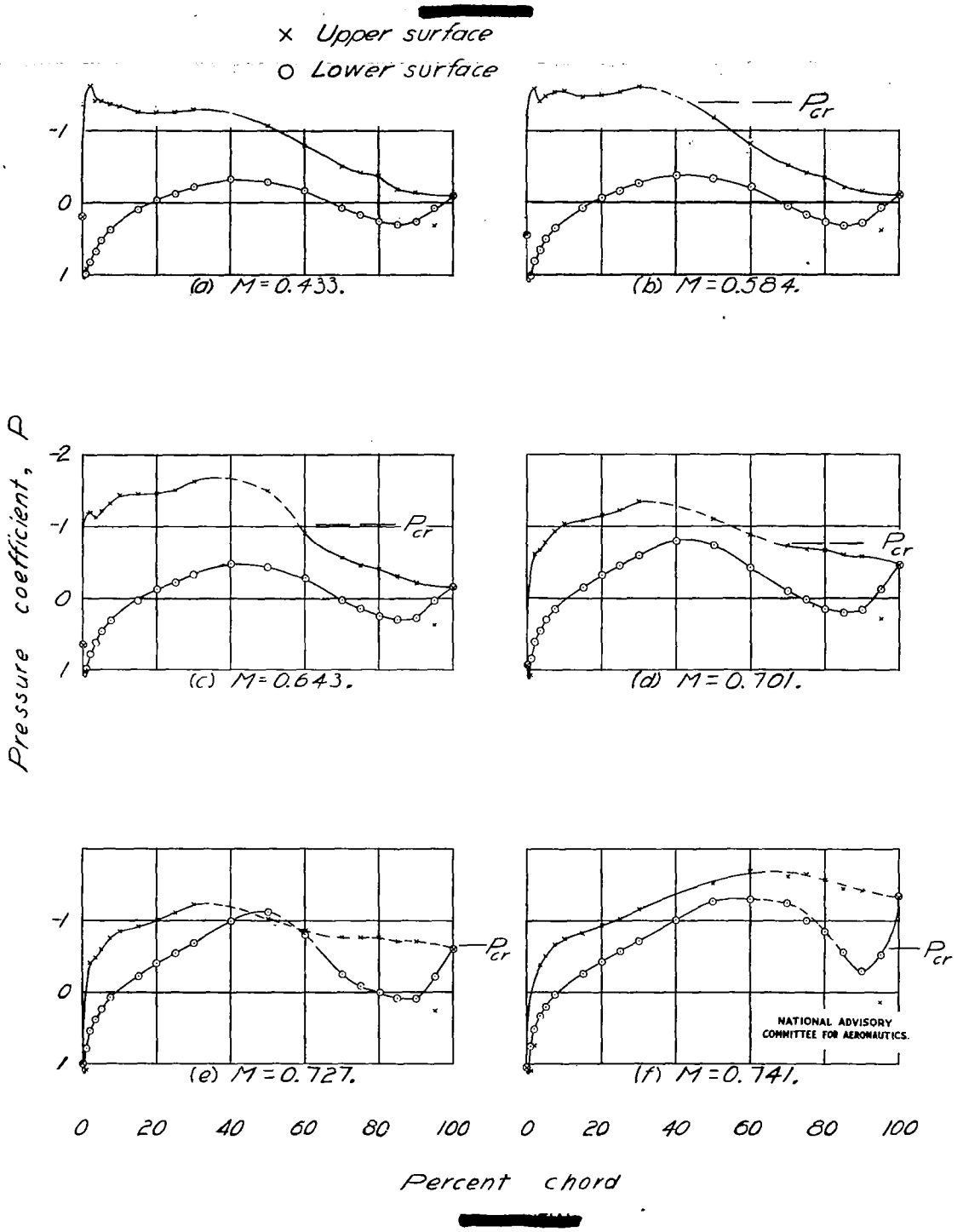

Figure 31.- Pressure distribution for a modified NACA 65,3-019 airfoil with 0.20-chord flap. $\alpha = 4^{\circ}$; $\delta = 12^{\circ}$.

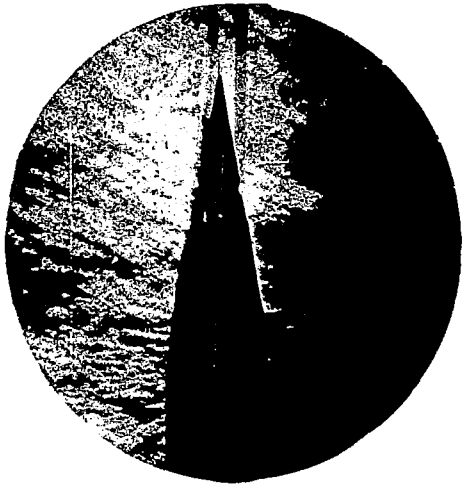

(a) M = 0.644.

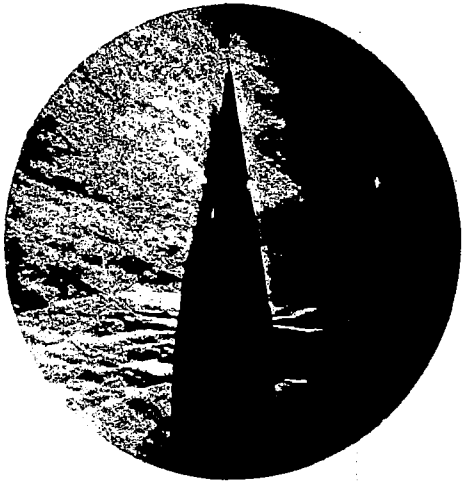

(b) M = 0.678.

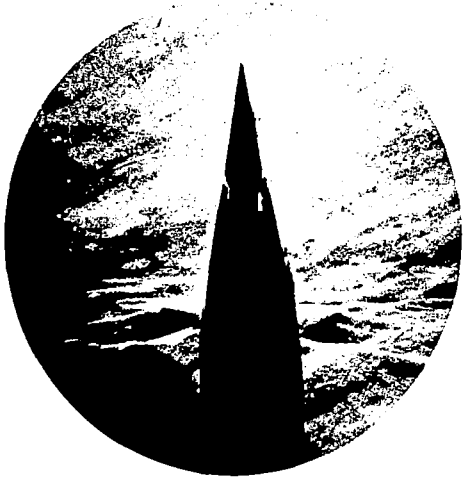

(c) M = 0.707.

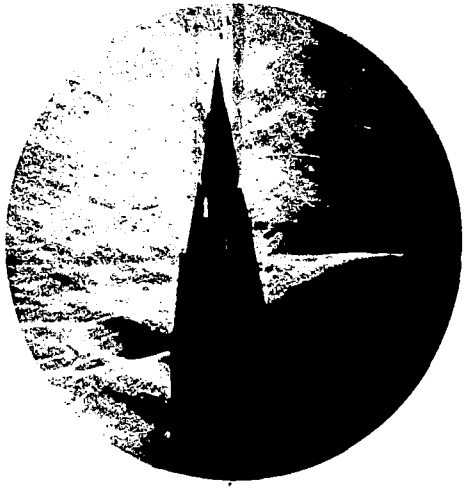

(d) M = 0.727.

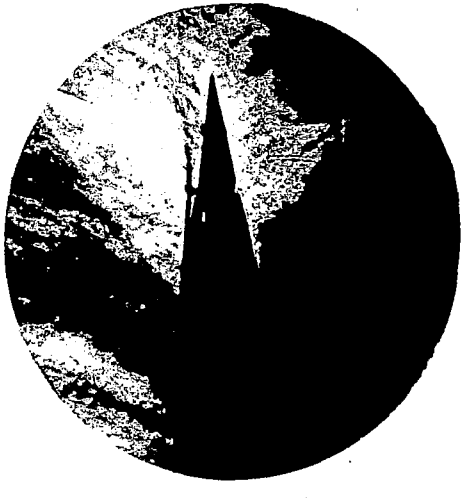

(e) M = 0.741.

Figure 32.- Schlieren photographs of the flow for a modified NACA 65,3-019 airfoil section with 0.20-chord flap. $\alpha = 0^{\circ}$; $\delta = 0^{\circ}$.

NATIONAL ADVISORY COMMITTEE FOR AERONAUTICS
LANGLEY MEMORIAL AERONAUTICAL LABORATORY - LANGLEY FIELD, VA.

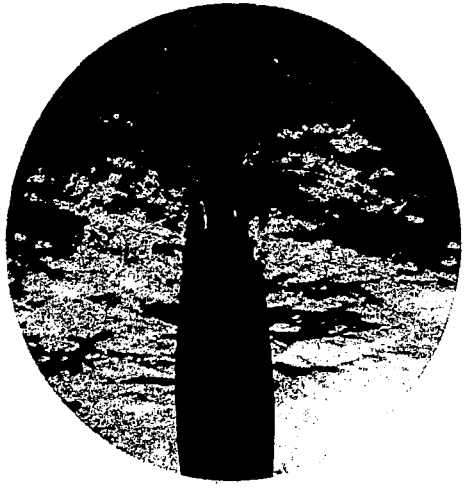

(a) M = 0.651.

(b) M = 0.677.

(c) M = 0.706.

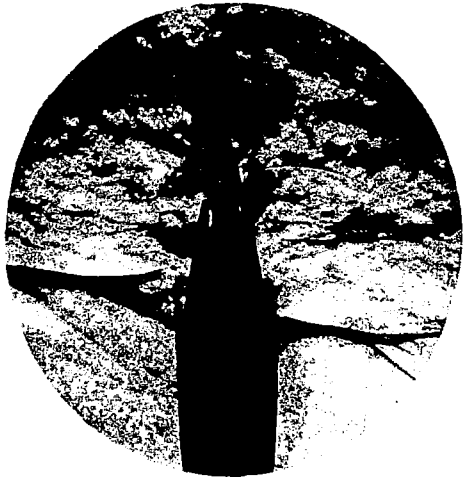

(d) M = 0.732.

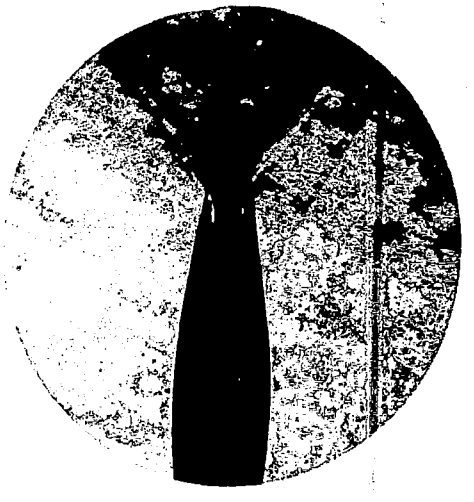

(e) M = 0.744.

Figure 33.- Schlieren photographs of the flow for a modified NACA 65,3-019 airfoil section with 0.20-chord flap. $\alpha = 0^{\circ}$; $\delta = -4^{\circ}$.

NATIONAL ADVISORY COMMITTEE FOR AERONAUTICS
LANGLEY MEMORIAL AERONAUTICAL LABORATORY - LANGLEY FIELD, VA.

(a) M = 0.589.

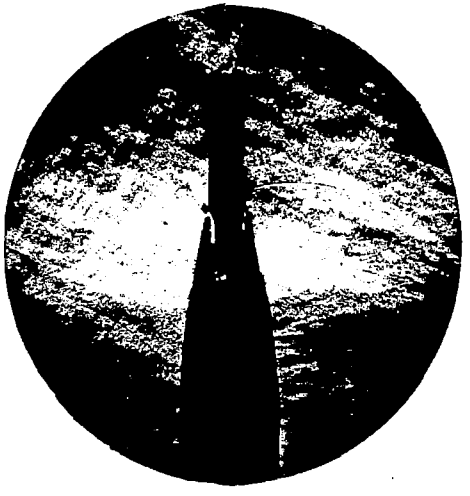

(b) M = 0.621.

(c) M = 0.650.

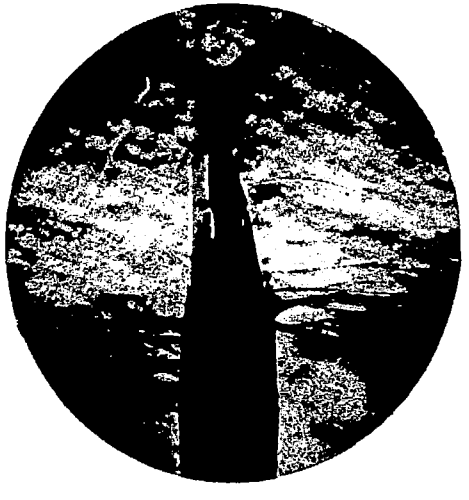

(d) M = 0.708.

(e) M = 0.735.

(f) M = 0.742.

Figure 34.- Schlieren photographs of the flow for a modified NACA 65,3-019 airfoil section with 0.20-chord flap. $\alpha = 0^{\circ}$; $\delta = -8^{\circ}$.

NATIONAL ADVISORY COMMITTEE FOR AERONAUTICS
LANGLEY MEMORIAL AERONAUTICAL LABORATORY - LANGLEY FIELD, VA.

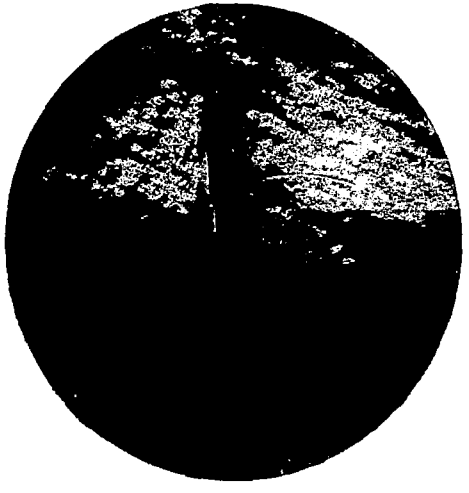

(a) M = 0.620.

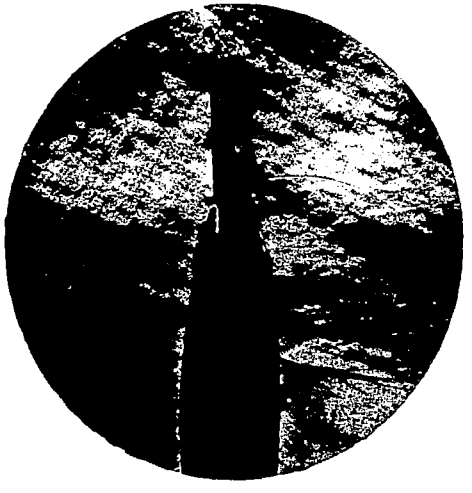

(b) M = 0.648.

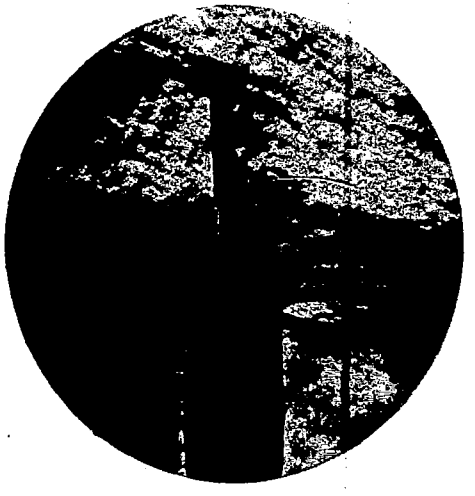

(c) M = 0.676.

(d) M = 0.706.

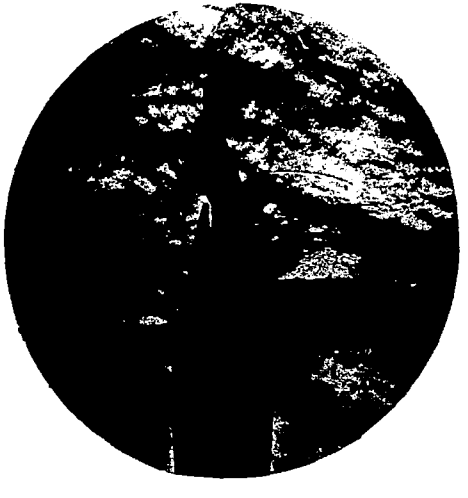

(e) M = 0.735.

(f) M = 0.743.

Figure 35.- Schlieren photographs of the flow for a modified NACA 65,3-019 airfoil section with 0.20-chord flap. $\alpha = 0^{\circ}$; $\delta = -12^{\circ}$.

NATIONAL ADVISORY COMMITTEE FOR AERONAUTICS
LANGLEY MEMORIAL AERONAUTICAL LABORATORY - LANGLEY FIELD, VA.

(a) M = 0.644.

(b) M = 0.673.

(c) M = 0.704.

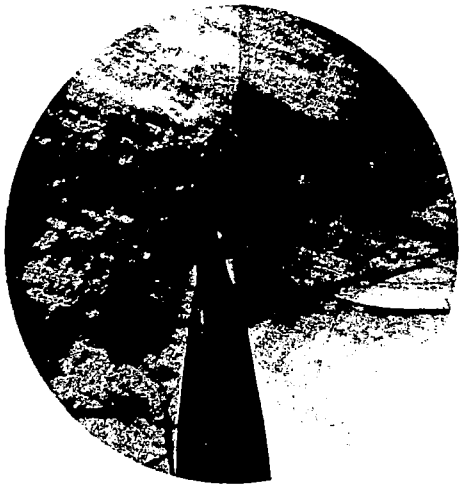

(d) M = 0.727.

(e) M = 0.738.

Figure 36.- Schlieren photographs of the flow for a modified NACA 65,3-019 airfoil section with 0.20-chord flap. $\alpha = 4^{\circ}$; $\delta = -4^{\circ}$.

NATIONAL ADVISORY COMMITTEE FOR AERONAUTICS
LANGLEY MEMORIAL AERONAUTICAL LABORATORY - LANGLEY FIELD, VA.

(a) M = 0.617. (b) M = 0.651. (c) M = 0.678.

(d) M = 0.703. (e) M = 0.727. (f) M = 0.741.

Figure 37.- Schlieren photographs of the flow for a modified NACA 65,3-019 airfoil section with 0.20-chord flap. $\alpha = 4^{\circ}$; $\delta = 0^{\circ}$.

NATIONAL ADVISORY COMMITTEE FOR AERONAUTICS
LANGLEY MEMORIAL AERONAUTICAL LABORATORY - LANGLEY FIELD, VA.

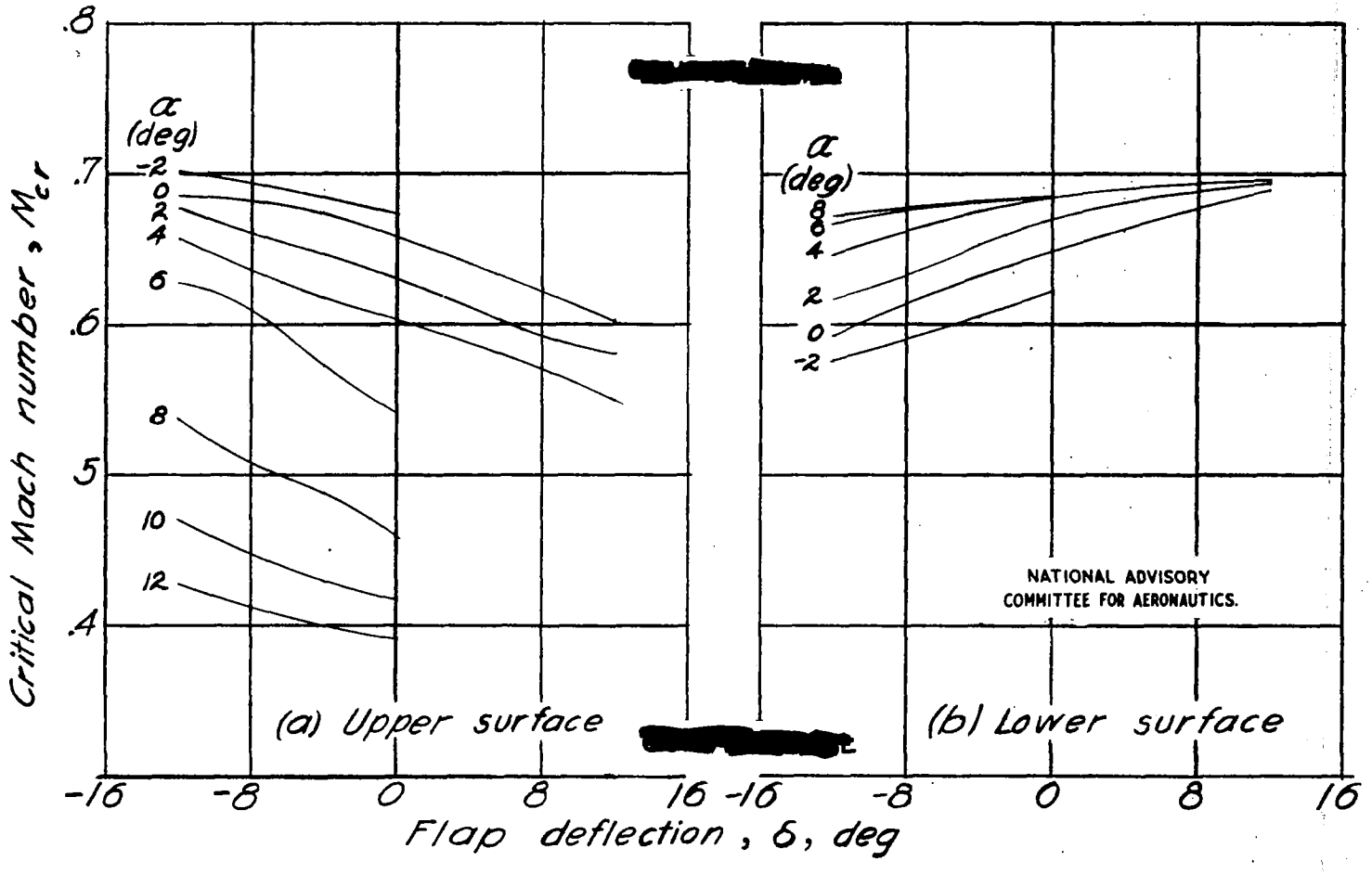

Figure 38.- Critical Mach number for each surface as a function of flap deflection at a constant angle of attack.

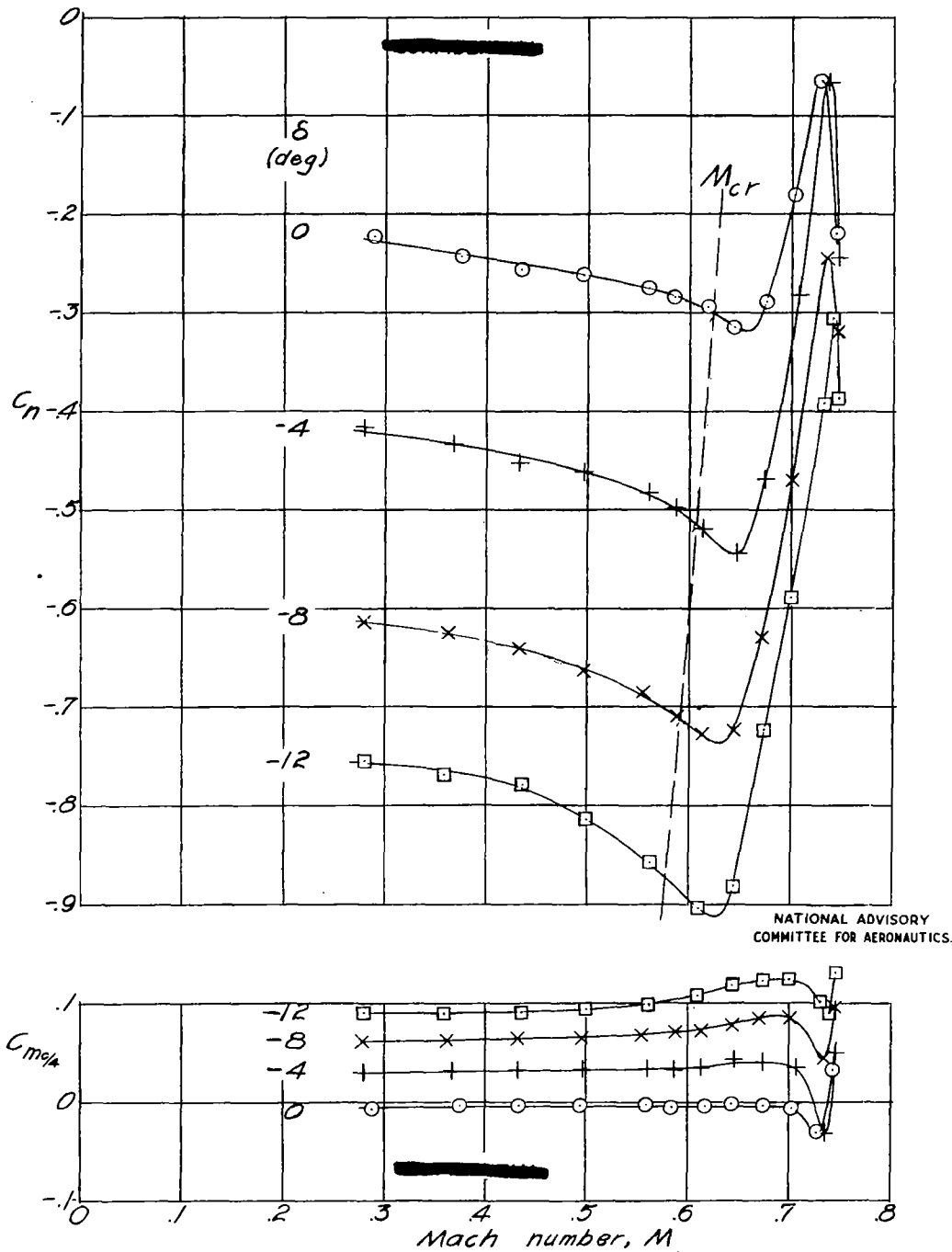

(a) $\alpha = -2^\circ$.

Figure 39.- Effect of compressibility on section normal-force and moment coefficients.

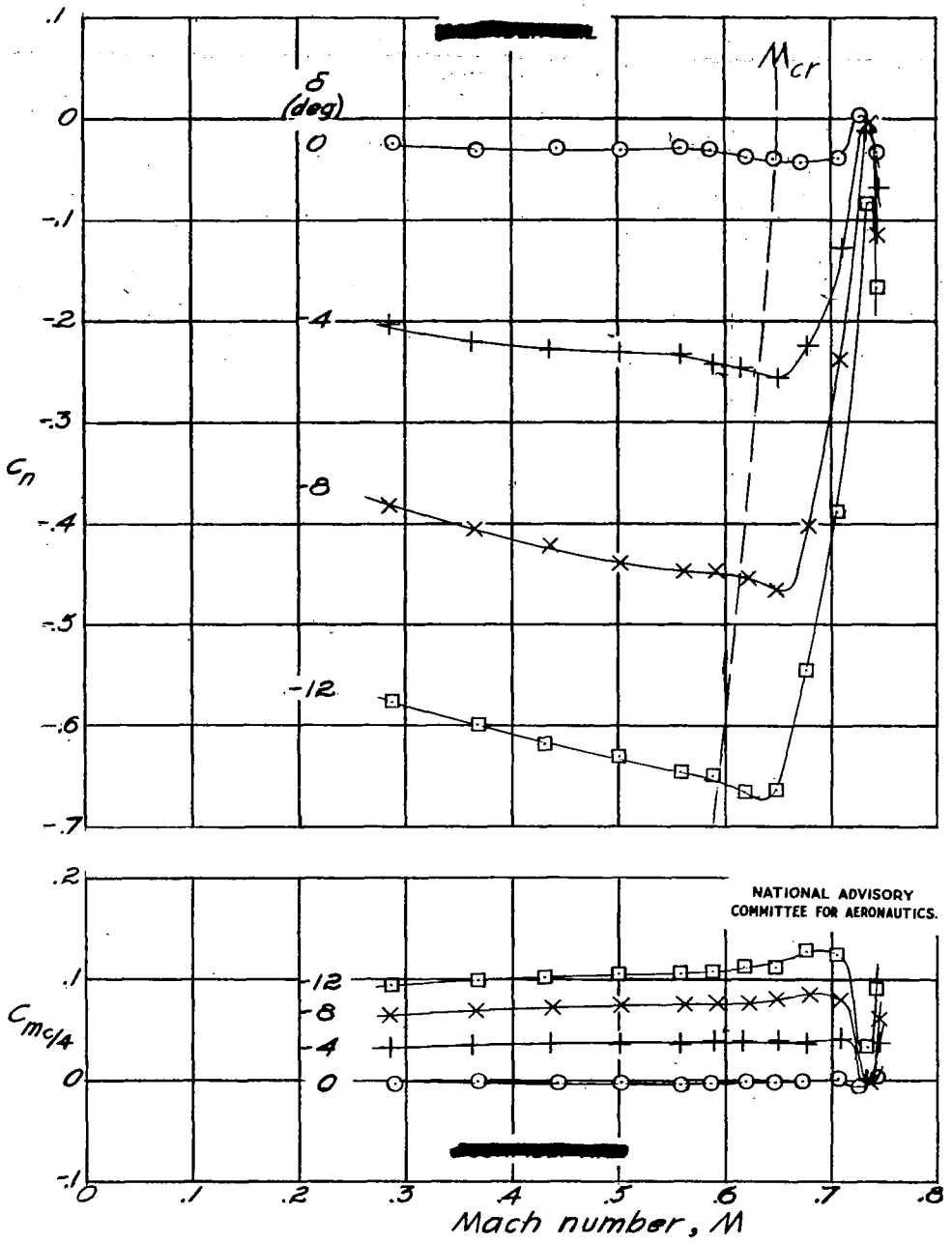

(b) $\alpha = 0^\circ$.

Figure 39.- Continued.

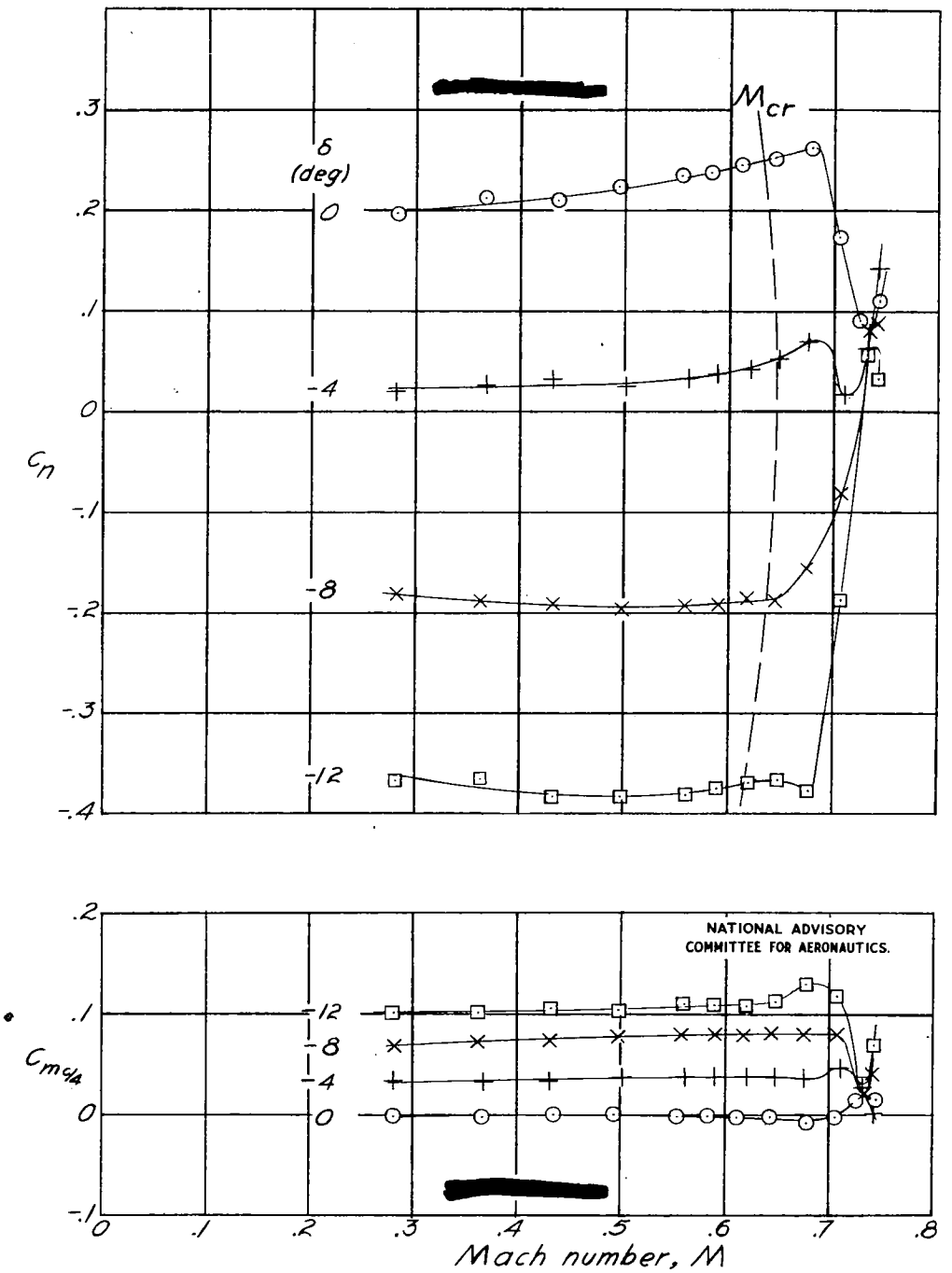

(c) $\alpha = 2^{\circ}$.

Figure 39. - Continued.

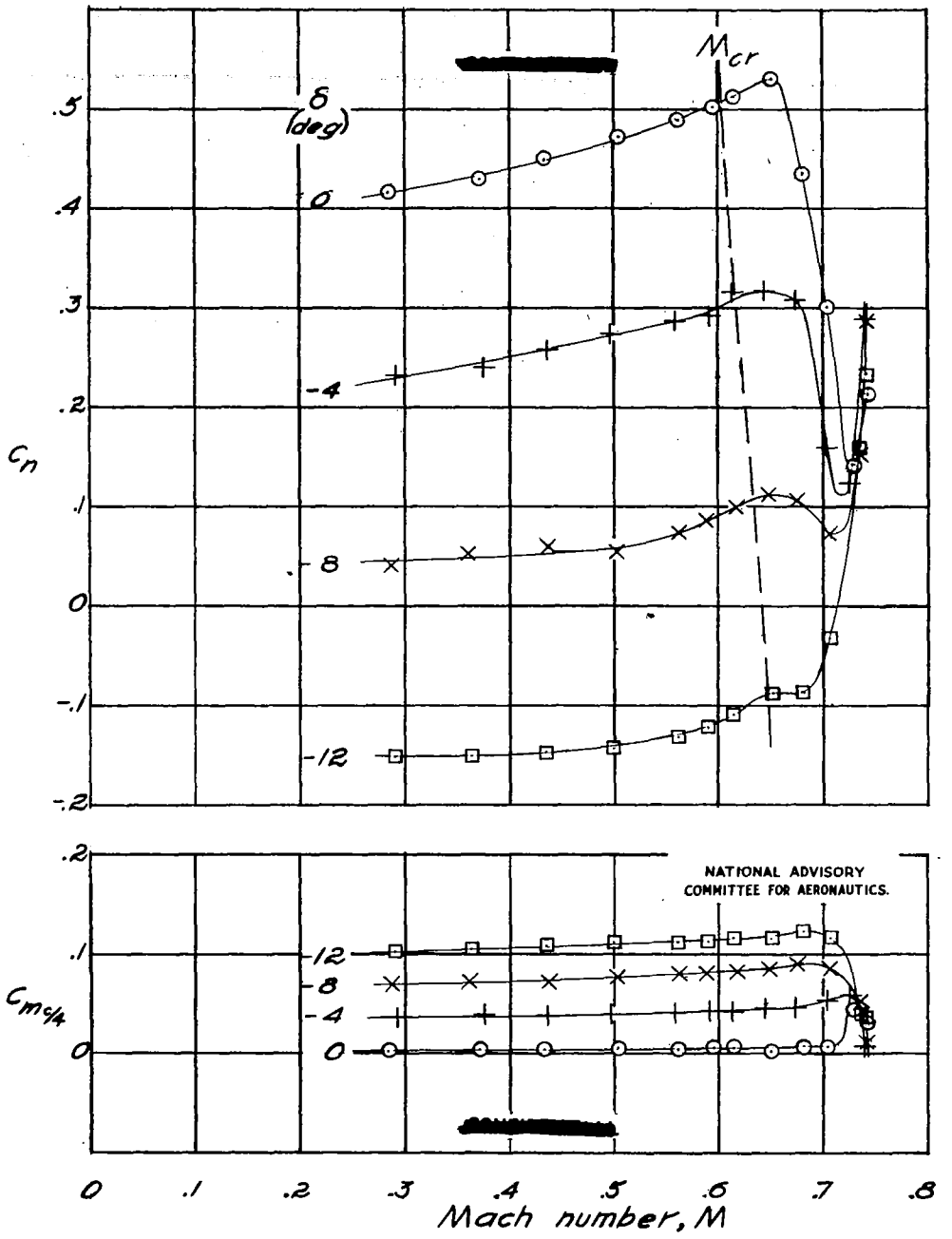

(d) $\alpha = 4^{\circ}$.

Figure 39.- Continued.

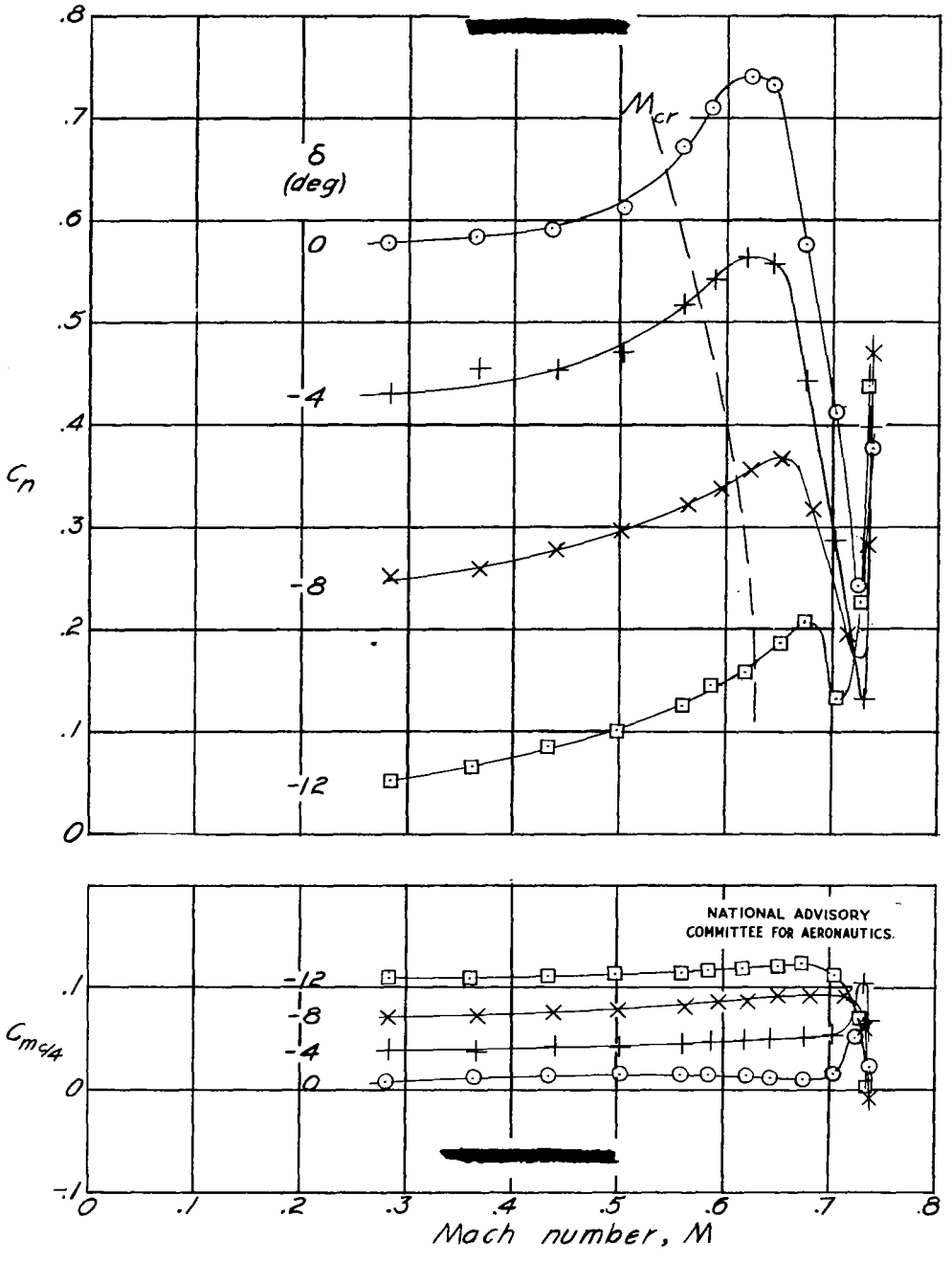

(e) $\alpha = 6^{\circ}$.

Figure 39. - Continued.

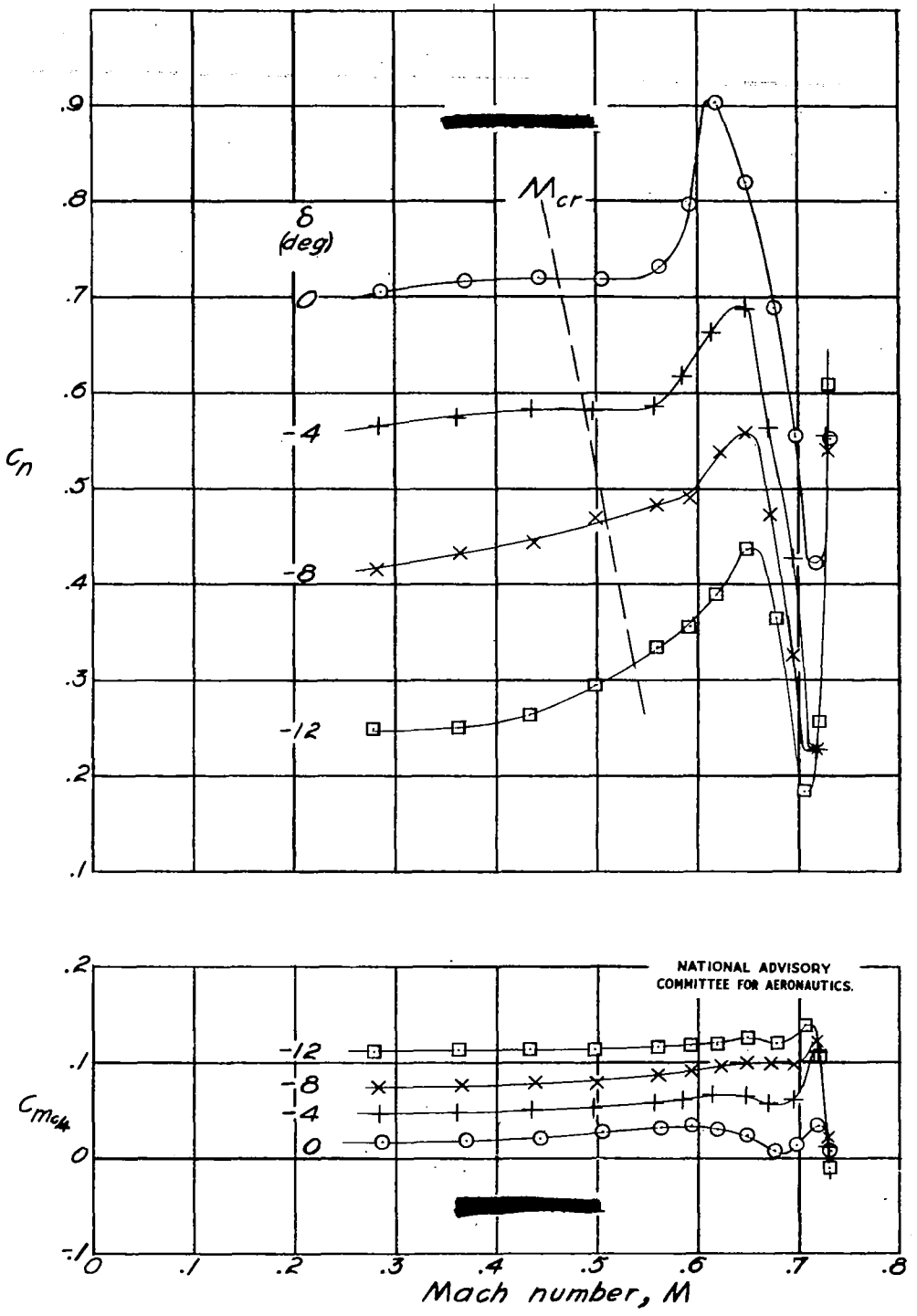

(f) $\alpha = 8^\circ$.

Figure 39.- Continued.

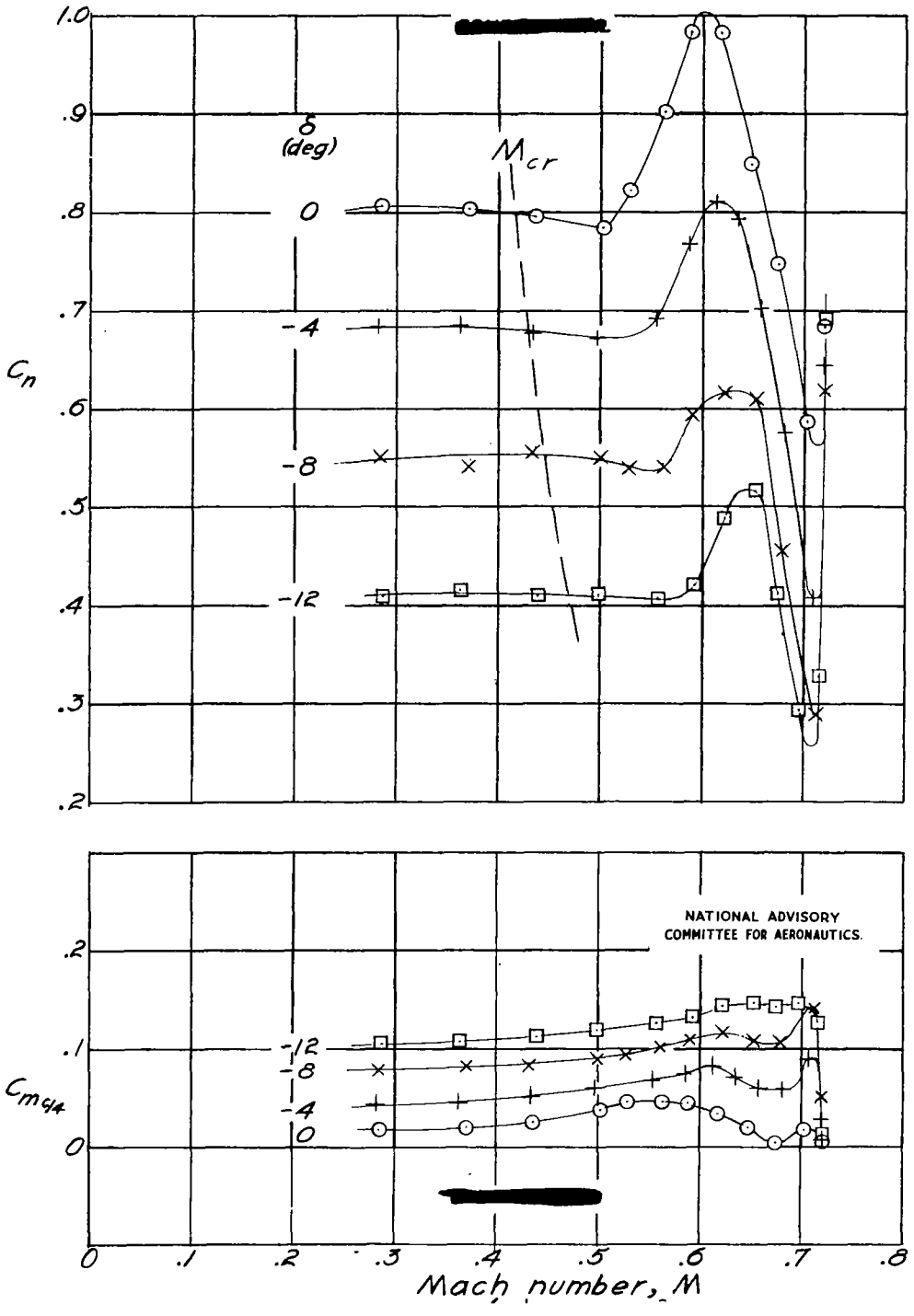

(g) $\alpha = 10^{\circ}$.

Figure 39.- Continued.

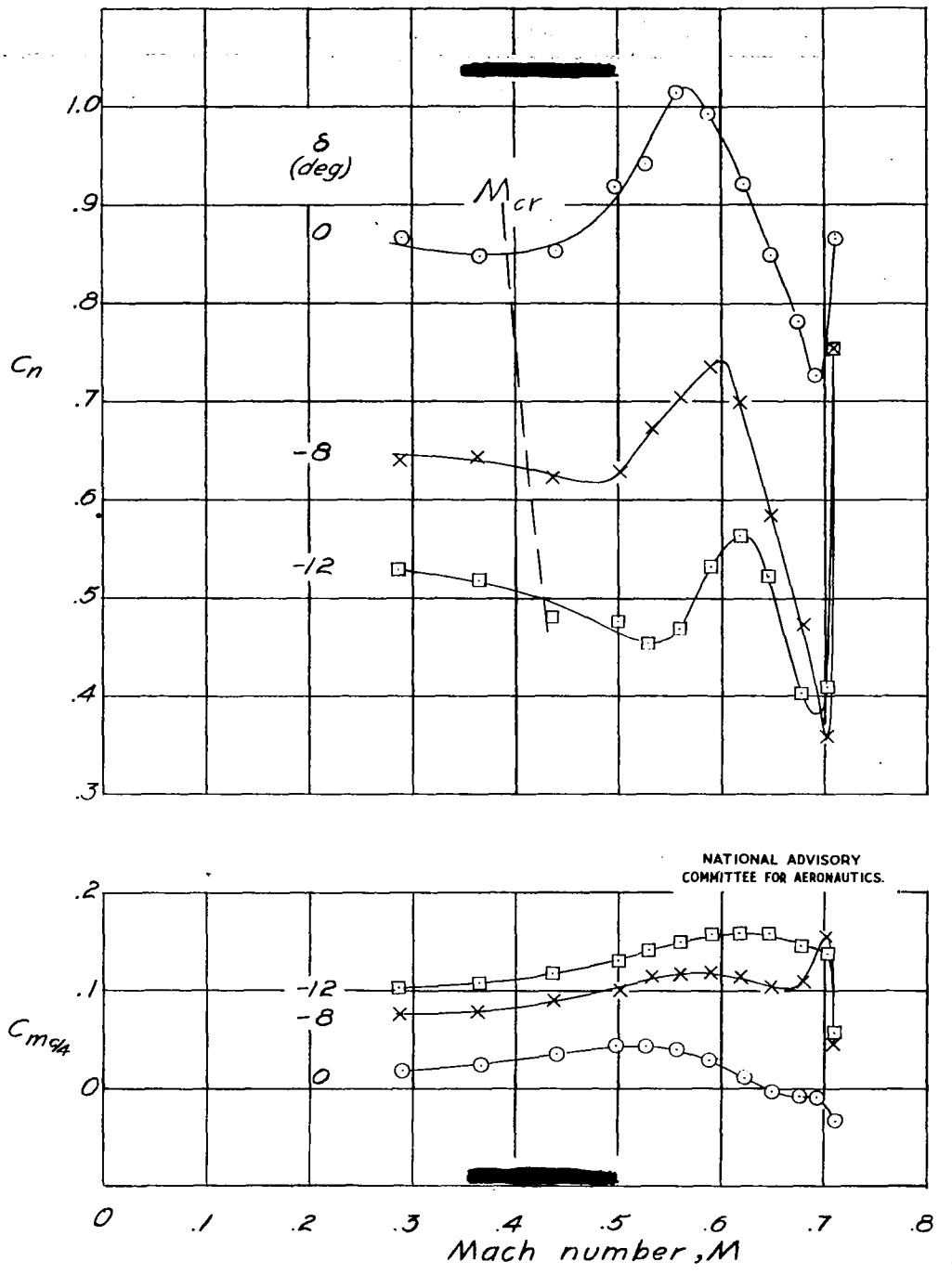

(h) $\alpha = 12^{\circ}$.

Figure 39.- Continued.

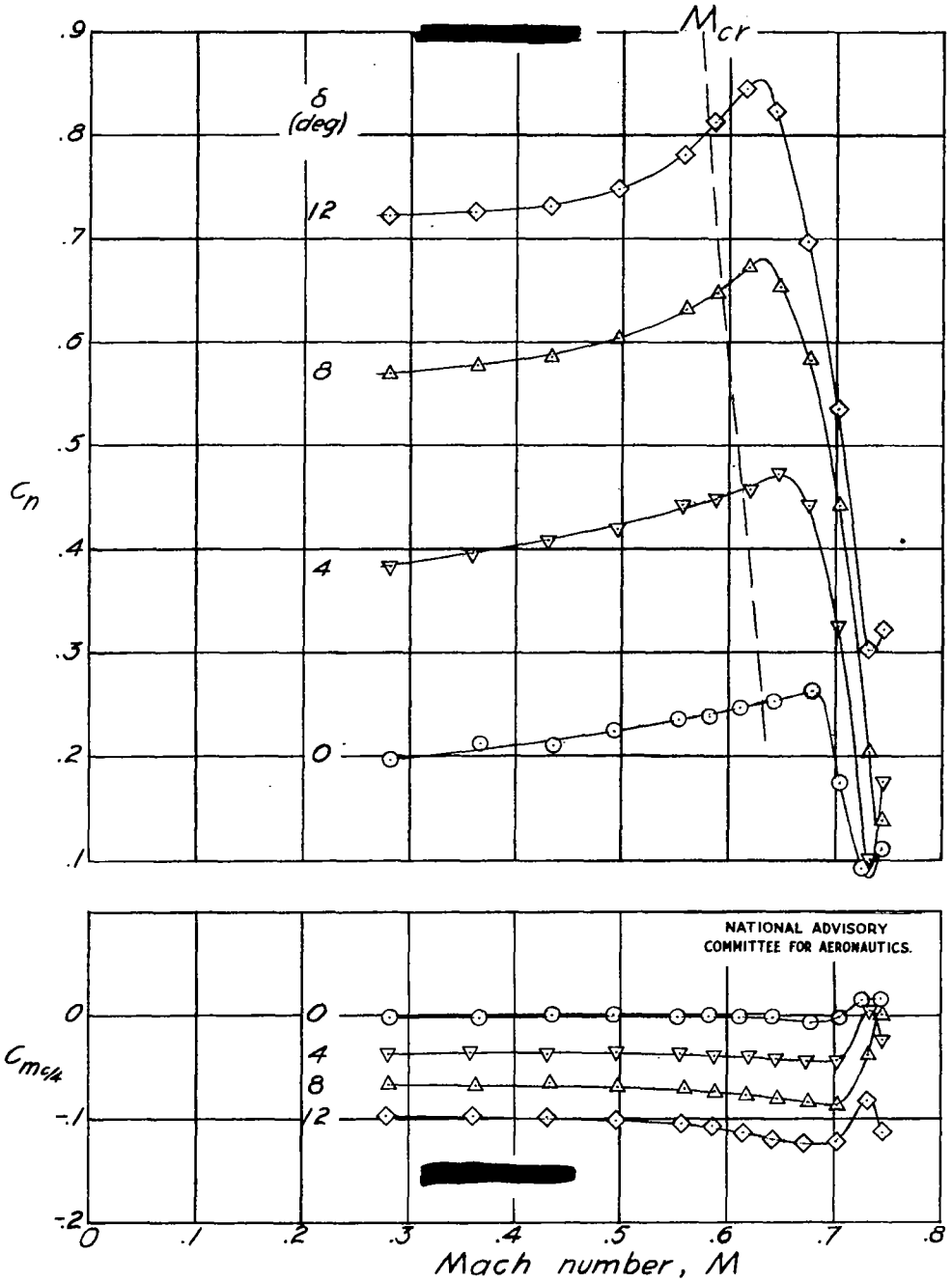

(i) $\alpha = 2^{\circ}$; positive flap deflections.

Figure 39.- Continued.

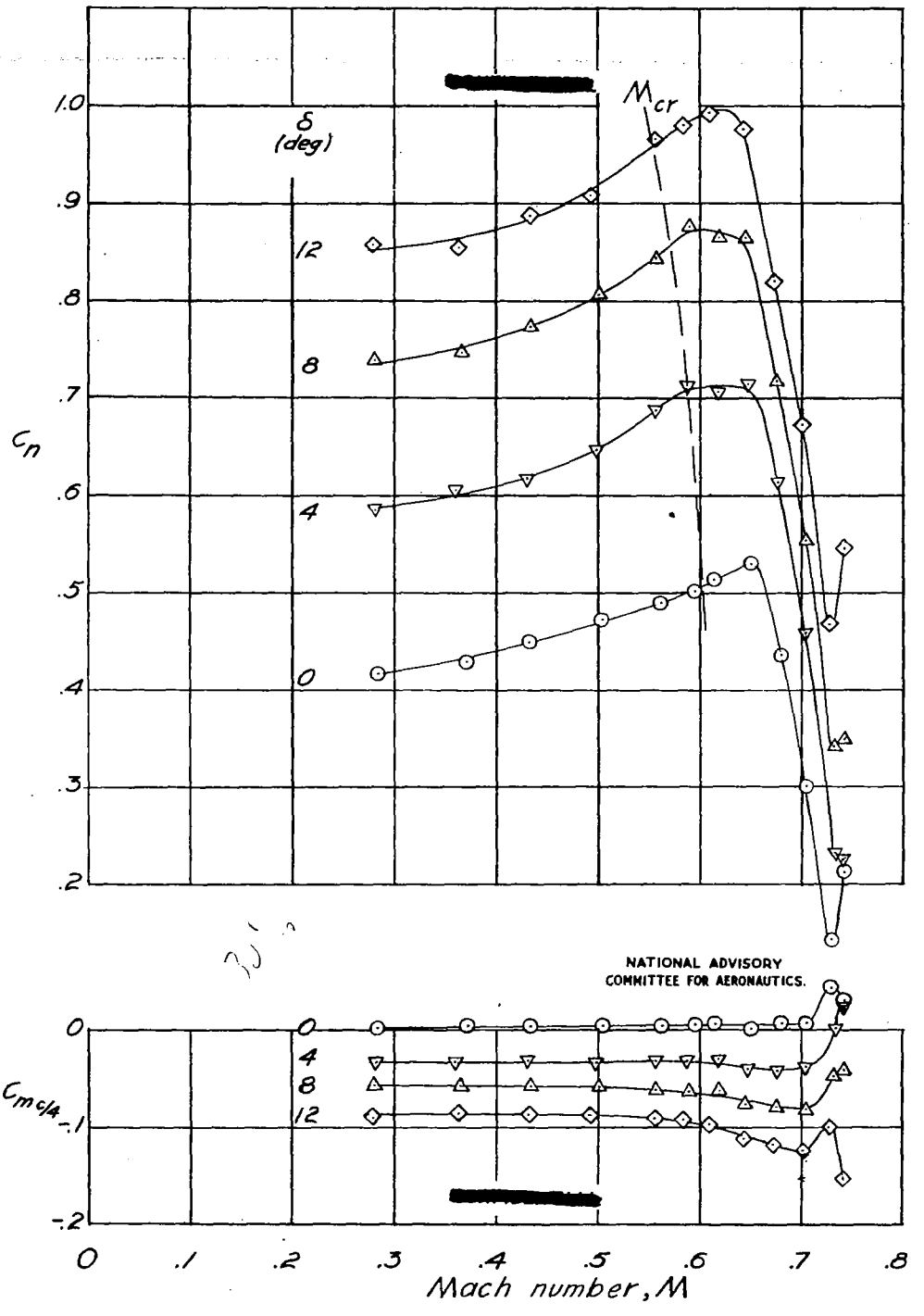

(j) $\alpha = 4^{\circ}$; positive flap deflections.

Figure 39.- Concluded.

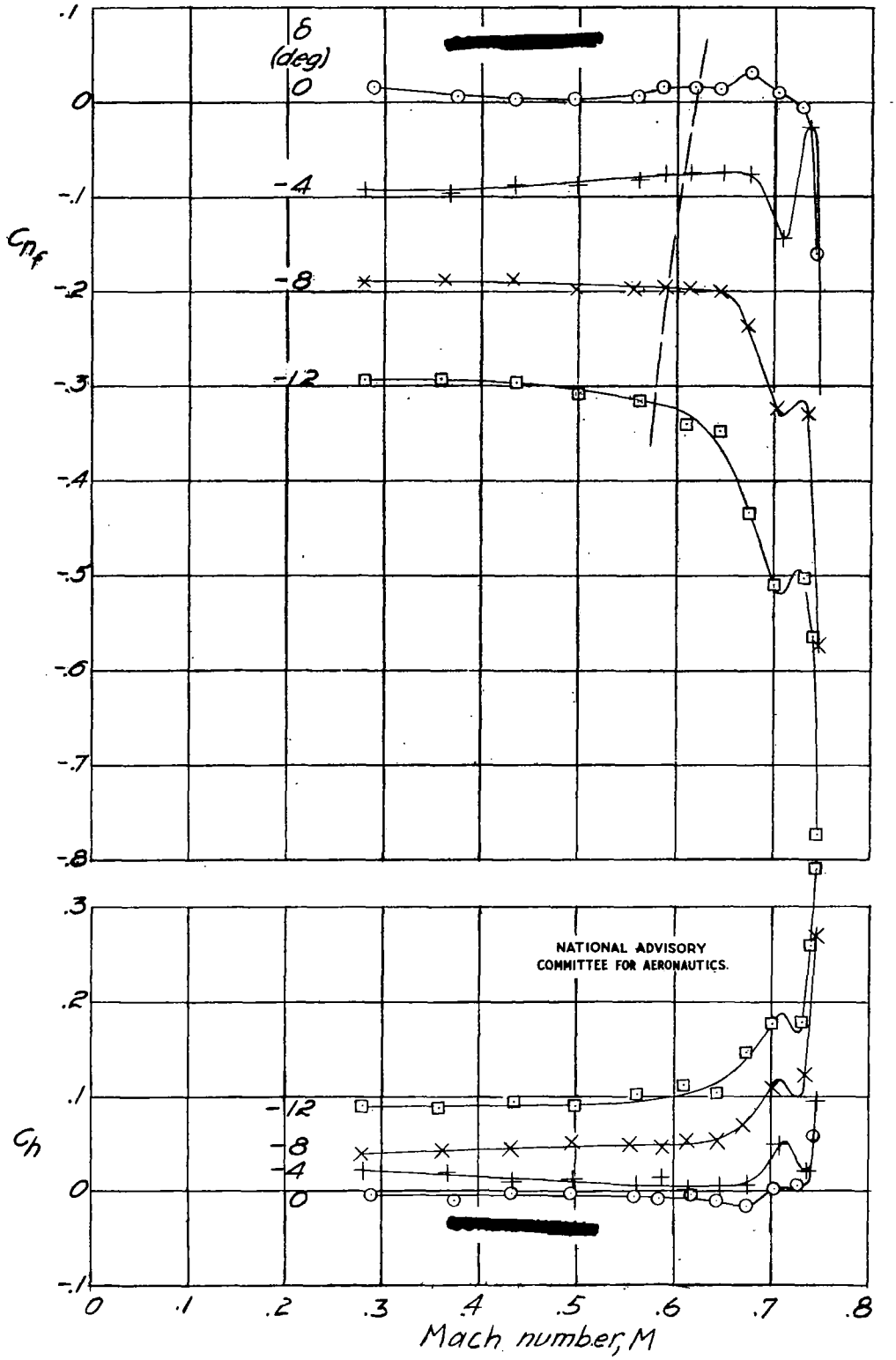

(a) $\alpha = -2^\circ$.

Figure 40. - Effect of compressibility on section hinge-moment and flap normal-force coefficients.

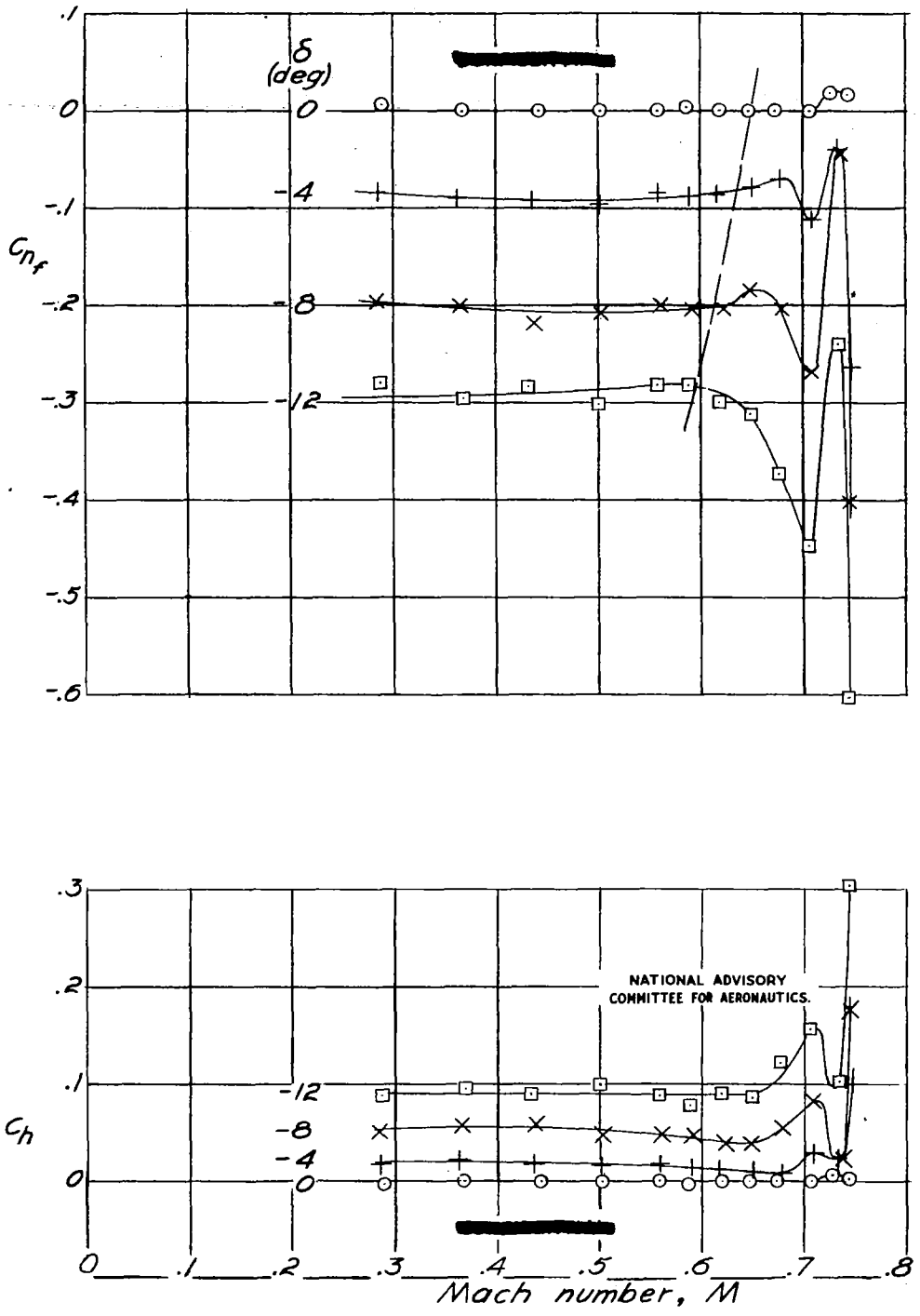

(b) $\alpha = 0^\circ$.

Figure 40.- Continued.

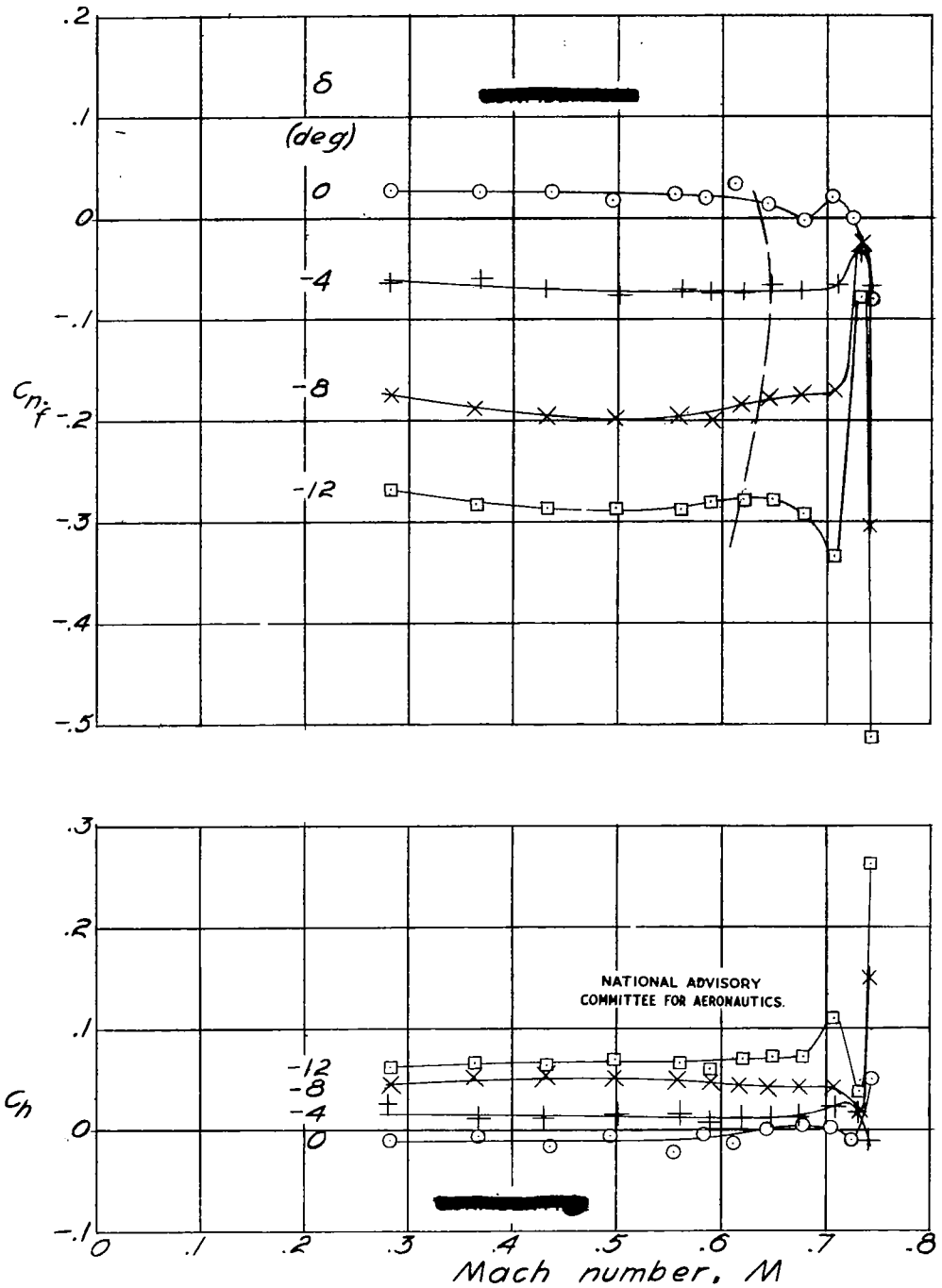

(c) $\alpha = 2^{\circ}$.

Figure 40.- Continued.

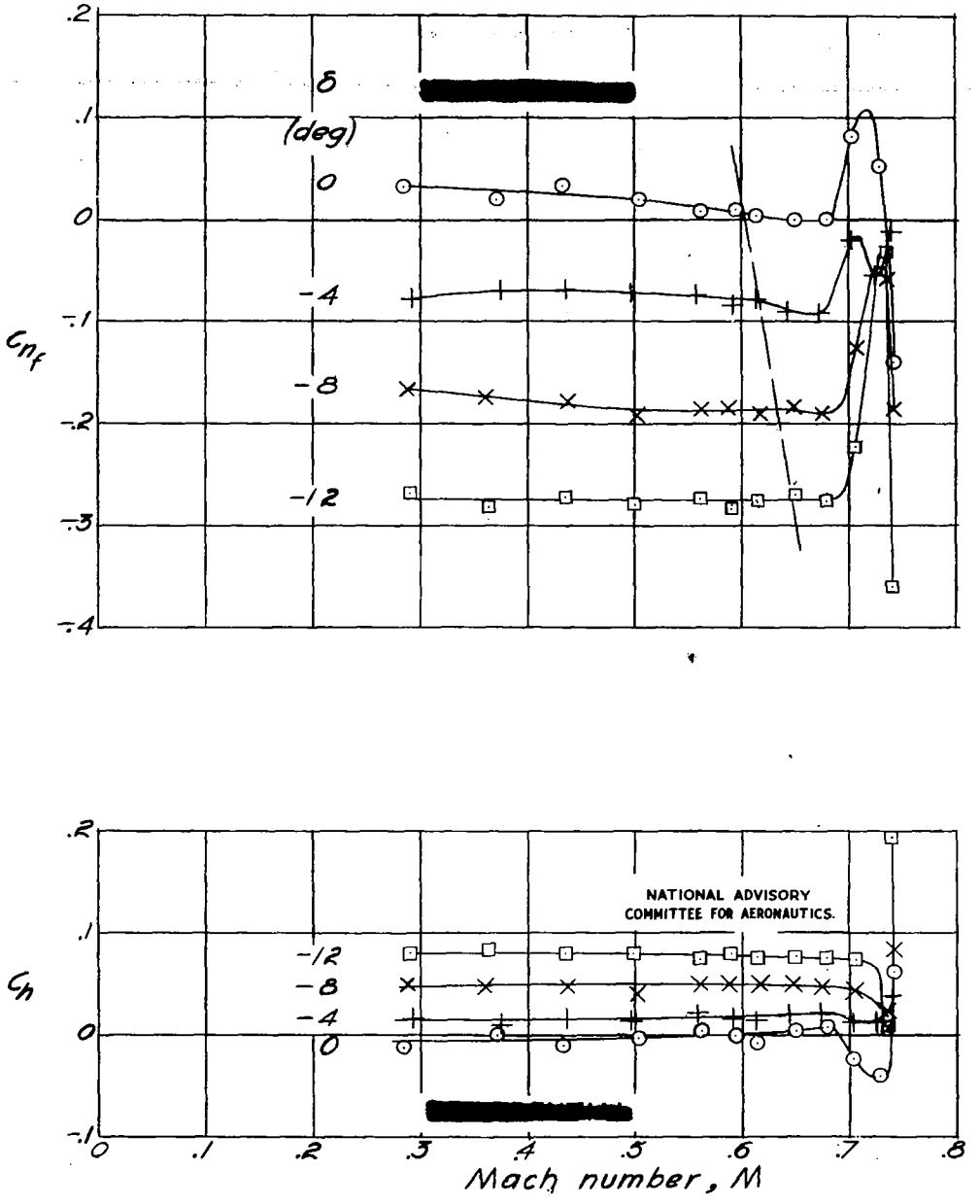

(d) $\alpha = 4^{\circ}$.

Figure 40.- Continued.

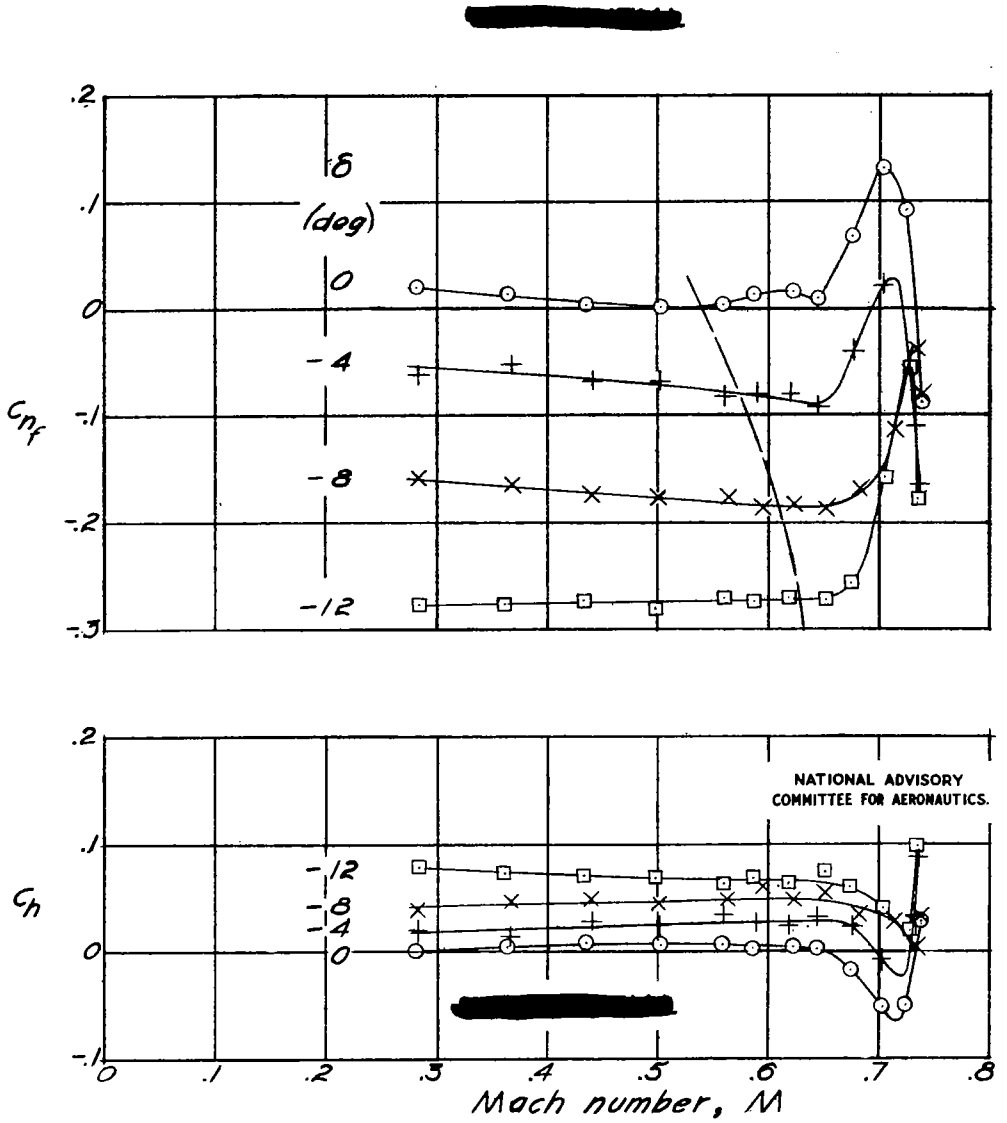

(e) $\alpha = 6^{\circ}$.

Figure 40.- Continued.

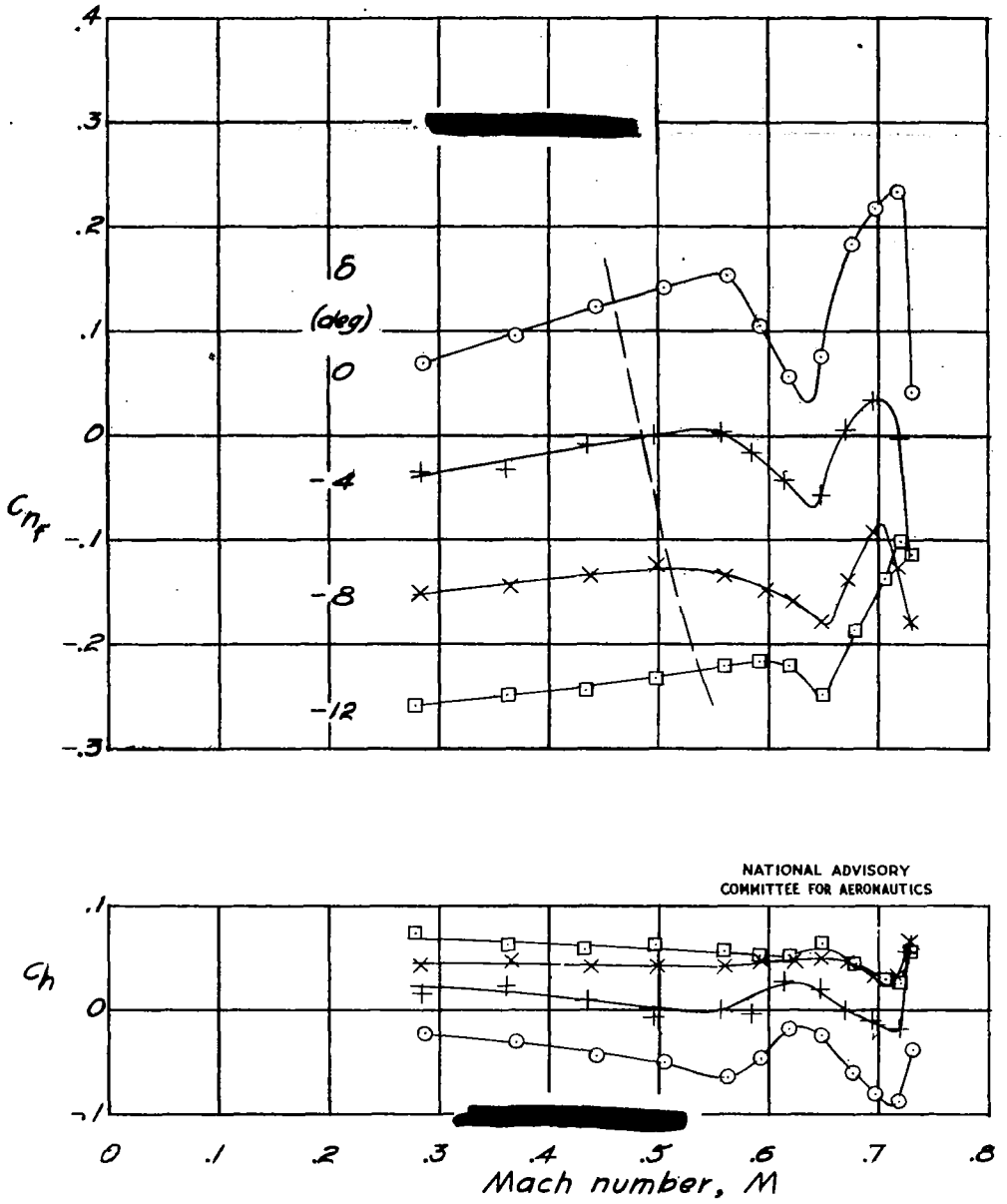

(f) $\alpha = 8^\circ$.

Figure 40.- Continued.

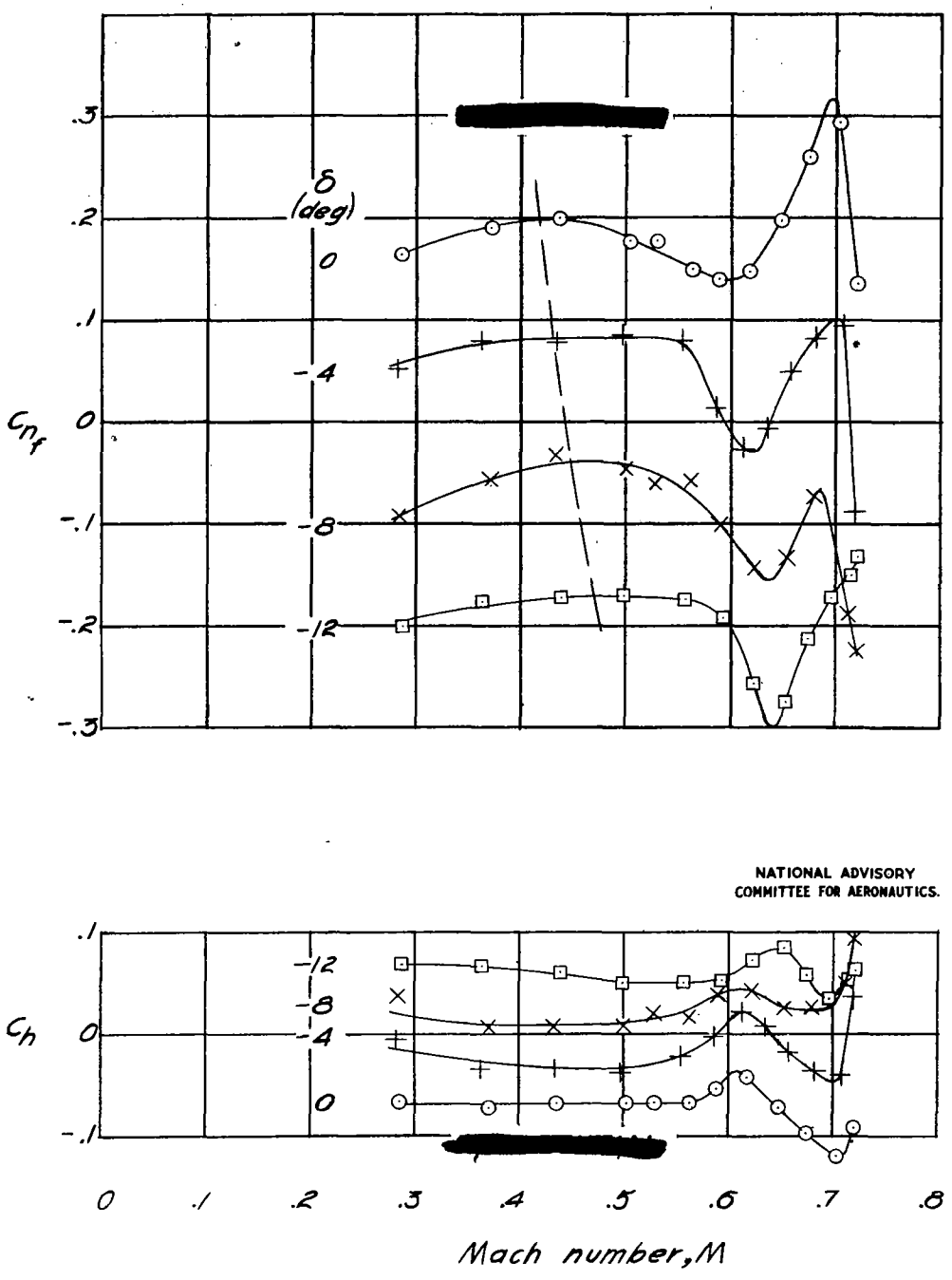

(g) $\alpha = 10^{\circ}$.

Figure 40.- Continued.

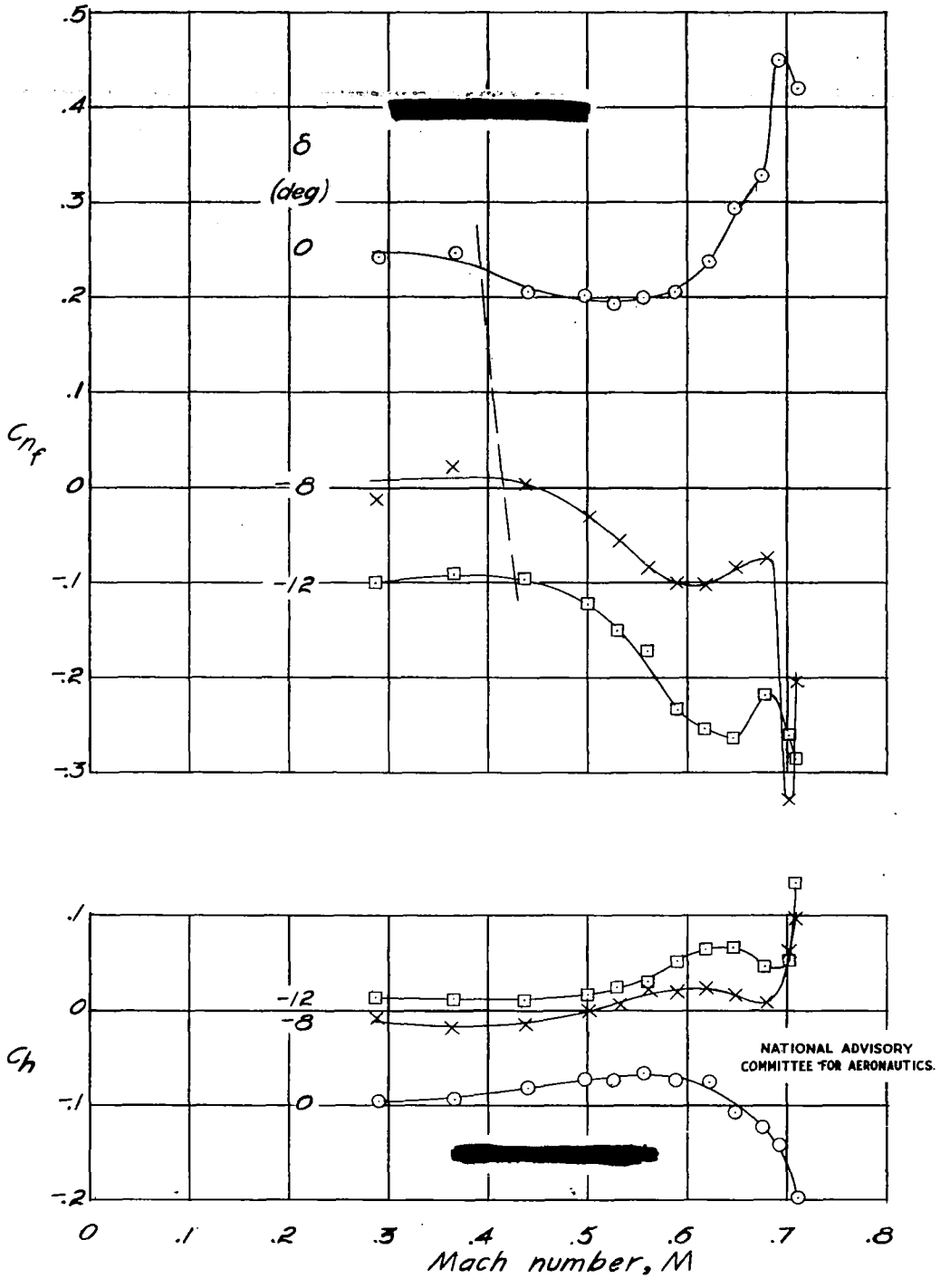

(h) $\alpha = 12^{\circ}$.

Figure 40.- Continued.

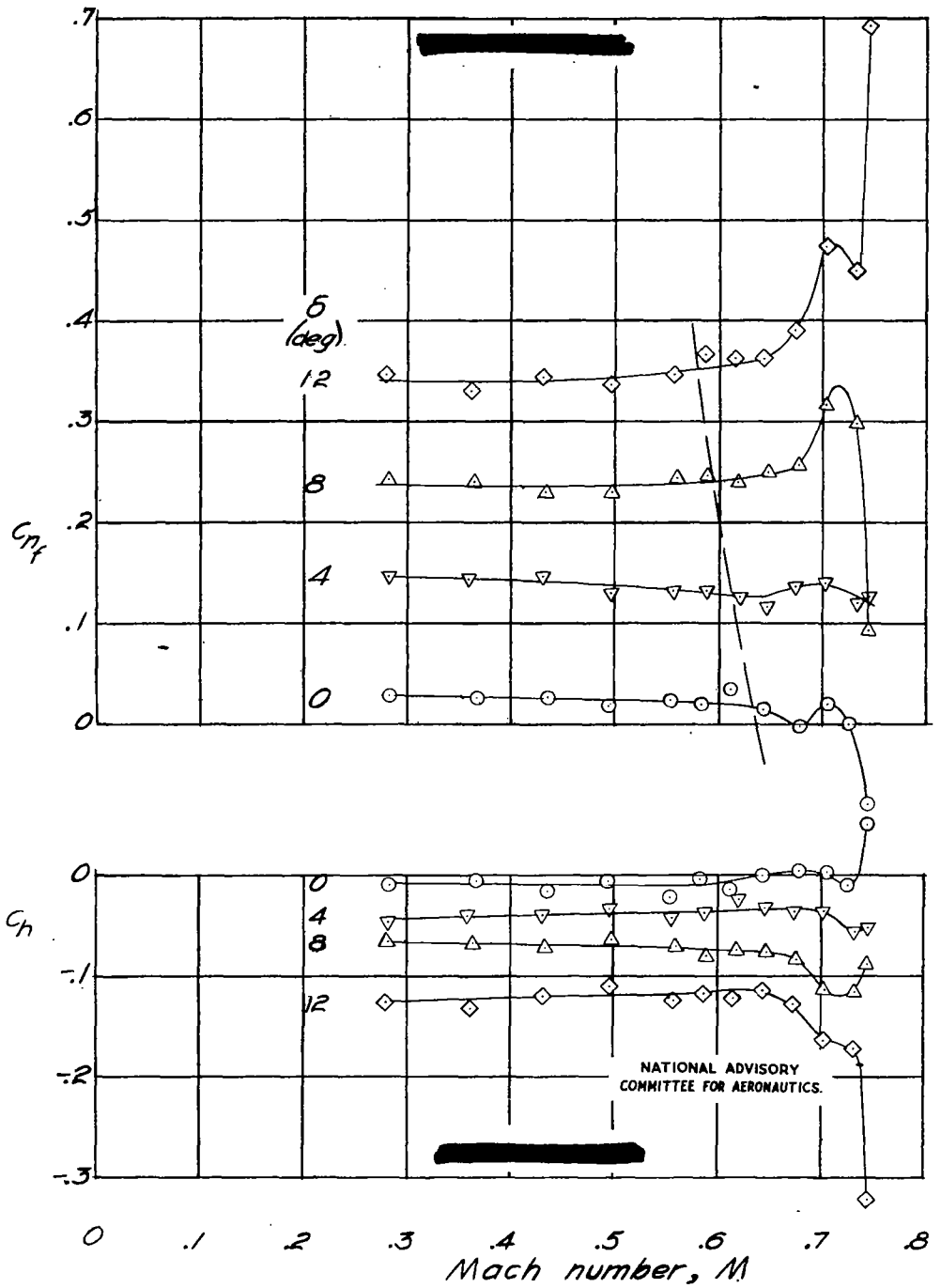

(i) $\alpha = 2^{\circ}$; positive flap deflections.

Figure 40.- Continued.

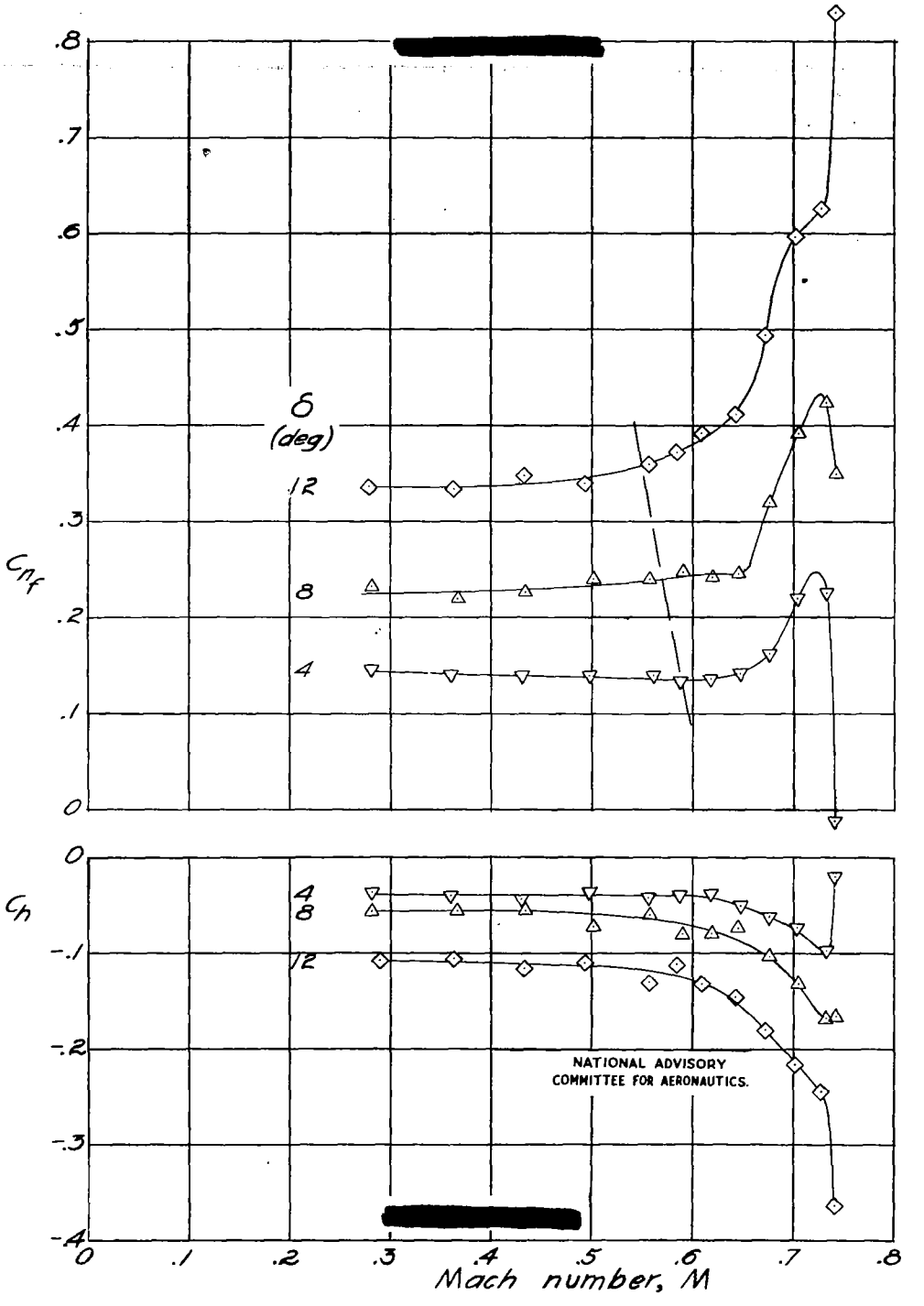

(j) $\alpha = 4^{\circ}$; positive flap deflections.

Figure 40.- Concluded.

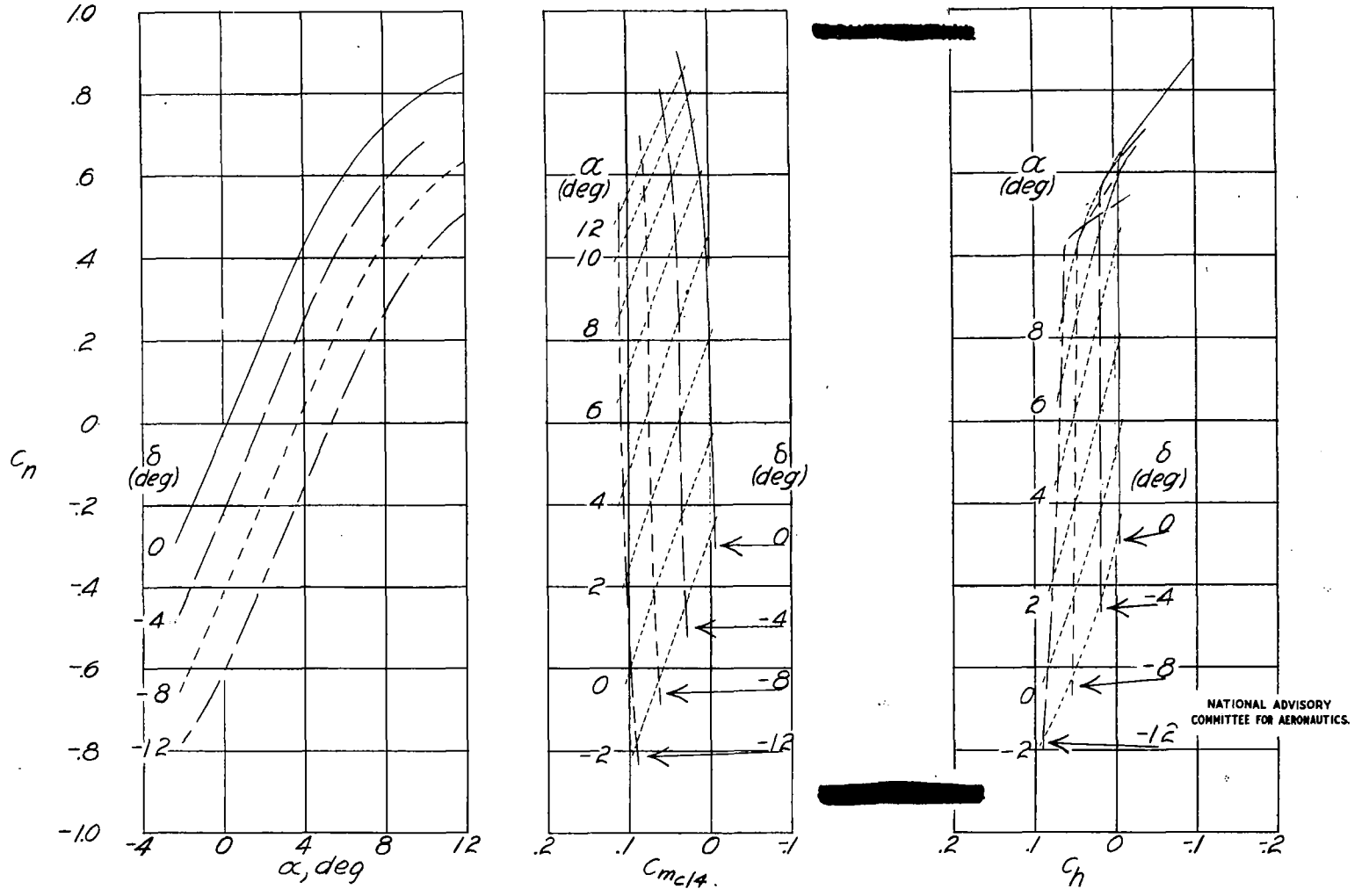

(a) M = 0.40.

Figure 41.- Section characteristics for the modified NACA 65,3-019 airfoil with 0.20-chord flap at constant Mach number.

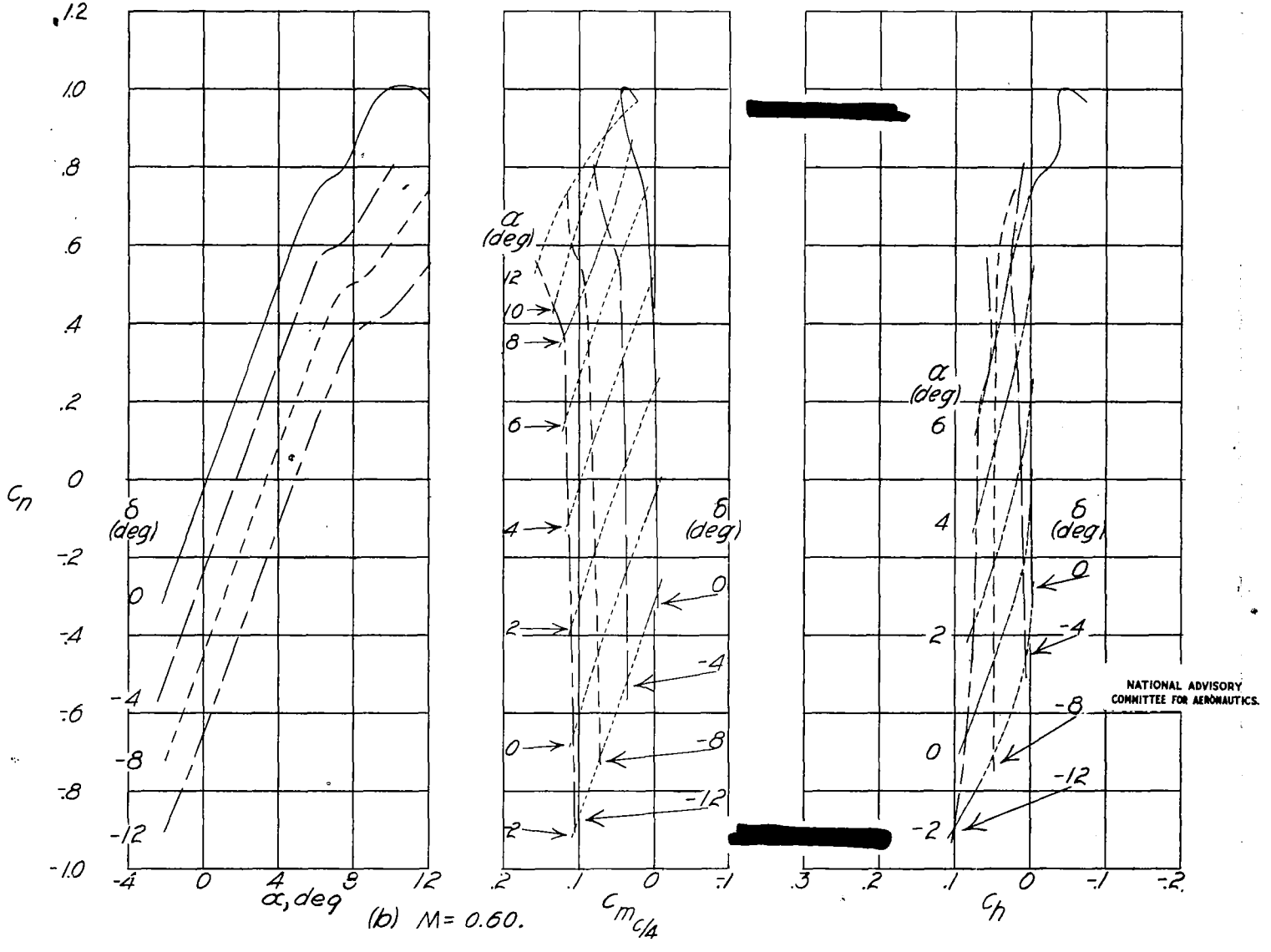

(b) M = 0.60.

Figure 41.- Continued.

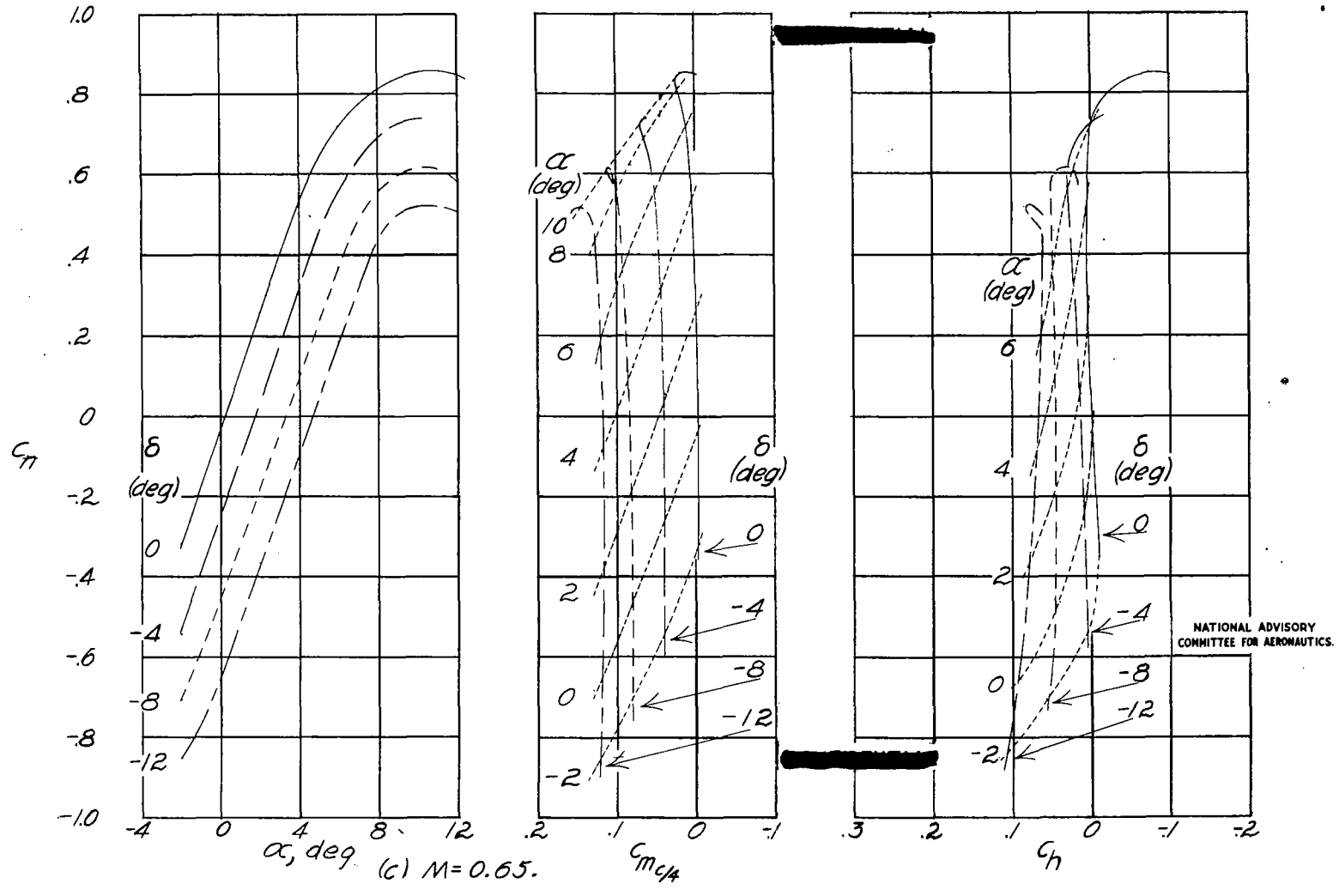

(c) M = 0.65.

Figure 41.- Continued.

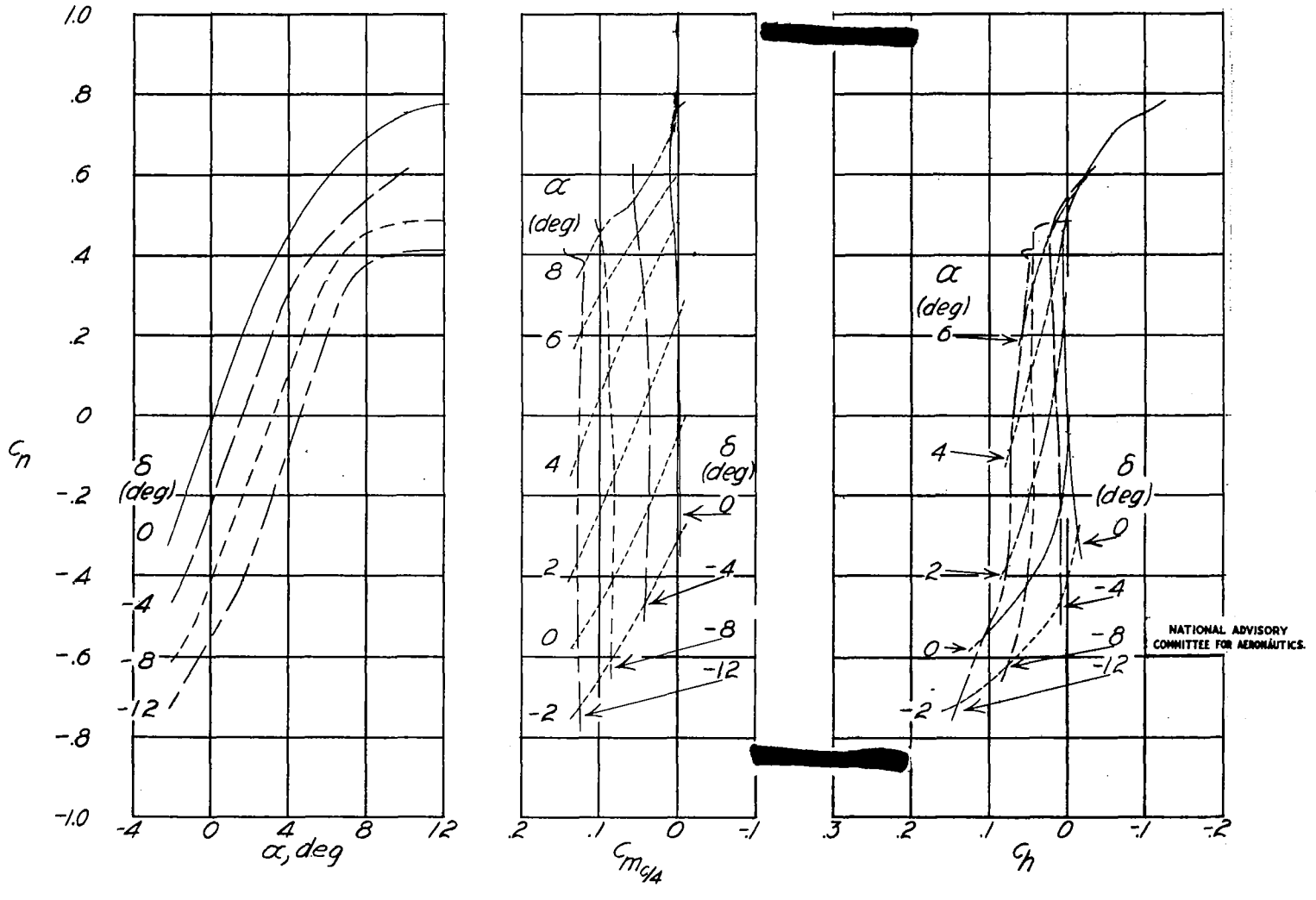

(d) M = 0.675.

Figure 41.- Continued.

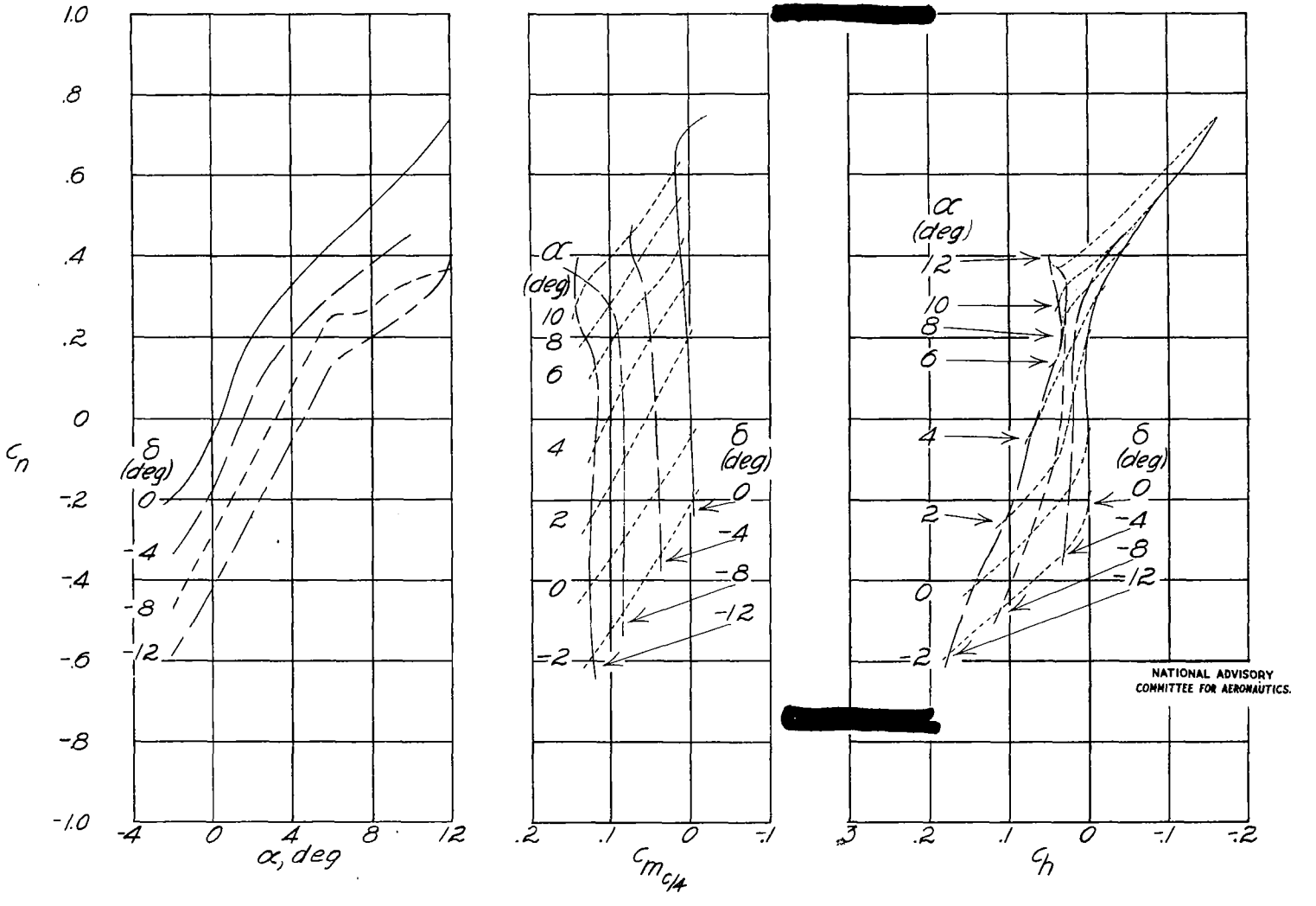

(e) M = 0.70.

Figure 41.- Continued.

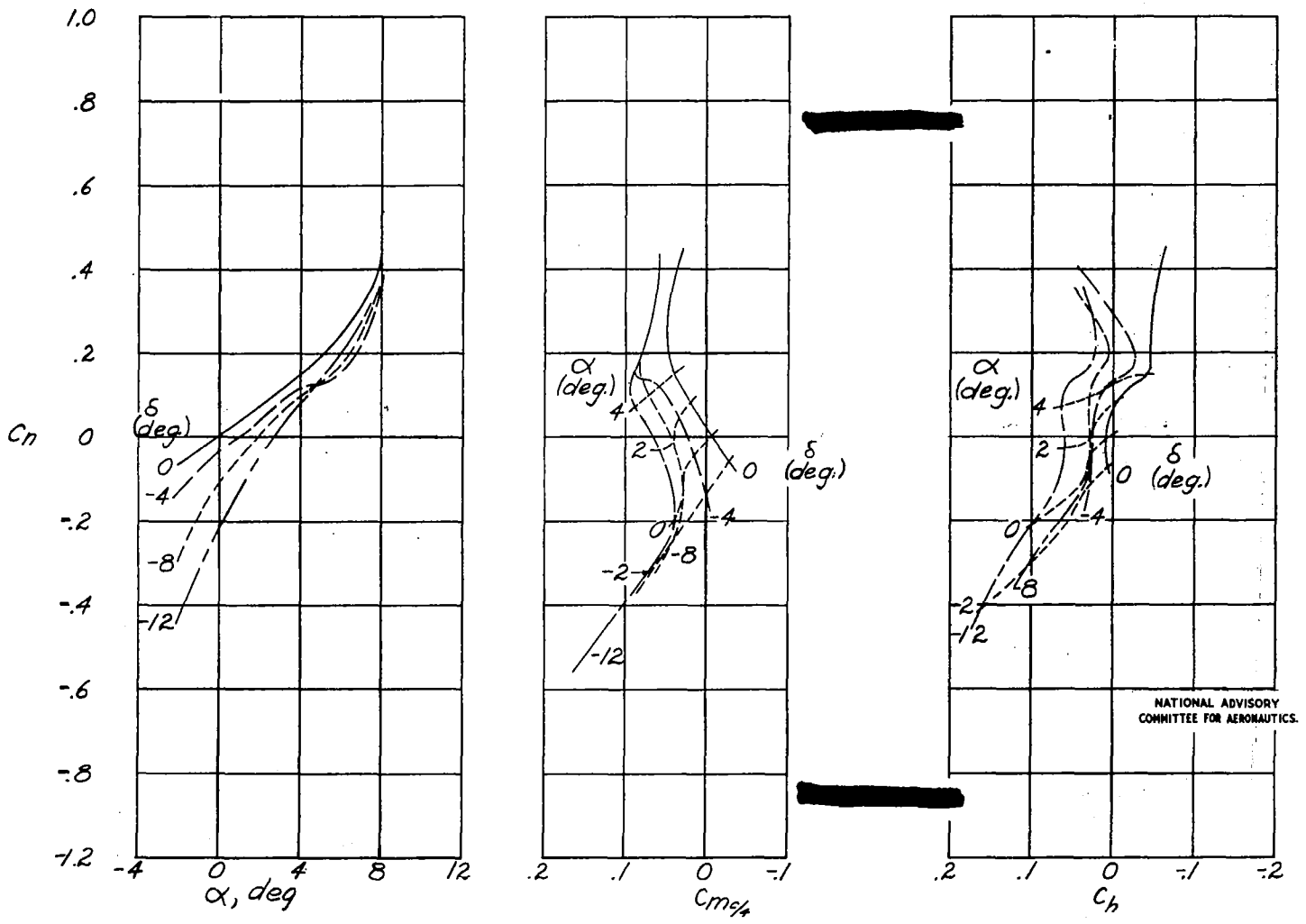

(f) M = 0.725.

Figure 41.- Concluded.

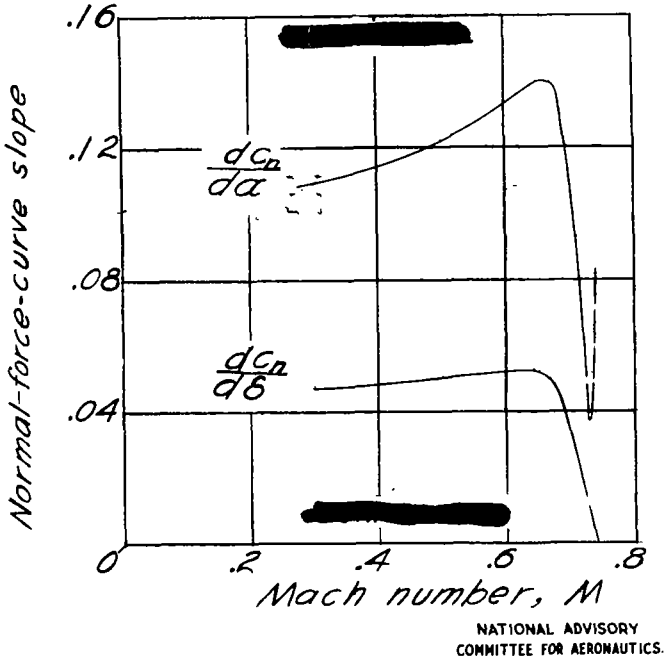

Figure 42.- Effect of compressibility on slope of normal-force curves.

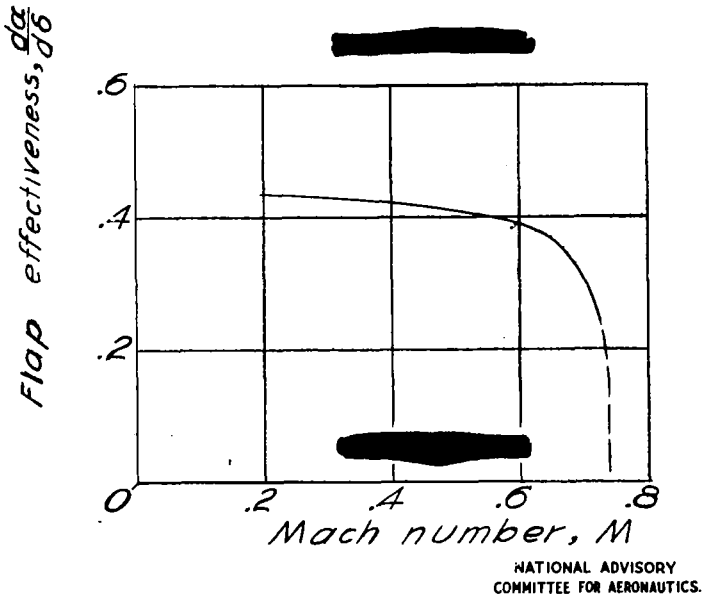

Figure 43.- Compressibility effect on flap effectiveness.

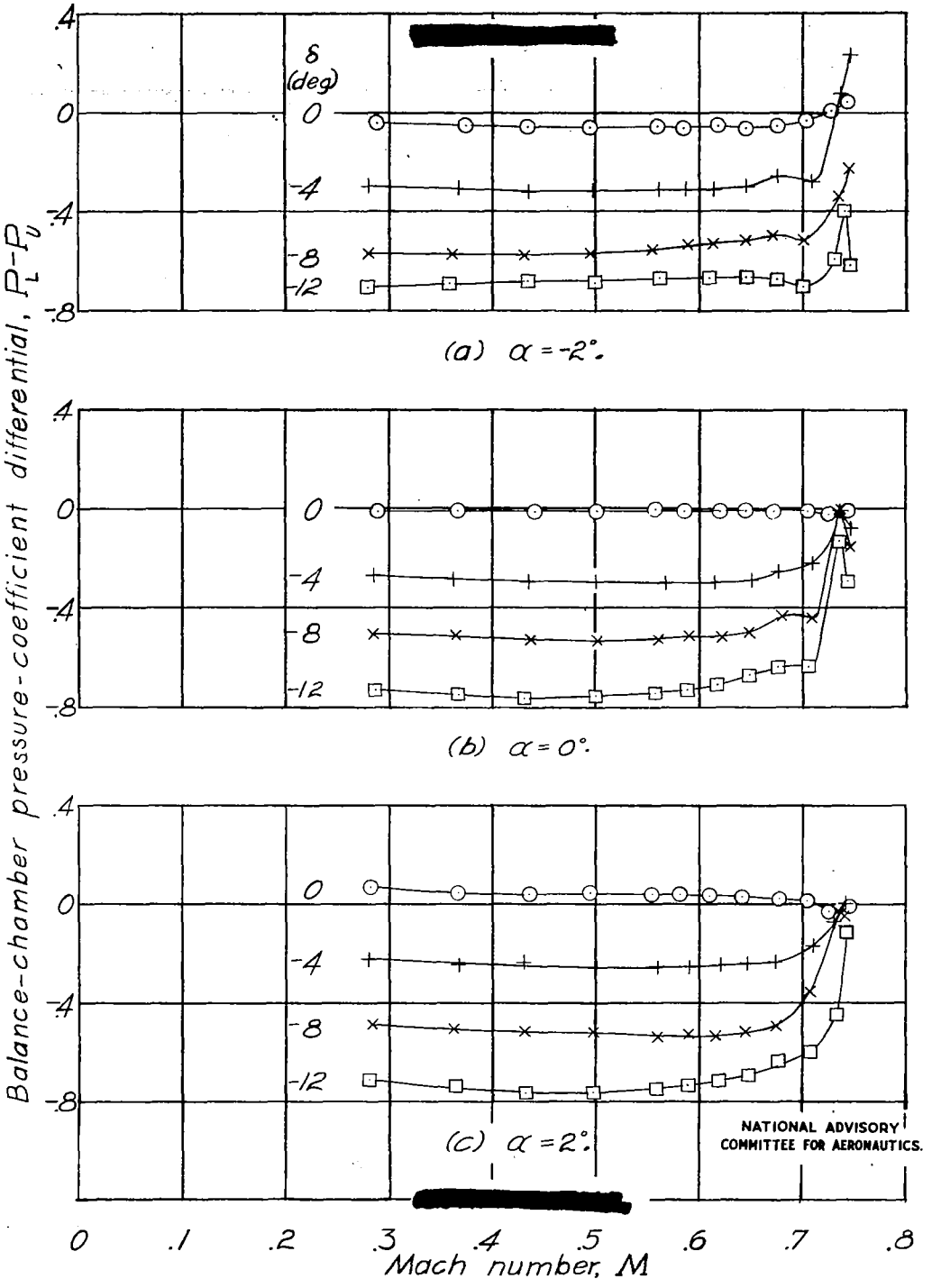

Figure 44.- Effect of compressibility on balance-chamber pressure-coefficient differential, P_L-P_U.

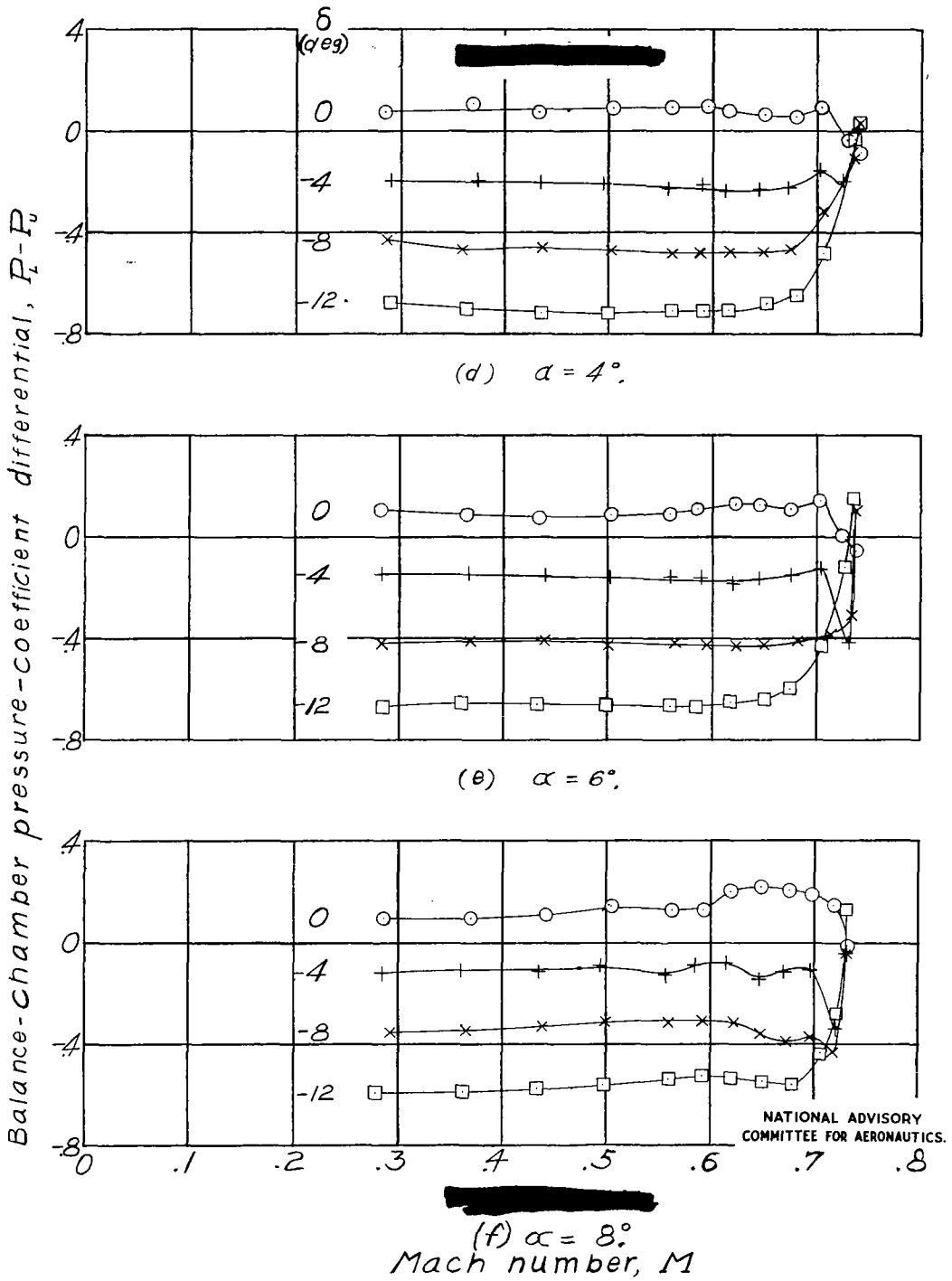

Figure 44.- Continued.

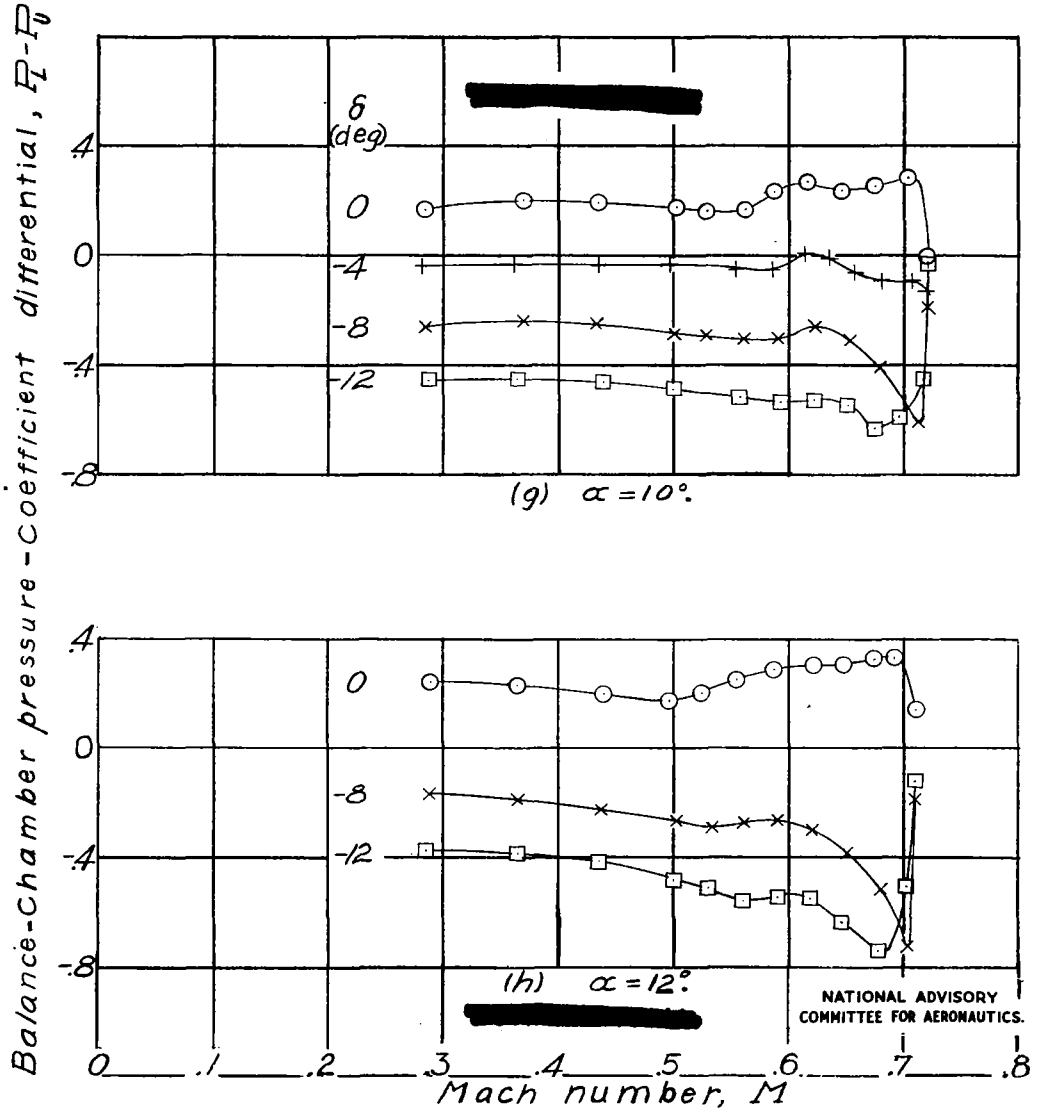

Figure 44.- Continued.

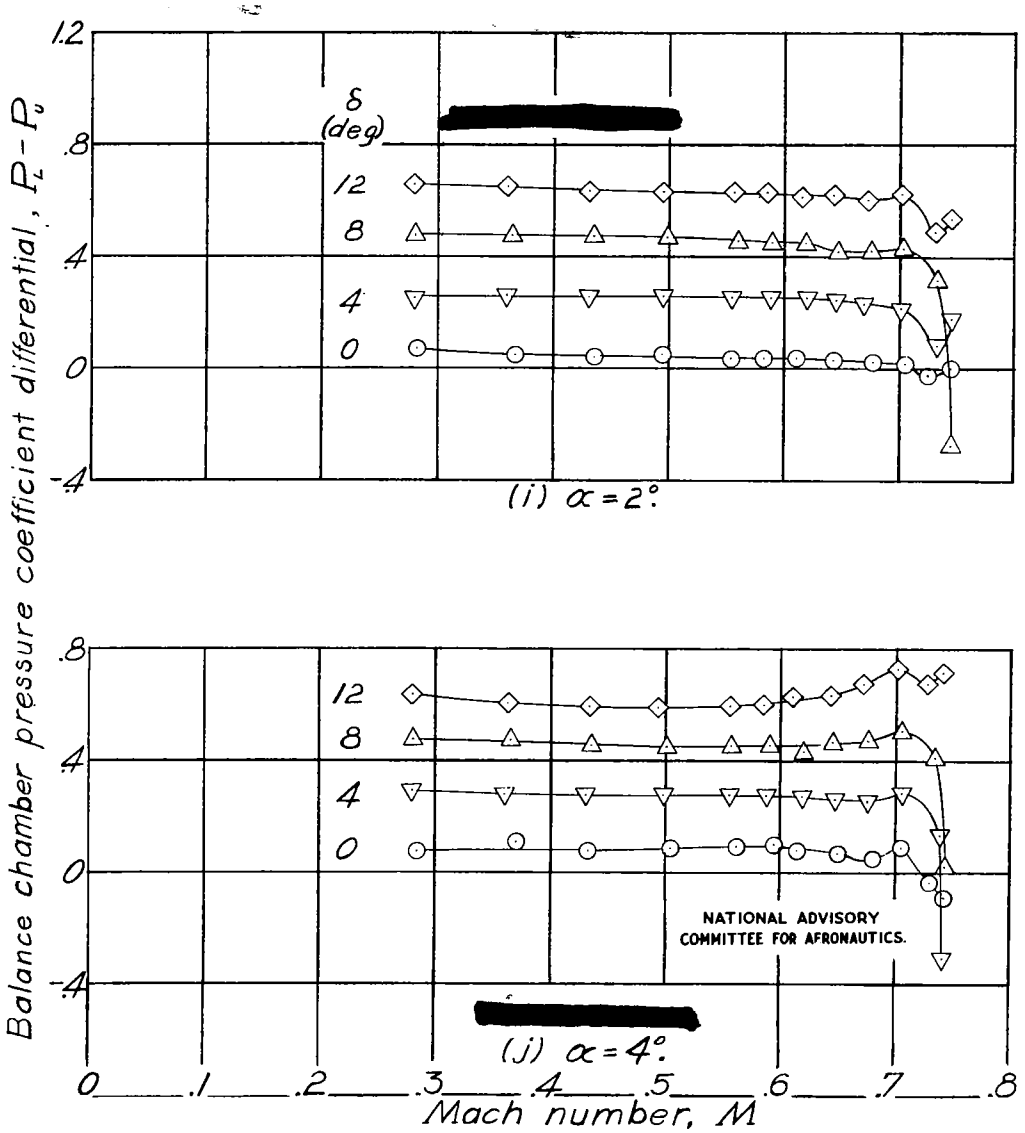

Figure 44.- Concluded.